UNIVERSITAT DE BARCELONA

Uncovering the elements that regulate IKKalpha function in response to DNA damage

Josune Alonso Martínez de Marañón

Uncovering the elements that regulate IKKα function in response to DNA damage

Josune Alonso Martínez de Marañón

TESIS DOCTORAL UB / 2022

Programa de Doctorado en Biomedicina

Programa de Investigación del Cáncer

Institut Hospital del Mar d'Investigacions Mèdiques (IMIM)

Director: Dr. Lluís Espinosa Blay

Tutor: Dr. Rosa Aligué Alemany

IMIM Parc de Salut MAR Barcelona
Institut Hospital del Mar d'Investigacions Mèdiques

Universitat de Barcelona

UNIVERSITAT DE BARCELONA

Programa de Doctorado en Biomedicina

Uncovering the elements that regulate IKKα function in response to DNA damage

TESIS DOCTORAL UB / 2022

Memoria de tesis doctoral presentada por Josune Alonso Martínez de Marañón
para optar al grado de doctora por la Universitat de Barcelona,
realizada bajo la dirección del Dr. Lluís Espinosa Blay.

Barcelona, 2022

ACKNOWLEDGEMENTS

ACKNOWLEDGEMENTS/AGRADECIMIENTOS

Hace cuatro años decidí adentrarme en una aventura, que de primeras parecía complicada, pero que ha resultado ser una etapa de lo más gratificante. Y eso ha sido posible gracias a la influencia y el respaldo de muchísimas personas que me han acompañado durante esta tesis. A todas ellas, gracias.

En primer lugar, quiero daros las gracias a Lluís y a Anna, por darme la oportunidad de hacer el doctorado en el grupo de BigSpin lab. Ese fue el punto de partida de esta emocionante historia. Lluís, gracias por todo lo que me has enseñado y por darme las herramientas necesarias para crecer como científica y ganar confianza en mí misma. Tu pasión por la ciencia y tu motivación me han servido de guía para querer aprender y mejorar cada día. Gracias por confiar en mis ideas, por tener en cuenta mi opinión, por dejarme cometer errores y aprender de ellos, por guiarme siempre que lo he necesitado y por tus buenas palabras de apoyo, incluso cuando los resultados no acompañaban. Anna, gracias por toda tu ayuda desinteresada y tus valiosas propuestas que han mejorado esta tesis, planteando nuevas preguntas y ofreciendo interesantes ideas. Y, en especial, quiero agradecerte tus valiosos consejos para ayudarme a mejorar en la manera de explicarme en público, algo que para mí es especialmente estresante. Ha sido una etapa muy enriquecedora y gracias a vosotros he aprendido mucho más de lo que podía imaginar, tanto a nivel profesional como personal.

Y esta etapa no hubiera sido la misma sin los grandes compañeros que he tenido. Gracias a vosotros he disfrutado del laboratorio cada día. Nunca olvidaré los buenos y divertidos momentos que hemos pasado juntos, el buen ambiente, los cotilleos, las bromas y las risas. Sobre todo, las risas. Porque otra cosa no, pero reír nos hemos reído, y mucho.

Para empezar, Dani, no solo eres un crack en tu trabajo, sino que has sido el socio perfecto. Me has ayudado, apoyado, escuchado, acompañado, enseñado, vacilado y aguantado tanto en los buenos como en los malos momentos. El proyecto en común duró poco (aunque el precioso esquema aguantó un poco más), pero desde entonces no hemos parado de trabajar juntos y ha sido de lo más divertido. Siempre recordaré las risas entre los miles y miles de westerns a primera hora de la mañana, las conversaciones absurdas en las tardes interminables de cultivos y las insuperables bromas que han hecho que trabajar no fuera aburrido. Formamos un buen equipo. De verdad, muchas gracias por todo.

Violeta, amiga, encontrar las palabras para expresar lo importante que has sido para mi en esta etapa es más difícil que elegir la combinación de colores perfecta. De ti he aprendido mucho, y no solo sobre ciencia. Has sido mi punto de apoyo, referente y consejera en muchos momentos de este doctorado, una fuente llena de palabras sabias. Pero sobre todo has sido mi amiga. Gracias por estar siempre a mi lado y estar pendiente de mí, por escucharme y por animarme. Eres una gran científica y una mejor amiga.

Luis, nuestra aventura empezó a la vez y ha sido un placer tenerte como compañero de viaje y de poyata. Para algunas cosas no podríamos ser más distintos, pero eso es lo que ha hecho más interesante y divertido compartir este camino contigo, aprendiendo uno del otro. Admiro mucho tu motivación y la ilusión que trasmites por el mundo de la investigación. ¡Por favor no la pierdas! Pero, en especial, aprecio tu gran corazón y tu buena energía. Se que siempre puedo contar contigo para lo que necesite, dentro y fuera del laboratorio, como compañero y amigo. Muchas gracias Zuis.

A Jessi y Arnau, los "jefes" del lab, os juro que intentaré no romper nada más en el tiempo que me quede (aunque no prometo nada…). Es increíble la paciencia que tenéis con todos nosotros y el gran trabajo que hacéis para mantener el orden en el medio del caos que es la vida del laboratorio. Gracias por estar siempre dispuestos a echarme una mano y los buenos consejos que me habéis dado en estos años.

A mis compis de ordenador Laura, David, Patri y Gayathri. Laura, has sido mi modelo a seguir como estudiante predoctoral. Trabajadora, ordenada y con las ideas claras, siempre dispuesta a darme buenos consejos. David, contigo no ha habido día que no llorará de la risa, con tus bromas y comentarios que hacían divertidos hasta los ratos más aburridos en el ordenador. Echo de menos las conversaciones entre los tres sobre libros, pelis y series frikis. Patri, mi nueva aliada, sé que siempre puedo contar contigo para los planes improvisados. Gayathri, our newest lab member! I am looking forward to share computer time with you.

A las postdocs Teresa, Yolanda, Roshana y Susanne por compartir vuestro conocimiento conmigo, por aconsejarme y darme ideas. Teresa, gracias por todo el apoyo que me diste con el proyecto de mucinas y gracias por ayudarme con la parte bioinformática, que ha mejorado los diferentes proyectos. A Laura e Irene, que hicisteis más fáciles los inicios del doctorado. Y, por último, a Joan, por estar siempre pendiente de como va el proyecto y tus palabras de ánimo.

Agradecer también al resto de grupos del departamento de Cáncer por estar siempre dispuestos a cooperar y ayudarnos mutuamente. A Marta, por toda la ayuda con las immunos. Al Dr. Alberto Villanueva y al Dr. Fernando Gallardo por su implicación y ayuda en el proyecto de melanoma. A la Dra. Rosa Aligué por aceptar ser la tutora de la tesis.

Lo más bonito que me llevo de esta época en Barcelona sois vosotras Uxue, Esti, Nerea, Itziar y Kizki. Vosotras habéis sido mi familia aquí, mi consejo de sabias y mi apoyo incondicional. Gracias por todos los momentos que hemos vivido juntas, por subirme la moral y hacerme reír. ¡Sois y siempre seréis mis brujitas favoritas! Uxue, eterna compañera, el inicio del doctorado coincidió con la mudanza al nuevo piso y nunca imaginamos todo lo que íbamos a vivir aquí. Gracias por nuestras conversaciones interminables. Gracias por tus consejos. Gracias por contagiarme tu manera de emocionarte por las cosas, tu ilusión, tu valor y tu tenacidad. Se que vas a llegar muy lejos porque lo vales. Simplemente, gracias por todo.

Gracias a toda mi gente de Vitoria que me ha apoyado desde la distancia. A la cuadrilla, Maider, Julen, Luisa, Ixone, Urko, Zuriñe, Carras, Lorena, Andrea, Alba, Durana, Mikel y Bea, por estar siempre ahí. Aunque pasen los años y nuestros caminos se separen, siempre seréis mi refugio, el lugar al que siempre querré volver. A Claudia, mi bióloga favorita, por creer en mí. A mi gran familia, por mantenerse siempre unida y por poder contar siempre con todos vosotros.

Y, por último, gracias Aita, Ama e Irati, porque sin vuestro apoyo incondicional no hubiera llegado a donde estoy ahora. Gracias por cuidar de mí y acompañarme en cada paso del camino. De vosotros aprendí los valores importantes que he necesitado durante esta aventura. Gracias por creer en mí siempre. A vosotros os dedico esta tesis.

Eskerrik asko bidelagunak!

ABSTRACT

ABSTRACT

Current treatment against most human cancers is based on DNA-damaging agents, such as chemotherapy or radiotherapy, that eradicate highly proliferative tumor cells. Unfortunately, a significant percent of them become resistant to the treatment, thus leading to tumor relapse and/or metastasis, which eventually results in to patient death. One of the elements involved in the acquisition of therapy resistance is the DNA damage response (DDR) pathway, which coordinates cell cycle, DNA repair and apoptosis. We previously identified a novel form of the IKKα kinase, that we called IKKα(p45), as an upstream regulator of ATM-mediated DNA repair downstream BRAF. We have now demonstrated that under non-damaged conditions, IKKα is already in a complex with ATM whose activity is regulated by NEMO. We have demonstrated that NEMO is dispensable for ATM-IKKα complex activation but is required for driving active ATM and IKKα to the sites of damage, thus leading to efficient DNA damage resolution. Moreover, recognition of damaged DNA by NEMO requires PARP activity since PARP1 depletion or inhibition results in defective recruitment of active ATM to the damaged sites and accumulation of DNA breaks. We propose that compounds that inhibit IKKα function in DDR, such as PARP or BRAF inhibitors in combination with conventional DNA damaging agents will provide a more durable therapeutic strategy for the treatment of cancer patients.

RESUMEN

La terapia actual contra la mayoría de los cánceres está basada en el uso de agentes que dañan el ADN, como la quimioterapia o la radioterapia, que erradican las células tumorales proliferantes. Desafortunadamente, un porcentaje significativo de los tumores se vuelven resistentes al tratamiento, recaen y/o metastatizan, causando eventualmente la muerte del paciente. Uno de los mecanismos implicados en la adquisición de la resistencia terapéutica es la vía celular de Respuesta al Daño del ADN (DDR), que coordina el ciclo celular, la reparación del ADN y la apoptosis. Previamente identificamos una forma nueva de la quinasa IKKα, llamada IKKα(p45), que regula la reparación del ADN mediante la activación de ATM tras ser activada en respuesta a agentes dañinos de manera dependiente de BRAF. En el presente estudio mostramos que IKKα forma un complejo con ATM en condiciones previas al daño, cuya actividad está regulada por NEMO. Nuestros resultados revelan que NEMO no es imprescindible para la activación de este complejo ATM-IKKα, pero es necesario para trasladar las formas activas de ATM e IKKα a los sitios de daño, permitiendo una reparación eficiente del ADN. Además, hemos observado que NEMO necesita la actividad de PARP1 para poder detectar los sitios dañados del ADN, debido a que la disminución o inhibición de PARP1 resulta en un reclutamiento defectuoso del ATM activado y, por lo tanto, en la acumulación de roturas del ADN. Basándonos en estos resultados, proponemos la utilización de inhibidores de la función de IKKα en DDR, como los inhibidores de PARP o BRAF, en combinación con los regímenes de tratamiento convencionales de pacientes con cáncer para mejorar la estrategia terapéutica de pacientes con cáncer.

TABLE OF CONTENTS

TABLE OF CONTENTS

FIGURES AND TABLES

FIGURES AND TABLES

INTRODUCTION

MATERIALS AND METHODS

RESULTS

PART I

DISCUSSION

ABBREVIATIONS AND ACRONYMS

ABBREVIATIONS AND ACRONYMS

53BP1	TP53-Binding protein 1
5-Fu	5-Fluorouracil
5-Fu+Iri.	5-Fluorouracil plus Irinotecan
ACTB	Actin Beta
AKT	Protein kinase B
APC	Adenomatous Polyposis Coli
AT	Ataxia-Telangiectasia
ATM	Ataxia Telangiectasia Mutated
ATP	Adenosine Triphosphate
ATR	ATM and RAD3-related
ATRIP	ATR-interacting protein
BAFF	B-cell-activating factor
Bcl-3	B-cell lymphoma 3-encoding protein
BER	Base excision repair
BioID	Proximity-dependent biotin identification
BirA	Biotin Ligase
BRAF	B-Rapidly Accelerated Fibrosarcoma
BRCA1	Breast cancer 1
BRCT	BRCA1 C terminus
BSA	Bovine Serum Albumin
Cas9	CRISPR-associated protein 9
CBP	CREB-binding protein
CC	Coiled-coil domain
CDK	Cyclin-dependent kinase
CDKN2A	Cyclin-dependent kinase inhibitor 2A
cDNA	Complementary DNA
CHK1/2	Checkpoint kinase 1/2
cIAP	Cellular inhibitor of apoptosis
CIMP	CpG island methylation
CIN	Chromosomal Instability
CMS	Consensus Molecular Subtypes

CNS	Central nervous
Co-IP	Co-Immunoprecipitation
CRC	Colorectal Cancer
CRISPR	Clustered Regularly Interspaced Short Palindromic Repeats
CRM1	Exportin 1
CT	Chemotherapy
CTD	Carboxyl terminal domain
C-terminal	Carboxy terminal
CtIP	CtBP-interacting protein
DAB	3,3'-Diaminobenzidine
DAPI	4,6-diamino-2-phenilindole
DBD	DNA-bindign domain
DDR	DNA damage response
DFS	Disease Free survival
DMEM	Dulbecco's modified Eagle's medium
DMSO	Dimethyl Sulfoxide
DNA	Deoxyribonucleic acid
DNA PKc	DNA-dependent protein kinase catalytic subunit
DPX	Dibutylphthalate Polystyrene Xylene
DSB	Double-strand break
DSP	Dithiobis(succinimidyl propionate)
E2F1	E2F transcription factor 1
ECL	Electrochemiluminescence
EDTA	Ethylenediaminetetraacetic acid
EGFR	Epidermal growth factor receptor
ELKS	Glutamate, leucine, lysine and serine
ERK1/2	Extracellular-signal regulated kinases 1/2
ERα	Estrogen receptor alpha
FA	Fanconi Anemia
FAP	Familial adenomatouspolyposis
FBS	fetal bovine serum
FDA	Food and Drug Administration
FDR	False Discovery Rate

GAPDH	Glyceraldehyde-3- phosphate dehydrogenase
GFP	Green fluorescent protein
GG	Global genome
H3	Histone 3
HDAC	Histone deacetylases
HE	Haematoxylin and eosin
HEPES	Hydroxyethyl piperazineethanesulfonic acid
HLH	Helix-loop-helix
HR	Homologous Recombination
HRP	Horseradish Peroxidase
ICL	Interstrand crosslink
IF	Immunofluorescen
IHC	Immunohistochemistry
IKK	IκB kinase
IKKK	IKK kinase
IL	Interleukin
IP	Immunoprecipitation
IR	Ionizing radiation
Iri.	Irinotecan
IκB	Inhibitor of κB
JNK	Jun amino-terminal kinase
KD	Kinase domain
kDa	KiloDalton
Ki67	Marker of proliferation ki67
KO	Knock-out
LC	Liquid chromatography
LC-MS	Liquid Chromatography Mass spectrometry
LPS	Lipopolysaccharides
LTβ	Lymphotoxin-β
LZ	Leucine zipper
MAPK	Mitogen-activated protein kinase
MDC1	Mediator of DNA damage checkpoint 1
MEKK3	MAPK/ERK kinase kinase 3

MGMT	O^6-methylguanine methyltransferase
MM	Malignant melanoma
MMR	Mismatch repair
MRE11	Double-strand break repair protein MRE11
MRN	MRE11-Rad50-NBS1 complex
MS	Mass spectrometry
MSI	Microsatellite Instability
MW	Molecular weight
Na_3VO_4	NA-orthovanadate
NBD	NEMO binding domain
NBS1	Nibrin
NCoR	Nuclear receptor co-repressor
NEMO	NF-κB essential modulator
NER	Nucleotide excision repair
NES	Nuclear export sequence
NF-κB	Nuclear Factor Kappa B
NHEJ	Non-Homologous End Joining
NIK	NF-κB inducing kinase
NLS	Nuclear localization signal
NRAS	Neuroblastoma Ras
N-terminal	Amino terminal
O/N	Overnight
PAMP	Pathogen-associated molecular patterns
PARP	Poly(ADP-ribose) polymerase
PBM	PAR-binding modules
PBS	Phosphate-buffered saline
PCR	Polymerase Chain Reaction
PCR2	Polycomb repression complex 2
PEI	Polyehylenimine
PFA	Paraformaldehyde
PI	Propidium Iodide
PIASγ	Protein inhibitors of activated STAT
PIDD	p53 inducible death domain-containing protein

PIKK	phosphatidylinositol 3-kinase-like protein kinase
PMSF	phenyl-methylsulfonylfluoride
PNK	Polynucleotide kinase
POLD	DNA polymerase delta catalytic subunit
PS	phosphatidylserine
PVDF	Polyvinylidene difluoride
qRT-PCR	Quantitative real time polymerase chain reaction
Rad50	DNA repair protein RAD50
RAD51	DNA repair protein RAD51 homolog 1
RANKL	Receptor activator for NF-κB ligand
RB	Retinoblastoma-associated protein
RGP	Radial-growth-phase
RHD	Rel homology domain
RIP1	Receptor interacting protein 1
RKT	Receptor tyrosine kinases
RNA	Ribonucleic Acid
ROS	Reactive oxygen species
RPA	Replication protein A
RPMI 1640	Roswell Park Memorial Institute medium
RT	Room temperature
SAINT	Significance Analysis of INTeractome
SCC	Squamous cell carcinoma
SCF	Skp1/Cul/F box
SCID	Severe immune deficiency
SCR-3	steroid receptor coactivator 3
SDD	Scaffold/dimerization domain
SDS	Sodium Dodecyl Sulphate
SDS-PAGE	SDS-polyacrylamide gel electrophoresis
SEC	Size exclusion chromatography
sgRNA	Single guide RNA
SMRT	Silencing mediator for retinoid and thyroid receptor
SSB	Single-strand breaks
ssDNA	Single-stranded DNA

SUMO	Small ubiquitin-related modifier
TAD	Transcription activation domain
TAD	Transcription activation domain
TAK1	Transforming growth factor-β activated kinase 1
TBP	TATA-Box binding protein
TBS	Tris buffered saline
TBS-T	Tris buffered saline plus Tween20
TC	Trancription coupled
TCGA	The Cancer Genome Atlas
TF	Transcription factors
TGF β	Transforming growth factor-β
TME	Tumor microenvironment
TMZ	Temozolomide
TNFα	Tumor necrosis factor α
TOP1	DNA topoisomerase 1
TOPBP1	Topoisomerase-binding protein-1
TRL	Toll-like receptor
TSA	Tyramide Signal Amplification
TSS	Transcription start site
UBAN	Ubiquiting binding domain
ULD	Ubiquitin-like domain
UV	Ultra Violet
VEGF	Vascular endothelia growth factor
VGP	Vertical-growth-phase
WB	Western blot
WT	Wild type
ZNF	Zinc-finger region
β-ME	β-Mercaptoethanol
γH2A.X	Phospho-Histone H2A family member X

INTRODUCTION

I1. COLORECTAL CANCER

The intestinal epithelium is continuously self-renewing through the combination of different cellular processes involving cell proliferation, differentiation, migration, and cell death. The maintenance of the equilibrium between these processes is complex but crucial for tissue homeostasis. Thereby, the alteration of one of these processes can lead to intestinal tumorigenesis. Colorectal cancer (CRC) is characterized by the abnormal and uncontrolled growth of colonic and rectum cells, caused by the accumulation of multiple genetic and epigenetic alterations.

I1.1 Epidemiology of colorectal cancer

CRC is the third most common cancer in men and women worldwide, accounting for approximately 9% of cancer-related death[1]. Generally, most CRC (about 95%) are considered sporadic and there are multiple risk factors (hereditary and environmental), such as other intestinal diseases, obesity, high fat diet, sedentary lifestyle, alcohol consumption, and long-term smoking, that increase the probability of developing CRC. Inherited CRCs are less common (about 5%-10%) and can be subdivided into polyposis syndromes, such as familial adenomatouspolyposis (FAP), and non-polyposis syndromes, such as Lynch syndrome[2].

I1.2 Molecular mechanisms of colorectal cancer development and progression

Normally, CRC tumorigenesis initiates with the transformation of normal colorectal epithelial cells by spontaneous mutations, environmental mutagens, and genetic or epigenetic alterations. The development of normal colon epithelial cells to aberrant crypt foci, followed by early and advanced polyps with subsequent progression to early cancer and then advanced cancer has been traditionally explained by the **adenoma-carcinoma sequence** (**Figure I1**). In the classical model, CRC cancer arises from a dysplastic polyp in an aberrant crypt, which usually presents a driver mutation in *APC* gene[3], that evolves into an early adenoma (<1cm in size). Then, the adenoma progresses to an advanced adenoma before finally becoming colon carcinoma and invasive colon cancer. Progressive accumulation of mutations and epigenetic alterations that cause hyperproliferation such as *KRAS/BRAF, SMAD4,* or *TP53* mutations allow the malignant transformation of these adenomas into colon carcinoma and metastasis[4,5].

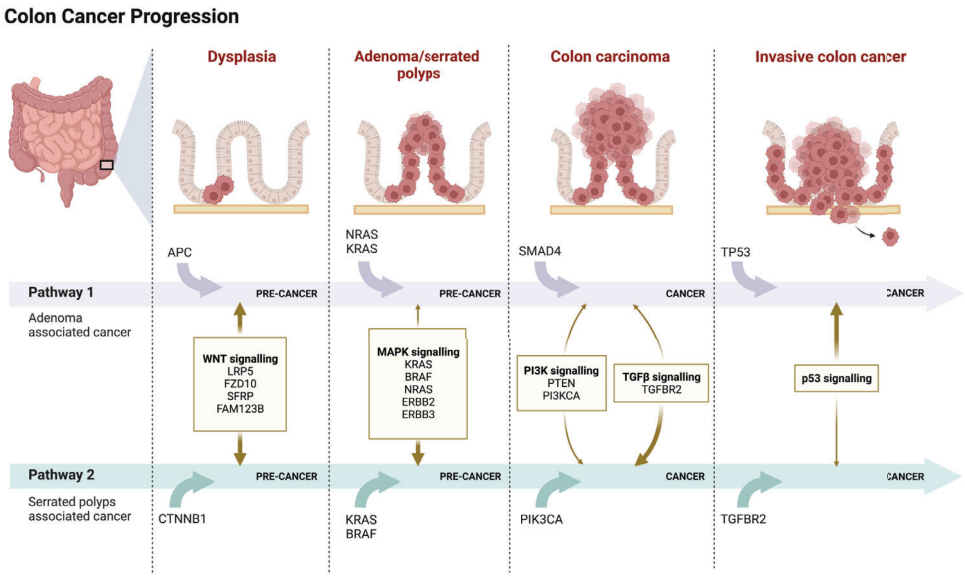

Figure I1. The adenoma-carcinoma sequence. CRC tumorigenesis is initiated by adenomas or serrated polyps, which driven by a series of defined genetic alterations, progress into colon carcinoma and then, in invasive CRC. Created with BioRender.com.

At the molecular level, CRC development and progression are driven by three major molecular mechanisms. The most common is the chromosomal instability (CIN) mechanism, which occurs in 70-85% of sporadic CRC cases and is characterized by aneuploidy, structural chromosomal abnormalities, loss of heterozygosity at tumor suppressor genes, and chromosomal rearrangements[6]. Indeed, these alterations are associated with mutations in specific oncogenic or tumor suppressor genes such as *APC, KRAS, BRAF, SMAD4,* or *TP53*, which regulate cell proliferation and cell cycle[7]. Another important mechanism in CRC is Microsatellite instability (MSI), which is caused by dysfunctional DNA mismatch repair[8] and is associated with genetic hypermutability[9]. The CpG island methylation phenotype (CIMP) comprises the third pathway to CRC. CIMP-positive tumors can be divided depending on their CIMP levels. CIMP^{high} tumors often showed mutations in BRAF, MLH1 methylation, and silencing of MGMT or CDKN2A, whereas CIMP^{low} tumors are associated with KRAS mutations[10]. The presence of the three mechanisms (CIN, MSI, CIMP) is not mutually exclusive and they influence several physiological pathways including WNT pathway, MAPK pathway, PI3K pathway, TGFβ signalling pathway, Notch pathway, and NF-κB pathway, among others[11]. In addition, CRC cells are highly influenced by the stromal and immune cells of the

tumor microenvironment (TME), particularly TME inflammation affects CRC tumorigenesis and modules cell polarization[12].

I1.3 Colorectal cancer classification

Classically, colon cancer classification is performed based on TNM. In this system, stages are assigned based on the characteristics of the primary tumor (T), the extent of regional lymph node involvement (N), and the presence of distant metastasis (M). Using this system CRC tumors are classified in four different stages (I, II, III and IV), with subcategories[13]. Although TNM is currently the most common guideline for CRC staging and an important basis to determine the treatment method, it is not a reliable tool for prognosis prediction. Indeed, the outcome after therapy for CRC patients is very variable, even when patients are assigned in the same TNM category[14], underlining the necessity of a better understanding of CRC molecular basis.

The emergence of the omics technology allowed the integration of genetic, transcriptomic, and proteomic data from different biological features. Recently, a new classification system that divided CRC tumors into four groups depending on their molecular characteristics was described, known as consensus molecular subtypes (CMS). CMS1 tumors are characterized by MSI, CIMP, and strong immune infiltration; CMS2 tumors showed canonical features such as WNT signalling activation; CMS3 tumors carry KRAS mutations with metabolic features; and CMS4 tumors present stromal infiltration and TGFβ activation[15].

I1.4 Colorectal cancer treatment

Treatment options for CRC patients include surgery, chemotherapy, targeted therapy, immunotherapy, gene therapy, and combination therapies. The standard guideline for primary colon cancer is surgical resection of the area containing the tumor and lymphoid nodes. Surgery is usually accompanied by chemotherapy/radiotherapy at adjunvancy (after surgery, to eliminate remaining tumor cells) or neoadjuvancy (prior to surgery, to reduce tumor mass)[5].

Regarding chemotherapy, the most commonly used chemotherapeutic agents include 5-Fluorouracil (5-Fu), Irinotecan (Iri.), Oxaliplatin, Calcium folinate, and Capecitabine. These agents are usually given together in different combination treatments: FOLFOX (5-Fu+Calcium folinate + Oxaliplatin), FOLFIRI (5-Fu + Iri. + Calcium folinate), CALPEOX (Capecitabine + Oxaliplatin) and FOLFOXIRI (5-Fu + Iri. + Calcium folinate + Oxaliplatin)[16].

Targeted therapies can be divided into two categories: small molecule signal transduction inhibitors and monoclonal antibodies[17]. Small inhibitors can eliminate cancer cells by specifically blocking signalling pathways necessary for tumor growth and proliferation. In contrast, monoclonal antibodies recognize tumor cells through specific antigens inducing their eradication. Examples of this targeted therapy are the clinically approved anti-EGFR antibody (Cetuximab) for KRAS wild-type CRC[18] or anti-VEGF (Bevacizumab) for blocking angiogenesis[19]. Targeted therapies can be also used in combination with chemotherapy for advanced and metastatic CRC cancer, to enhance their effectiveness against tumor cells[17].

Immunotherapy fights tumors by activating the immune system to directly attack tumor cells. Some immune checkpoint inhibitors have been approved for CRC treatment, such as the PD-1 inhibitors nivolumab and pembrolizumad[20]. Regarding gene therapy, recent clinical studies have shown promising results, however efficient and reliable delivery methods are still under development[21].

The appearance of new therapeutic agents and combination therapies has considerably improved cancer treatment in the last years. However, therapeutic resistance is still a major problem in cancer patients because it is the main cause of relapse and death. For that reason, uncovering druggable mechanisms involved in therapy resistance is one of the main focus of cancer research.

I2. DNA DAMAGE RESPONSE PATHWAY

The maintenance of genome integrity and fidelity is essential for the proper function and survival of all organisms. However, the genome is constantly assaulted by endogenous factors and by a large variety of exogenous genotoxic agents. To counter this threat, cells have evolved an intricate network of mechanisms to detect DNA damage, signal its presence and mediate its repair, collectively termed as the **DNA damage response (DDR)**[22,23]. In order to ensure genome integrity, DDR coordinates accurately the complex network of signal sensors, transducers, and effectors[24]. DNA damage is directly recognised by DDR sensors, which activate the signalling cascade of DDR transducers, resulting in the activation of DDR effectors, that are involved in the regulation of a wide variety of cellular processes such as DNA replication, DNA repair, cell cycle control, and programmed cell death[25]. Failure to repair DNA lesions may result in blockages of transcription and replication, mutagenesis, and cellular cytotoxicity, which has been shown to be involved in a variety of genetically inherited disorders, aging, and carcinogenesis[26,27].

I2.1 DNA damage and repair

Based on its origin, DNA damage can be categorized as endogenous or exogenous DNA damage. Most of the endogenous DNA damage arises from the chemically active DNA engaging oxidative reactions with reactive oxygen species (ROS), that are naturally present within cells[28]. But it could also be generated due to the accumulation of replication errors, DNA base mismatches, spontaneous base deamination, or DNA methylation[29]. On the other hand, exogenous DNA damage occurs when DNA is injured by environmental, physical, and chemical agents, such as UV radiation, ionizing radiation, alkylating agents, and crosslinking agents[30].

DNA lesions can vary from breaks in phosphodiester bonds of the DNA helix -such as single-strand breaks (SSBs)[31] and double-strand breaks (DSBs)[32]- to base damage including pyrimidine dimers, mismatches, and crosslinks. SSBs are often generated from oxidative damage or from the defective activity of the DNA topoisomerase 1 (TOP1) enzyme. Unresolved SSBs during DNA replication can be converted to more deleterious DSBs, resulting in chromosome breakages and translocations, leading to severe genome instability[33].

The type of ends and the structures of the DNA breaks dictate the selection and the recruitment of repair factors[34]. Although some breaks can be repaired by direct reversal[35] and interstrand crosslink

(ICL)[36] mediated via proteins such as O^6-methylguanine methyltransferase (MGMT), most are mediated by series of protein phosphorylation events. There are five major DNA repair pathways that are active throughout different cell cycle stages[37]: Base excision repair (BER), Nucleotide excision repair (NER) and Mismatch repair (MMR) for SSBs, Homologous recombination (HR) and Non-homologous end joining (NHEJ) for DSBs (**Figure I2**).

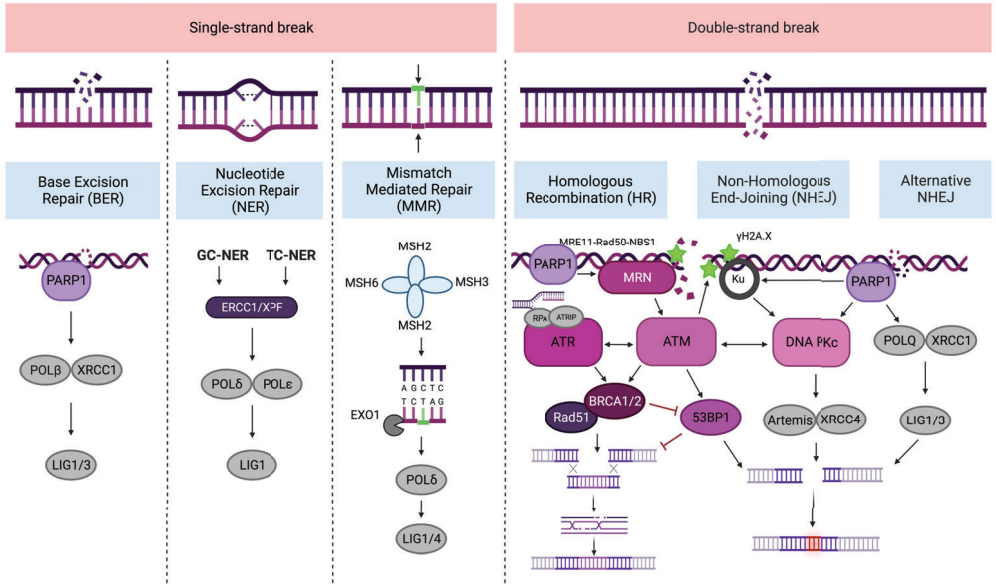

Figure I2. DNA repair pathways. Specific types of DNA damage (SSBs or DSBs) result in the activation of specific signalling and repair cascades. For the repair of DSBs PIKK members (ATM, ATR and DNA PKc) are crucial regulators. DSBs could be repaired through rapid non-homologous end joining (NHEJ) or through higher fidelity homologous recombination (HR). PARP1 is key to mediating multiple DNA damage repair pathways. Created with BioRender.com.

In BER pathway, a DNA glycosylase recognizes and excises damaged base, while DNA polymerases (POLβ), nucleases (XRCC1) and ligases (LIG1, LIG3) mediate lesion reparation[38]. NER pathway is used to correct SSBs involving helix-distorting bulky lesions and is mediated by two different mechanisms: transcription-coupled (TC) NER, which repairs damaged active transcription sites of RNA polymerase II, or global-genome (GG) NER, which fills in the gap formed by ssDNA due to base pairing disruption. Endonucleases XPF-ERCC1/4 and XPG cut the damaged strands, then DNA polymerases POLδ and POLε and ligase LIG1 perform damage reparation[39]. MMR pathway is activated to repair DNA replication errors containing a mismatched nucleotide, insertions, or deletions. In this pathway,

damage is detected by either MSH2-MSH6 or MSH2-MSH3 complexes and removed by exonuclease EXO1[40].

Depending on the cell cycle phase, DSBs can be repaired by NHEJ or HR[41]. In NHEJ pathway, DSBs are recognised by Ku70/Ku80 heterodimers. This complex binds to DNA PKcs (DNA-dependent protein kinase catalytic subunit) and activates it, which mediates the recruitment of DDR factors including Artemis, XRCC4, LIG4, XLF, and APLF[42,43]. In alternative NHEJ, PARP1 is recruited to the damage site by the MRE11-Rad50-NSB1 (MRN) complex, POLQ repairs the damage and XRCC1 and LIG1/3 handle the ligation[44,45]. In NHEJ broken ends are ligated without the need of a homologous template, therefore it can operate in any phase of the cell cycle.

By contrast, HR is restricted to S/G2 phases because sister-chromatin sequences are used as the template for DNA repair[46]. This highly regulated pathway starts with the generation of 3' single-stranded DNA (ssDNA) overhangs through resection of 5'DNA ends, promoted by endonucleases including the MRN complex[47]. Then, DDR effectors BRCA1/2 (Breast cancer 1 and 2) and Rad51 locate the area of homology in the undamaged template, allowing DNA synthesis and ligation[48].

DNA repair pathway selection is critical for maintaining genomic stability and is strictly regulated during different cell cycle phases. One key element that determines whether DSBs are repaired by NHEJ or HR is the DDR member 53BP1 (TP53-Binding protein 1)[49]. Despite that 53BP1 is not essential in NHEJ pathway performance, it abrogates DSBs resection during the G1 phase, conserving DSB ends and thereby favouring NHEJ over HR. Upon entry into S phase, BRCA1 assists in switching the mode of DSBs repair towards HR pathway by excluding 53BP1-RIF1 complexes and allowing DSBs end resection[50,51].

I2.2 DNA-damage signalling

The DDR signalling is primarily mediated by proteins of the PIKKs (phosphatidylinositol 3-kinase-like protein kinase) family and members of PARP (poly(ADP-ribose) polymerase) family[22]. DDR is initiated with the recruitment and activation of these key DDR proteins into sites of damage, which orchestrate a large network of cellular processes to maintain genomic integrity.

The PIKK family

The central components of DDR signal transduction response are three members of PIKKs family ATM (Ataxia telangiectasia mutated), ATR (ATM- and Rad3-related), and DNA PKcs[52]. All these

proteins are huge polypeptides with similar domain organization and common structural features. In their C-terminal is located the PI3K kinase domain, which harbours the catalytic site of the kinases, whereas the N-terminal region is poorly conserved between family members and is believed to be important for the interaction with various substrates[53].

Deficiency of these PIKKs members is linked to a diverse group of pathologies such as neurodegeneration, immune deficiency, and cancer. Mutations in ATM are found approximately in 0.5-1.0% of the population[54], predisposing carriers to cancer. People with mutations is both alleles of ATM suffer from ataxia-telangiectasia (AT), a neurodegenerative disorder that occurs early in childhood[55]. Mutations in ATR are rare and they are associated with a rare disease called Seckel syndrome, characterized by growth retardation and microcephaly[56]. The DNA PKcs mutations are associated with autoimmune diseases and patients with DNA PKcs presented classical SCID (severe immune deficiency) phenotype[57].

ATM is the master regulator of DSB repair signalling and stress responses[58]. Upon damage, ATM can be activated through different pathways. In the canonical form, activation of ATM is dependent of both DSBs and the MRN complex, which is considered the primary sensor of DSBs. MRN recruits the ATM homodimer, induces its monomerization and promotes the interaction of ATM monomers with DNA ends and its DDR substrates[59,60]. ATM can also be activated by autophosphorylation at Ser1981, promoted by acetylation of Lys3016 by the acetyltransferase TIP60[61]. Indeed, Ser1981 phosphorylation has been widely considered a marker of ATM activation. But not only by DSBs, recent studies have demonstrated that other DNA structures such as SSBs, topoisomerase cleavage complexes, splicing intermediates, and R-loops or oxidative stress could also induce ATM activation[62–65].

ATM is the apical kinase responsible for global orchestration of cellular responses to DSBs, which include DNA repair, checkpoint activation, apoptosis, and alterations in chromatin structure and transcription[66]. To achieve this, ATM phosphorylates hundreds of substrates in response to DNA damage. ATM activation promotes DNA repair via both NHEJ and HR. On one hand, ATM-dependent activation and recruitment of 53BP1 to damaged sites prevents end resection and promotes NHEJ[67,68]. However, ATM implication on NHEJ could be extended by direct phosphorylation of DNA PKcs and other NHEJ factors (such as Artemis), promoting efficient DNA repair[69]. On the other hand, several factors involved in HR pathway such as BRCA1, BRCA2, BLM and EXO1 are also targets of ATM and it also supports efficient recruitment of CtIP (CtBP-interacting protein) necessary for DSBs

end resection and HR initiation[70,71]. The complex mechanisms whereby ATM-regulated 53BP1 and BRCA1 assemblies counteract each other are still emerging.

Another important step in the repair of DSBs is the phosphorylation of the histone variant H2A.X on Ser139 that occurs in a megabasepair chromatin region surrounding DNA breaks[72,73]. The phosphorylation of H2A.X, also known as **γH2A.X**, is primarily catalysed by ATM[74], but also by DNA PKcs[75] and ATR[76]. This phosphorylation generates a binding site for MDC1 (mediator of DNA damage checkpoint 1), which acts as a molecular scaffold recruiting chromatin modifiers to relax heterochromatin around DSBs [77,78]. Thereby γH2A.X is considered central for the efficient accumulation of DNA repair factors at break site, and for that reason, it has been widely used as marker of DNA damage.

By contrast, ATR is activated in response to many different types of DNA damage, including DSBs, base adducts, crosslinks, and particularly by replication stress[79]. When replication is blocked, DNA polymerases are unable to continue coupled to replicative helicase, generating ssDNA tracts that rapidly become coated with RPA (Replication protein A). ATR is recruited to ssDNA in association with its partner ATRIP (ATR-interacting protein). Then, ATR activator TOPBP1 (topoisomerase-binding protein-1) binds and activates ATR in ATRIP-dependent manner, leading to phosphorylation of the downstream effectors involved in DNA repair and stabilization of replication forks[80,81]. ATR has common substrates with ATM[82], but it also has unique targets particularly involved in the Fanconi Anemia (FA) pathway, which promotes the repair of DNA interstrand crosslinks. Furthermore, ATR has been reported to phosphorylate ATM in response to UV exposure[83].

Regarding DNA PKcs, it is activated when it is recruited to DBSs by Ku proteins and its major role is to promote NHEJ[84]. Mechanistically, NHEJ is started by the binding of Ku70/80 and DNA PKcs binding to DSBs, resulting in DNA PKcs holoenzyme which allows DNA-end tethering. Subsequently, additional NHEJ core factors are recruited for the ends to be closely aligned and ligated[85,86]. Activation of DNA PKcs dependent of ATM and ATR phosphorylation may be also important for DNA repair[87]. However, recent evidence suggests that DNA PKcs also phosphorylates ATM to restrain its activity[88]. Indeed, the common target sharing and the interdependent activation of PIKKs members highlight the functional importance of their crosstalk for an effective DNA repair.

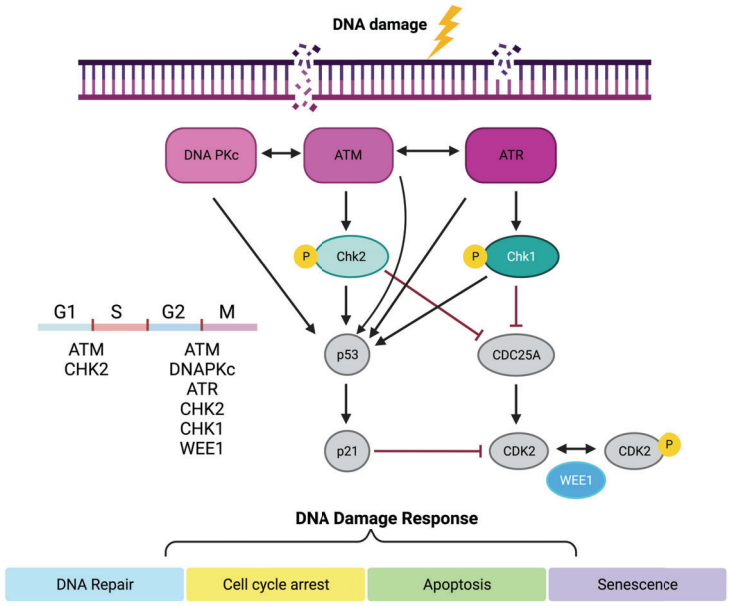

Figure I3. PIKK-dependent DNA damage induced cell cycle checkpoint signalling. Once activated, these kinases can phosphorylate several downstream effectors to execute cellular responses that lead either to cell cycle arrest or to apoptosis. While ATM and ATR have prominent roles in mediating cell cycle checkpoints through the activation of Chk1/2 and p53, DNA PKc usually activates the p53- mediated apoptosis pathway. Created with BioRender.com.

Apart from their role in DNA repair signalling, ATM, ATR and DNA PKcs also operate as cell cycle checkpoints[89] (**Figure I3**). The two most studied targets of ATM and ATR are the protein kinases Chk2 and Chk1, respectively[90]. Together with ATM and ATR, these kinases act to reduce CDK (cyclin-dependent kinase) activity by several mechanisms, some of which involve activation of the p53 transcription factor or phosphorylation and subsequent degradation of Cdc25 phosphatase. Inhibition of CDKs slows down or arrests cell cycle progression at G1-S, intra S and G2-M cell cycle checkpoints, to increase the time available for DNA damage repair before replication or mitosis occurs[91,92]. Both ATM and ATR contribute to control the intra-S and G2/M checkpoints, whereas it is believed that G1/S checkpoint is controlled primarily by ATM rather than ATR[93]. DNA PKcs mostly controls G2/M checkpoint in ATM-deficient cells[94]. After DNA reparation is completed efficiently, DDR is inactivated and the normal cell cycle is restored. Alternatively, if the damage is severe and cannot be repaired, DDR signalling triggers programmed cell death by apoptosis or cellular senescence[95].

The PARP family

One of the earliest events in DDR is the recruitment of PARP family member PARP1 (poly(ADP-ribose) polymerase 1) to diverse types of DNA lesions. PARP1 catalyses the polymerization of ADP-ribose (PAR) units, resulting in the attachment of either linear or branched PAR polymers to itself or to multiple target proteins. This poly(ADP)ribosylation, also known as PARylation, contributes to DNA repair, stabilization of DNA replication forks, and modification of the chromatin structure[96]. For that reason, the roles of PARP1 in DDR have been widely studied in the last years.

PARP1 structure is highly conserved among eukaryotes and compromises three main domains: an amino-terminal DNA-binding domain (DBD) containing three zinc finger motifs and nuclear localization signal; a BRCT (BRCA1 C terminus) domain, containing automodification domain; and a highly conserved carboxy-terminal domain that contains active site and NAD+ binding site. Together these domains mediate the response of PARP1 to different kinds of activators, including DNA damage[97,98].

Induced by DNA damage, PARP1 is rapidly recruited to damage sites through its DNA-binding ability and catalyses the synthesis of PAR chains on itself, histones and other proteins[99]. This enzymatic reaction results in the attachment of ADP-ribose units to Glu, Asp or Lys residues of acceptor proteins by transesterification reaction[100]. DDR proteins can bind to PAR chains both covalently and non-covalently resulting in their recruitment to sites of DNA damage[101]. Target proteins that interact with PAR chains non-covalently usually contain PAR-binding modules (PBM), which frequently overlap with important functional domains that can be activated through PAR binding[102].

PARP1 is implicated in different DDR pathways for the reparation of DNA damage (**Figure I2**). SSBs are very rapidly detected and bound by PARP1, followed by PARylation and activation of PARP1 and its target proteins involved in NER or BER pathway (such as XRCC1, LIG3, POLβ), stimulating the repair process[103,104]. Regarding DSBs repair, PARP1 is required for the robust detection of this type of break and for the initial response through its interaction with MRE11 and ATM[97,105]. Indeed, both MRE11 and ATM contain PAR-binding motifs and their interaction with PAR stimulates their recruitment and activity[106]. Thereby PARP1 deficiency or inhibition results in delayed activation of ATM downstream targets such as γH2A.X, p53 or SMC1 among others[107]. Moreover, it has been described that PARP1 has a role in both HR pathway, regulating DNA end resection and recruiting

indirectly BRCA1 to DSBs[108] and in NHEJ pathway, through direct interaction and activation of DNA PKcs and mediating alternative NHEJ together with MRE11[109,110].

Apart from its role in DNA repair, several studies have shown that PARP1 regulates a broad range of biological processes in the nucleus including chromatin regulation (interacting with histones and chromatin remodelers)[111], replication fork stabilization[112], gene expression (controlling component of the transcription machinery)[113], ribosome biogenesis[114] and RNA processing [115].

I2.3 DNA damage response and cancer therapy

Defects in the DDR pathway cause genomic instability in normal cells, aiding in cancer initiation and progression via accumulation of driver genomic aberrations. In contrast, active DDR is considered also one of the main contributors of the appearance of resistance to current antitumoral therapies in cancer cells, which are based on the genotoxic agents (such as radiotherapy or chemotherapy) that directly or indirectly induce DNA damage and activate specific DNA repair pathways. Thus, a deeper understanding of DDR mechanisms provides new targetable vulnerabilities in cancer cells that can be exploited for clinical benefit with specific use of DDR inhibitors[116]. Not only to enhance the effectiveness of standard genotoxic treatments against resistant cancer cells, but also to exploit synthetic lethality in cancers with specific DDR alterations. The synthetic lethality concept was proposed a long time ago to describe the condition whereby a defect of either one of two genes has no/little effect, but the combination of both genes leads to cell death[117].

PARP inhibitors (PARPi) were the first clinically approved drugs designed to exploit synthetic lethality[118]. They trap PARP1 at the site of DNA damage, binding to its catalytic site and blocking auto-PARylation, thus preventing its release and removing PARP1 from its normal catalytic cycle and affecting DNA repair[119]. PARPi compounds can be classified into three allosteric types with different potency to retain PARP1 on DNA break[120,121]. HR-deficient tumor cells, particularly cells carrying mutations in BRCA1 and BRCA2, were found to be highly sensitive to PARPi, because they only rely on NHEJ to repair DSBs. Therefore, blockage of PARP1 function leads to accumulation of genome instability and increases cell death in HR-deficient cancer cells.

Despite the remarkable success of PARPi therapy in improving both progression-free and overall survival, most cancers eventually develop resistance. Several genetic and epigenetic mechanisms involved in PARPi resistance have been identified, including BRCA reversion mutations, formation of RAD51-ssDNA filaments, loss of expression of 53BP1-Rif1-SHIELDIN antiresection pathway and

fork protection[122]. In order to overcome this resistance, several promising targets have been identified as alternative objectives to lead to PARPi hypersensitivity[123].

However, the use of other antitumor agents targeting key components of the DDR is currently limited to early-phase clinical trials [124]. ATM and ATR inhibitors are prime targets of DDR inhibitors, given their central role in activating DDR for both SSBs and DSBs. Inhibitors of these kinases have been tested in monotherapy or in combination with chemotherapy, radiotherapy, and PARP inhibitors in clinical trials of different solid tumours[125]. DNA PKcs inhibitors that block NHEJ have been tested in combination with radiotherapy, as NHEJ is the predominant pathway to repair the damage generated by radiotherapy[126]. Inhibitors of Chk1 and WEE1 that prevent checkpoint regulation are also emerging and being tested because of their capacity in potentiating the effect of DNA damaging agents and overcoming PARPi resistance[127].

All in all, the complex nature of DDR emphasizes the need for further investigation to uncover the intricate and dynamic DDR protein network to maximize the benefit of the implementation of DDR inhibitors in cancer treatment strategies.

I3. NF-κB SIGNALLING PATHWAY

Nuclear factor-κB (NF-κB) pathway is considered a central coordinator of immune system and inflammation. It was found more than 30 years ago as a DNA-binding factor in the nucleus of activated B cells that specially recognizes an enhancer element found in the gene encoding the immunoglobulin-κ light chain[128]. Further investigation demonstrated the impact of NF-κB pathway in different biological processes and its contribution to tumorigenesis by direct modulation of cellular functions such as proliferation, apoptosis inhibition or cellular migration[129,130].

I3.1 NF-κB family, structure and classification

NF-κB transcription factors

The mammalian NF-κB family is composed of five transcription factors (TF): RelA (p65), RelB, c-Rel, p105/p50 (NF-κB1) and p100/p52 (NF-κB2). All the members can form homodimers and heterodimers and shuttle from the cytoplasm to the nucleus in response to cell stimulation. NF-κB dimers can bind to specific DNA sequences (consensus κB sites) and both induce and repress expression of target genes through the recruitment of coactivators and corepressors[131,132]. The genes regulated by NF-κB include those controlling apoptosis, cell adhesion, proliferation, the innate- and adaptative-immune responses, inflammation, the cellular-stress response, and tissue remodelling[133,134].

All NF-κB members share a highly conserved N-terminal Rel homology domain (RHD) that includes the nuclear localization signal (NLS) responsible for DNA binding, dimerization, and interaction with the inhibitor proteins[135]. RelA, RelB and c-Rel are synthetized in their mature form and contain a transcription activation domain (TAD) necessary for the positive regulation of gene expression. p50 and p52 subunits are synthesized as large precursors p105 and p100, respectively, and require proteolysis of the C-terminus (which contains multiple ankyrin repeats) to mature[136]. They lack TAD, thus p50 and p52 may repress transcription unless associated with TAD-containing NF-κB members[137]. Despite structural similarities and their ability to bind DNA, different studies have demonstrated that all NF-κB subunits have distinct and non-overlapping functions.

Inhibitor of NF-κB (IκB)

In unstimulated cells, NF-κB proteins are predominantly localized in the cytoplasm bound to a family of NF-κB inhibitor proteins (IκB), which include IκBα, IκBβ, IκBε, IκBγ, IκBζ and Bcl-3 (B-cell lymphoma 3-encoding protein). The proteins of this family are characterized by C-terminal ankyrin repeats that are essential for their interaction with NF-κB factors. Through these motifs they bind to NF-κB dimers masking their NLS, thereby retaining them in the cytoplasm and preventing their nuclear translocation and subsequent DNA binding[138]. Moreover, IκB proteins also present a nuclear export sequence (NES) in the N-terminal, reflecting their involvement in maintaining the equilibrium of NF-κB dimers shuttling process[135,139]. Degradation of IκB is a rapidly induced signalling event that is initiated upon specific phosphorylation by Inhibitor of KappaB kinase (IKK) complex that marks the inhibitor protein for ubiquitination and subsequent proteasomal degradation[140]. Degradation of IκB drastically alters the dynamic balance between cytoplasmatic and nuclear localization signals to encourage nuclear translocation of NF-κB factors and promote gene transcription.

Apart from NF-κB pathway regulation, alternative nuclear functions for various IκB have been identify[141]. It has been described a physical association of IκBα to histone deacetylases (HDACs) that increases NF-κB-independent transcription by cytoplasmatic retention of HDACs. In addition, previous studies from our group demonstrated that IκBα can also interact with the chromatin at specific genomic regions to regulate gene transcription through modulation of the chromatin editing polycomb repression complex 2 (PRC2). Indeed, phosphorylated and SUMOylated IκBα can bind directly to the acetylated N-terminal tail of histones, specially H4, and this association facilitates the recruitment of PRC2 to specific genes related with development, stemness and tissue homeostasis[142–145].

IκB kinase complex (IKK complex)

The IKK kinase complex is the master coordinator of the NF-κB signalling pathway. It is composed by two catalytic subunits IKKα and IKKβ and the regulatory subunit IKKγ/NEMO[146]. Biochemical purification of this complex showed a molecular size from 700 to 900 kDa[147], revealing the presence of other components such as Hsp90, Cdc37 and ELKS, although their attachment to core IKK complex is transient and stimulus-dependent[148–150]. This core complex catalyses the phosphorylation of IκB at serine residues (Ser32/36 IκBα, Ser19/23 IκBβ, Ser18/22 IκBε) leading to its degradation and inducing NF-κB pathway activation[151].

The kinases IKKα and IKKβ show a similar structure (50% sequence identity), which includes a N-terminal kinase domain (KD), a scaffold/dimerization domain (SDD) with a helix-loop-helix motif (HLH), that modulates kinase activity, and leucine zipper (LZ), which allows homo- or heterodimerization of the kinases, and a C-terminal NEMO-binding domain (NBD) that permits recognition and binding to NEMO[152]. Moreover, IKKβ contains a ubiquitin-like domain (ULD), that is not found in IKKα, which is critical for its catalytic activation and seems to be involved in the positioning of IKK complex with IκBα[153]. Both proteins exhibit kinase activity towards IκBα, although it is reported that IKKβ has higher efficiency than IKKα. In contrast, IKKα presents a predicted nuclear localization signal[154], that is related with NF-κB-independent nuclear activities.

One of the most important IKKα nuclear function is the regulation of gene expression through phosphorylation of Histone 3 (H3) at Ser10. This phosphorylation induced by TNFα stimulation triggers subsequent CBP-mediated acetylation on Lys14 of H3, modulating chromatin accessibility and promoting NF-κB gene expression (for instance IκBα, IL-6 and IL-8)[155,156].

The activation of these subunits is induced by the phosphorylation of two serine residues in the kinase domain: Ser176/180 for IKKα and Ser177/181 for IKKβ. This event leads to a conformational change in the activation loop, which activates their catalytic function[157,158]. Even though it has been intensively studied, the molecular mechanisms of IKK activation are still not fully understood. Consensually, TGFβ-activated kinase 1 (TAK1) has been identified as one IKK kinase (IKKK). TAK1 is activated and recruited into the proximity of IKK complex by a wide variety of proinflammatory mediators, phosphorylating and activating the kinases in the cytoplasm, and resulting in the initiation of NF-κB pathway[159,160]. RIP1 (Receptor interacting protein 1) and MEKK3 (MAPK/ERK kinase kinase 3) kinases have also been postulated to play a role in IKK phosphorylation and TNFα-mediated NF-κB activation[161–163]. Even though IKKα and IKKβ kinases are very similar and are present in the same complex, several biochemical and genetic approaches have indicated that they have different substrates and non-overlapping functions.

NF-κB essential modulator (IKKγ/NEMO) is the non-catalytic regulatory subunit of the IKK complex and is required for the activation of IKK and NF-κB pathway. NEMO is a 48 kDa polypeptide containing several domains that are crucial for its regulatory function including a N-terminal α-helical region followed by two coiled-coil domains (CC), that function as the interaction interface with IKKα and IKKβ; a ubiquitin-binding domain (UBAN), that allow NEMO to recognise and bind K63-polyubiquitination chains; and C-terminal zinc-finger region (ZNF), involved in the interaction

with substrates[164,165]. Indeed, NEMO has been shown to interact with many proteins that participate in NF-κB activation. Recently, a series of studies have revealed the existence of stimuli-induced posttranslational modifications of NEMO that are involved in NF-κB pathway regulation, including polyubiquitination, SUMOylation and phosphorylation [166]. Additionally, NEMO has also been shown to interact with several negative regulatory proteins including deubiquitinases (A20 and CYLD) and phosphatases (PP2A)[167,168].

The gene encoding NEMO (*IKBKG* gene) is located on X chromosome thereby mutations in this gene are associated with inherited diseases, such as Incontinentia pigmenti, characterized by severe skin disorder and neurological disorders that are lethal in males[169], and X-linked recessive anhidrotic ectodermal dysplasia associated with immunodeficiency (EDA-ID) associated with perturbed immune response and recurrent infections[170].

I3.2 Activation of NF-κB signalling pathway

The NF-κB signalling pathway can be activated by a variety of factors eliciting different responses.

Classical NF-κB pathway (canonical)

The canonical NF-κB pathway is mainly induced by PAMP (Pathogen-associated molecular patterns) and pro-inflamatory cytokines, such as Interleukin-1 (IL-1), Tumor necropsis factor (TNFα) or Toll-like receptor (TRL) ligands like lipopolysaccharides (LPS). The stimulation of receptors initiates the signalling cascade and the recruitment of several proteins (TRADDs, FADDs, cIAPs, LUBAC, TRAFs, RIP1, among others) that result in the activation of TAK1[171,172], which catalyses the phosphorylation of IKK complex. Subsequently, active IKK complex phosphorylates IκBs in the N-teminal serine residues[140]. Then, the ubiquitin-ligase machinery SCF (Skp-1/Cullin/F-box) will recognise the phosphorylated IκB, inducing its polyubiquitination and proteasomal degradation[173]. The degradation of IκBs liberates NF-κB dimers (except for p52/RelB dimer), thereby they translocate to the nucleus to activate specific gene transcription[174] (**Figure I4**).

Alternative NF-κB pathway (non-canonical)

Activation of non-canonical NF-κB signalling is induced by specific members of TNF cytokine family, including CD40 ligand, B-cell-activating factor (BAFF), lymphotoxin-β (LTβ) and Receptor activator for NF-κB ligand (RANKL)[175–177]. Contrary to canonical NF-κB pathway, non-canonical NF-κB pathway totally depends on IKKα activity (is IKKβ and NEMO independent) and specifically mediates the

activation of p52/RelB NF-κB dimer. Upon ligand induction, NF-κB inducing kinase (NIK) is stabilized which phosphorylates and activates IKKα[178]. Under normal conditions NIK is targeted for continuous degradation by TRAF3, which is degraded upon TNF receptor activation[179]. Then, IKKα phosphorylates NF-κB precursor p100, causing its proteolysis processing into the active form p52. After this processing, p52/RelB heterodimer translocate to the nucleus and promote the regulation of genes related with specific immunological processes such as lymphoid organogenesis and lymphocyte function[180,181] (**Figure I4**).

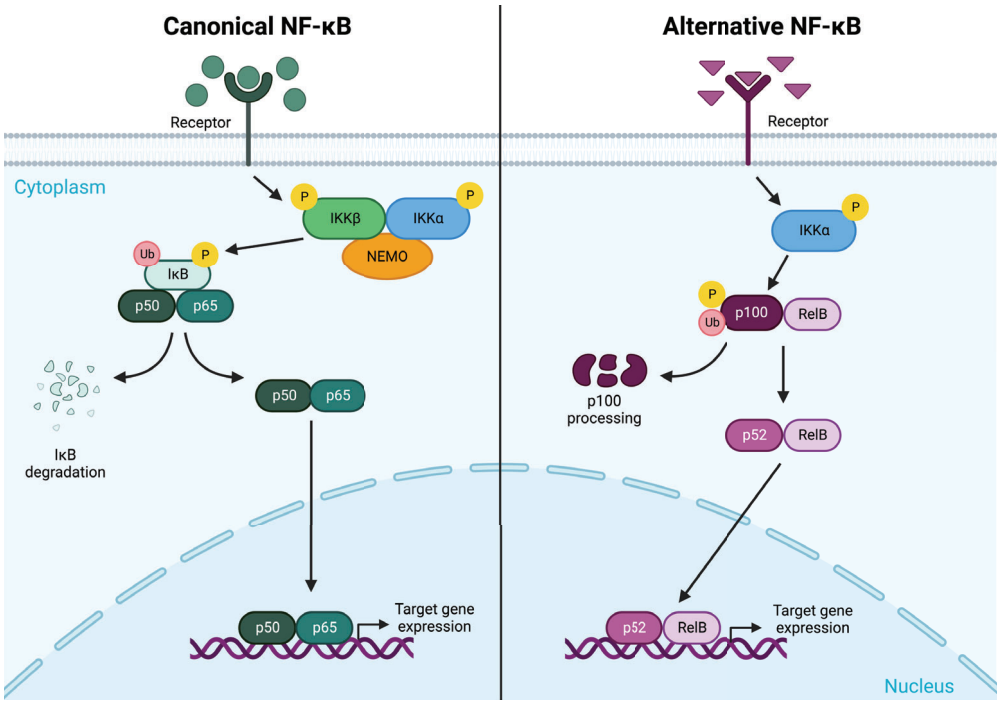

Figure I4. NF-KB pathway. In the canonical NF-κB pathway (left) the stimulation of multiple receptors leads to the activation of the IKK complex (IKKα, IKKβ and NEMO) which catalyses the phosphorylation of the inhibitor IκB. This phosphorylation is essential for signalling the ubiquitination and protein degradation of IκB, leading NF-κB members free to translocate to the nucleus an promote gene transcription. In the alternative NF-κB pathway (right), upon ligand induction, active IKKα phosphorylates p100, and as a result, it is processed into the active form p52 and together with RelB, translocates to the nucleus an active gene transcription. Created with BioRender.com.

Activation of NF-κB pathway through DNA damage

Apart from extracellular signals, NF-κB pathway can also be activated by double-strand breaks (DBS) produced by genotoxic agents. In this DNA damage-dependent NF-κB activation the regulatory subunit NEMO has found to be required with an IKK-independent function[182,183] (**Figure I5**).

Upon genotoxic stress, NEMO is SUMOylated in its ZF domain at lysine residues 277 and 309 by protein inhibitor of activated STATγ (PIASγ). Mutations in this SUMO acceptor lysines have minimal impact in the canonical NF-κB activation but totally abrogate DNA damage-dependent NF-κB activation. Moreover, even though the ZF domain is crucial for NEMO SUMOylation, the interaction between NEMO and PIASγ is controlled by the CC region located in N-terminal. The SUMOylation of NEMO alters its intracellular distribution promoting its nuclear localization[184–186].

Another crucial element in DNA damage-dependent NF-κB signalling activation is PARP1. PARP1 is capable of directly sensing DNA damage and its PARylation activity serves as a scaffold for the recruitment of elements, a step that might be critical for NF-κB activation. Indeed, automodified PARP1 has been shown to rapidly assemble a signalling complex containing PARP1, NEMO, ATM and PIASγ. It is described that PIASγ directly binds to PAR chains by a PAR binding motif in its C-teminal. This interaction between PIASγ and PARP1 is required for NEMO SUMOylation and nuclear accumulation[187,188]. Additionally, also other elements have been found to promote NEMO SUMOylation, such as the nuclear complex formed by p53 inducible death domain-containing protein (PIDD) and RIP1, which resulted SUMOylated itself[189,190].

Following DNA damage, nuclear events trigger the activation of the kinase ATM that will associate with NEMO and phosphorylate it on Ser85[191]. This phosphorylation is a prerequisite for subsequent NEMO monoubiquitination but not for SUMOylation[192]. However, SUMOylation and phosphorylation are both required for DNA damage-dependent NF-κB activation. The monoubiquitination of NEMO is catalysed by cellular inhibitor of apoptosis-1 (cIAP1) and occurs in the same lysine residues that are SUMOylated[191,193]. It is still unclear if NEMO has to be deSUMOylated prior to ubiquitination or if both posttranslational modifications can coexist. However, kinetic analysis of these modifications indicates that NEMO proceeds through transient SUMOylation before phosphorylation and subsequent monoubiquitination. The monoubiquitination of NEMO is also associated with its cellular distribution, appearing to promote its nuclear export for cytoplasmic signal transduction and NF-κB activation[194].

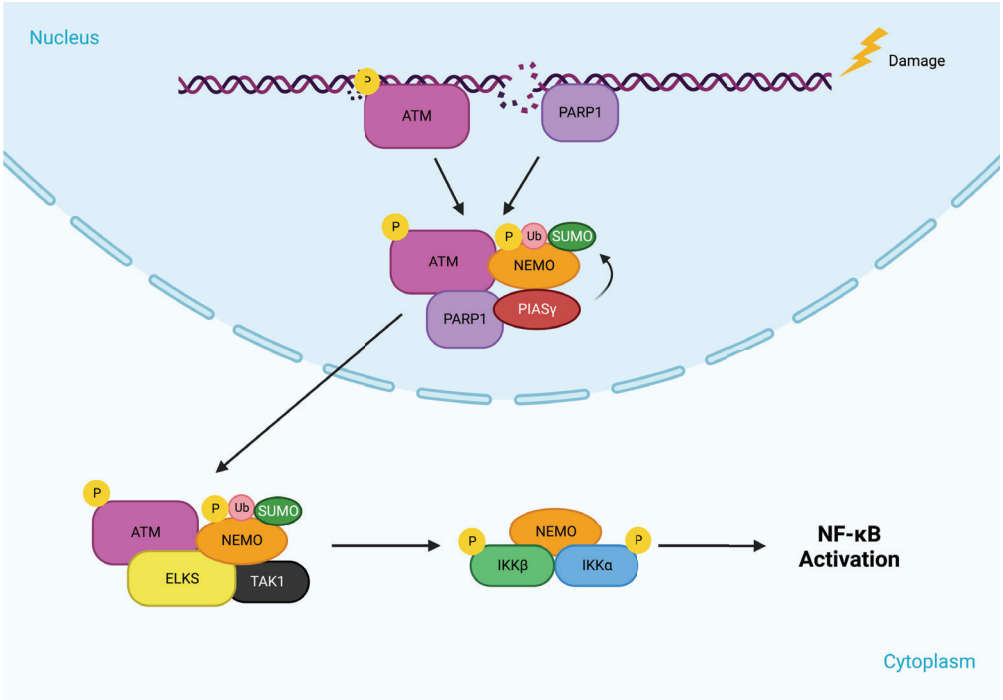

Figure I5. DNA damage dependent NF-κB activation. In response to genotoxic treatments, NEMO translocates to the nucleus, forms a complex with ATM, PARP1 and PIASy and suffers several posttralational modifications, including SUMOylation, phosphorylation and ubiquitination. Then, this activated NEMO, together with ATM, is exported to cytoplasm and forms a complex with ELKS and TAK1, which results in the activation of IKK complex and subsequent NF-κB activation. Created with BioRender.com.

ATM has also been reported to have a putative cytoplasmic role mediating NF-κB activation. It is described that NEMO and ATM form a cytoplasmatic complex with ELKS (protein rich in glutamic acid, leucine, lysine, serine), that recruits TAK1 and regulates its activation upon damage[195,196]. Moreover, ATM activates TRAF6, resulting in Ubc13-mediated K63-polyubiquitination and cIAP1 recruitment that will stimulate TAK1 phosphorylation[197]. Then, this NEMO/ATM/ELKS/TAK1 complex activates IKK complex by mechanisms that still remain to be elucidated, thus resulting in the activation of NF-κB pathway.

I3.3 NF-κB independent IKK functions and cancer association

The substrate spectrum of IKK complex is not only restricted to IκBs and precursors, but it also includes a wide range of NF-κB pathway intrinsic (such as RelA) and external substrates (such as

p53), remarking the implication of its members in other physiological processes independently from NF-κB pathway [198]. Particularly, these unconventional and NF-κB independent functions of IKK members (especially nuclear IKKα) have been shown to be related with multiple protumoral mechanisms in several cancer types.

In breast cancer, the nuclear activity of IKKα increases phosphorylation and recruitment of estrogen-induced transcription factors, such as estrogen receptor alpha (ERα), steroid receptor coactivator 3 (SCR-3), E2F transcription factor 1 (E2F1), to promoters of genes required for cell cycle progression (*CYCLIN D1* and *C-MYC*, for example), enhancing transcription and inducing proliferation of cancer cells[199,200]. Additionally, upon activation, IKKα enters into the nucleus of cancer cells and phosphorylates p27/Kip1 inducing its nuclear export and resulting in enhanced cell proliferation[201].

In prostate cancer, IKKα negatively regulates in the nucleus the expression of the metastasis suppressor Maspin, facilitating the recruitment of DNA methyltransferase activity to its promoter[202]. In lung cancer, nuclear IKKα phosphorylates CREB-binding protein (CBP) to increase its affinity for p65 and NF-κB pathway, but as a result its association with p53 is reduced, decreasing p53-dependent gene expression[203]. In skin cancer, nuclear IKKα promotes G2/M phase progression by binding to H3 in 14-3-3σ locus and preventing its hypermethylation by SUV39h1, which results in de-repression of 14-3-3σ that controls the cytoplasmatic export of cell cycle-regulatory phosphatase CDC25[204]. Indeed, high levels of nuclear active IKKα are predictive of higher metastatic capacity in squamous cell carcinoma (SCC)[205].

Regarding CRC cancer, nuclear IKKα phosphorylates the nuclear co-repressors silencing mediator for retinoid and thyroid receptors (SMRT) and nuclear receptor co-repressor (NCoR), leading to their cytoplasmic export by 14-3-3σ and the transcriptional activation of genes, including Notch target genes such as *HES1, HES5* and *HERP2*[206,207]*.* Moreover, IKKα contributes to oncogenic transformation of the intestine through the regulation of stemness-related genes[208].

A few years ago, our group identified a truncated form of IKKα with a predicted weight of 45 kDa, called IKKα(p45). It is generated by the proteolytic cleavage of full length IKKα in the endosomal compartment and is present in different cell types, but specially in the nucleus of cancer cells. Activated IKKα(p45) has been shown to prevent apoptosis of CRC cells *in vitro* and is required for tumor growth *in vivo.* IKKα(p45) presents the KD but lacks some regulatory domains at the C-terminal region. For that reason, many of the described nuclear functions of IKKα are associated

with this truncated form including H3 phosphorylation, regulation of specific gene transcription and cancer progression. In fact, nuclear active IKKα(p45) together with full length IKKα and NEMO forms a complex that regulates the phosphorylation of SMRT and H3[209,210].

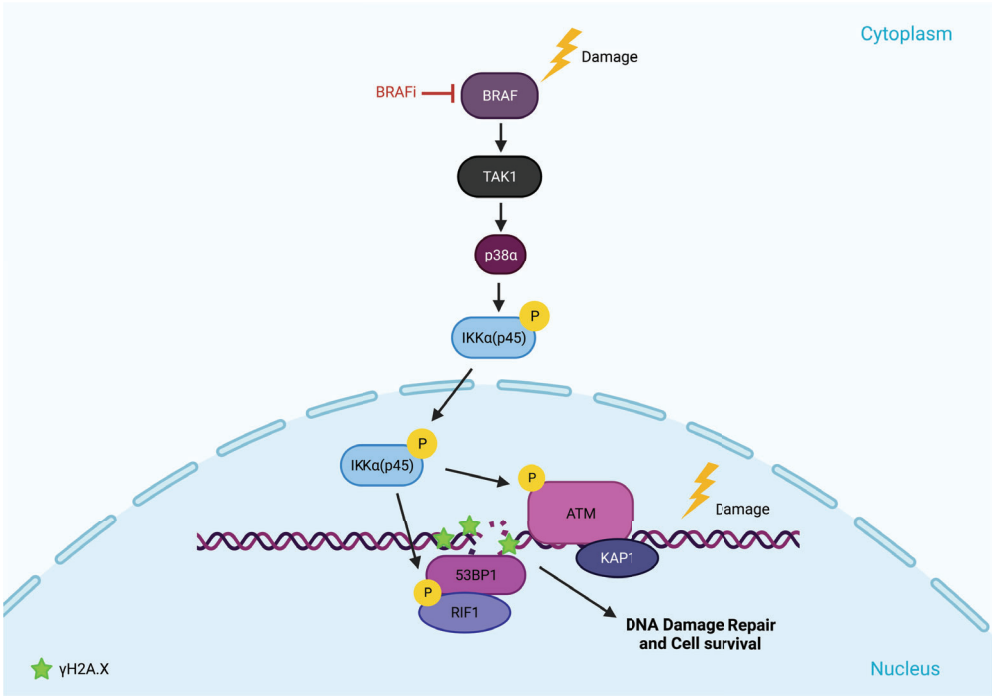

Figure I6. NF-κB independent IKKα function in DDR. The truncated form of IKKα, p45-IKKα, is rapidly activated in response to DNA damage downstream BRAF, TAK1 and p38α and regulates different elements of DNA repair machinery through direct ATM and 53BP1 phosphorylation, leading to efficient DNA repair and cell survival. Created with BioRender.com.

Additionally, in response to damage, this truncated form is phosphorylated and activated downstream BRAF/TAK1/p38 MAPK, inducing its nuclear translocation. Importantly, it regulates DNA damage response (DDR) activation through direct phosphorylation of ATM (**Figure I6**). Active p45-IKKα is essential for an efficient DNA repair, therefore inhibition of IKKα or BRAF abrogates the activation of key DDR elements, compromising DNA repair and synergistically potentiating the antitumoral effect of chemotherapy/radiotherapy in CRC, leading to the eradication of resistant cells[211].

Due to their association with tumorigenesis[212], inside and outside NF-κB pathway, chemical inhibition of IKK members has become an attractive approach for cancer therapy. There is a variety of inhibitors including natural products, biomolecular and peptide inhibitors and synthetic small-molecule inhibitors with different inhibitory strategies[213]. Some of them have been shown enhance the sensitivity of cancer cells to standard chemotherapy-induced death, through suppression of genes encoding antiapoptotic and antioxidant molecules[214]. However, the inhibitors developed to date have showed severe toxic effects, as they are not specific enough and affect intensely cellular homeostasis[215]. Therefore, further investigation for identifying specific mechanisms involved in IKK activation and regulation of their protumoral functions will open new doors for the development of new therapeutic strategies.

I4. MALIGNANT MELANOMA

Malignant melanoma (MM) is the most serious type of skin cancer. It arises from the malignant transformation of melanocytes, the pigment-producing cells in the basal layer of the epidermis and hair follicles, predominantly found in the skin and eyes. Melanocytic neoplasms range from benign lesions, termed naevi, to malignant ones like melanoma[216].

I4.1 Malignant melanoma epidemiology

Skin cancer is a common cancer (fifth in both men and women) in the Western world with an increasing incidence. Malignant melanoma is the least common (1% of all skin cancer cases) but the deathliest skin cancer, with about 48,000 melanoma-related deaths every year[1]. It is highly aggressive and metastatic with a 5-year survival rate of less than 15%. The major risk factor of MM development is ultraviolet radiation by sun exposure (and subsequent sunburns)[217,218]. As well as sun exposure, distinct inherited genetic alterations have been associated with melanoma, even though they account for a small proportion of melanoma cases (around 8-12% of cases)[219]. Furthermore, the presence of atypical melanocytic naevi, which have larger and more asymmetric and irregular forms, is also an additional risk factor[220].

I4.2 Molecular biology of Malignant Melanoma

The malignant transformation of melanocytes is a result of a process that requires a complex interaction between exogenous and endogenous events. Mutations in critical growth regulatory genes, production of autocrine growth factors, and loss of adhesion receptors contribute to disrupter intracellular signalling in melanocytes, allowing them to escape from their tight regulation by keratinocytes and resulting in an uncontrollable proliferation[221,222].

Initially, a normal melanocyte acquires an initiating drive mutation that leads to melanocyte hyperplasia and naevi development. Further accumulation of molecular alterations will give these melanocytic neoplasms malignant potential becoming them dysplastic naevi[223]. Then, these dysplastic naevi can progress into radial-growth-phase (RGP) and vertical-growth phase (VGP) and develop melanoma, that depending on its invasive capacity can be considered *in situ* melanoma (cancer cells are mainly restricted to the epidermis), invasive melanoma (cancer cells can enter the subjacent mesenchymal tissue) and metastatic melanoma (melanoma cells colonized other

tissues)[224]. However, not all melanomas pass through each phase and can progress directly to metastatic malignant melanoma[225].

Multiple driver mutations and alterations in several signalling pathways have been identified to impulse MM progression[226]:

MAPK Signalling pathway

The principal molecular pathway activated in melanocytic tumors is the Mitogen-activated protein kinase (MAPK) signalling pathway. This pathway regulates cell fate decisions, such as proliferation, differentiation, apoptosis, and stress responses, downstream of receptor tyrosine kinases (RKT), cytokines, and heterotrimeric G-protein-coupled receptors[227,228].

MAPK family is highly conserved in eukaryotes[229] and is formed by kinases that phosphorylate their own (autophosphorylation) and substrates dual serine and threonine residues to activate or deactivate their target[230]. In mammals, the MAP kinases can be grouped into three main families[231]: extracellular-signal-regulated kinases (ERKs), which respond primarily to growth factors and mitogens to induce cell growth and differentiation[232]; Jun amino-terminal kinases (JNKs), that are activated by environmental stress and inflammatory cytokines and play an important role in apoptosis, inflammation, cytokine production, and metabolism[233]; and stress-activated proteins kinases (p38MAPK), which are also activated upon environmental stresses and inflammatory cytokines and contribute to inflammation, apoptosis, cell differentiation, and cell cycle regulation[234]. In the majority of solid tumors, including melanoma, the canonical MAPK signalling pathway formed by RAS/RAF/MEK/ERK is commonly affected and hyperactivated[235,236].

In MM, the most commonly mutated component of MAPK pathway is BRAF. Indeed, BRAF is mutated in 50-70% of melanomas, being the substitution of a glutamic acid for valine at position 600 (V600E) the most common mutation. Also, the upstream activator of BRAF, NRAS is mutated in between 15-30% of melanomas, and in this gene, the most common substitution is leucine for a glutamine at position 61 (Q61L). Mutations in NRAS and BRAF, stimulate constitutive activation of ERK signalling, promoting proliferation and survival in tumor cells[237–239] (**Figure I7**).

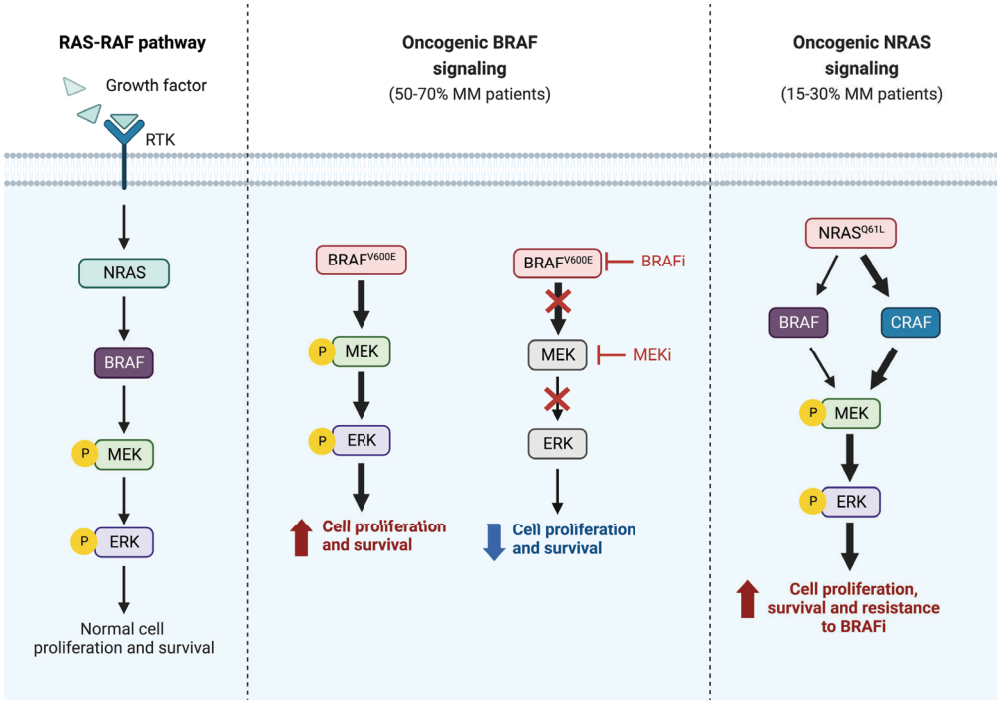

Figure I7. Schematic representation of MAPK oncogenic signalling in MM. In normal situation, upon ligand binding, receptor tyrosine kinase (RTK) homodimerize leading to activation of NRAS signalling cascade. One of NRAS downstream targets in BRAF, that will subsequently activate MEK and ERK to activate several transcription factors responsible of cell growth and survival. MM patients are characterized by mutations in BRAF or NRAS, which result in constitutive activation of this pathway, resulting in anormal cell proliferation, and in the case of NRAS mutations, resistance to BRAF inhibitor treatments. Created with BioRender.com.

Cell cycle regulation pathway

Uncontrolled cell cycle progression is another hallmark characteristic of melanoma development. Multiple components involved in this process have been found to be mutated in MM including cyclin-dependent kinase inhibitor 2A (CDKN2A), retinoblastoma-associated protein (RB), cyclin D1, and cyclin-dependent kinase 4/6 (CDK4/6). Particularly, mutations in CDKN2A are associated with familial melanomas. Indeed, as CDKN2A encodes the two proteins $p16^{INK4A}$ and $p14^{ARF}$, which regulate cell cycle by inactivating CDK4/6 or RB, germline mutation in this gene leads to uncontrolled cell cycle progression[240–242]. In addition, mutations in TP53 have also been identified in melanoma, especially in metastatic melanoma[243].

AKT signalling pathway

Dysregulation in the protein kinase B (AKT) pathway occurs in 70% of melanomas, which results in AKT amplification and PTEN loss by epigenetic silencing[244]. AKT activation of this pathway is controlled positively by PI3K kinases and negatively by PTEN and is involved in cell metabolism, growth, proliferation, and apoptosis[245]. Moreover, this pathway is also implicated in the activation of NF-κB pathway and IKKα, which have also been described to have protumoral functions in MM[246].

I4.3 Malignant melanoma classification

Histopathologically, MM is diagnosed using the TNM guideline, in which classification is established by tumor thickness (T), lymph node involvement (N), and presence of metastasis (M). In this type of cancer, the most important criteria for assessing prognosis, and further treatment, are tumor thickness and presence of ulceration, related with poor prognosis[247]. Moreover, different histological subtypes can be distinguished: superficial spreading melanoma, nodula melanoma, acral lentiginous melanoma, and lentigo-maligna melanoma[248]. However, this subdivision has no prognostic importance and little correlation with treatment outcomes.

The increasing understanding of MM molecular basis has associated genetic alterations with disease progression and response to treatments. Therefore, subclassifications of melanoma based on their molecular features have emerged and are continuously evolving[249,250]. For example, The Cancer Genome Atlas analysis of a large cohort of melanoma samples classified four different genetic subtypes based on activating mutations: BRAF-mutant melanomas, Ras-mutant melanomas, NF1-mutant melanomas, and triple-wild-type melanomas[251]. The emergence of these molecular classifications imposed relevant implications in the treatment strategies of MM patients[252].

I4.4 Malignant melanoma treatment

MM treatment option totally depends on the tumor stage, location and size and it varies from patient-to-patient reflecting the specific characteristics of tumor cells. Treatment for primary melanoma usually includes surgery to remove the tumor[248]. In contrast, treatment options for late-stage melanoma may include targeted therapy, immunotherapy, chemotherapy, or radiotherapy[253].

Until now, chemotherapy and radiotherapy have shown very little benefit as adjuvant or palliative strategies. Alkylating agents, such as Dacarbazine and Temozolomide (TMZ), generate DNA damage

by introducing alkyl groups to guanine bases, eventually causing cell death. They both are able to cross the blood-brain barrier, making them useful treatments for brain metastasis[254]. However, different clinical trials evaluating these alkylating agents and other cytotoxic chemotherapies (such as platinums, taxanes or nitrosoureas) have evidenced that single treatment of these chemotherapeutic agents has modest activity in improving patient survival. For that reason, there is an increasing interest in the development of combination therapy regiments[255,256].

Regarding targeted therapies, because of the high prevalence of BRAF mutations in MM and its essential contribution to tumor, several inhibitors of BRAFV600E (such as Vemurafenib, Dabrafenib or Encorafenib) are currently used in the clinical practice alone or in combination with MEK/ERK inhibitors (such as Trametinib, Cobimetinib or Binimetinib) to block MAPK pathway reactivation [257–259]. However, in BRAF wild-type tumors treatment with Vemurafenib results in increased MAPK signalling due to stabilization of BRAF/cRAF dimers, which can be mitigated by second-generation RAF inhibitors such as PLX7904 and PLX8394[260–262]. Drugs targeting other altered molecular pathways are also being developed[263].

MM is also considered a strong candidate for immunotherapy[264]. The American Food and Drug Administration (FDA) has approved the use of monoclonal antibodies that block immune checkpoint interactions, such as Ipimumab (blocks CTLA-4) or Pembrolizumab and Nivolumab (block PD-1), for patients with unresectable or metastatic melanoma due to their strong and durable responses[265,266]. This immune checkpoint blockade therapy is also given in combination with BRAF and MEK inhibitors in BRAF mutant patients[267].

Despite considerable progress made in the treatment of patients with advanced MM, the majority of the patients experience a disease progression due to acquired resistance, highlighting the importance of uncovering additional mechanisms of tumor progression and therapy resistance.

OBJECTIVES

OBJECTIVES

1. Characterize the interactomes of IKKα under basal conditions and upon cellular damage.
    a. Uncover the candidate elements that support IKKα activation after damage.
    b. Identify downstream effectors of IKKα involved in DNA damage response (DDR).
2. Study the functional relevance of the IKKα-DDR axis in the therapeutic resistance of cancer cells.
    a. Validate experimentally the contribution of the different IKKα-associated elements to the DNA damage repair.
    b. Propose and validate novel biomarkers to predict therapy response or resistance.
    c. Design new therapeutic strategies to eradicate cancer cells.

MATERIALS AND METHODS

MATERIALS AND METHODS

MM1. CELL LINES AND REAGENTS

CRC cell line CaCo2 [ATCC, Ref. HTB-37], melanoma cell lines NRAS mutated SK-MEL173 [ATCC, Ref. CVCL_6090], BRAF mutated SK-MEL37 [ATCC, Ref. CVCL_3878] and SK-MEL131 [ATCC., Ref. CVCL_6081] and metastatic SK-MEL93 [ATCC, Ref. CVCL_5651], and HEK293T [ATCC, Ref. CRL-3216] were obtained from the American Type Culture Collection [ATCC, USA]. All adherent cells were grown in Dulbecco's modified Eagle's medium (DMEM) [Invitrogen] plus 10% fetal bovine serum (FBS) [Biological Industries], 4.5 g/L glucose [Life Technologies], 2 mM L-glutamine [Biological Industries], 56 U/mL penicillin and 56 µg/mL streptomycin [Biological Industries] and were maintained in a 5% CO_2 incubator at 37°C.

Large cell lymphoma SU-DHL10 cell lines (PARP1/2 WT, PARP1 KO and PARP2 KO) were provided by Dr. Jose Yelamos laboratory (IMIM). Suspension cells were grown in Roswell Park Memorial Institute medium (RPMI 1640) [Invitrogen] supplemented with 10% FBS, 4.5 g/L glucose, 2 mM L-glutamine, 56 U/mL penicillin and 56 µg/mL streptomycin and were maintained in a 5% CO_2 incubator at 37°C.

For cell treatment, chemotherapeutic agents 5-FU [Accord, Ref. 606544.3], Irinotecan [Fresenius Kabi, Ref. 687014.3], Doxorubicin [Accord, Ref. 174247] and Temozolomide [Sun Pharmaceutical Industries, Ref. 47335-890-80], PARP inhibitor Olaparib (AZD2281) [Selleckchem, Ref. S1060], BRAF inhibitors Vemurafenib (PLX4032) [Selleckchem, Ref. S1267], AZ628 [Selleckchem, Ref. S2746] and Sorafenib (BAY 43-9006) [Selleckchem, Ref. S7397], CRM1 inhibitor Leptomycin B [Sigma, Ref. L2913] and Biotin [Sigma, Ref. B4639] were used at indicated concentrations. Cells were also damaged irradiating them in GS Gene linker UV Chamber [Bio-rad] at 130mJ.

MM2. CELL TRANSFECTION

Transfection is the process of introducing nucleic acids into cells. In cell biology research the term is used for non-viral methods in eukaryotic cells. For this, we used PEI (Polyethylenimine, Linear, MW 25.000) [Polysciences Inc., Ref. 23996]. PEI is a high-charge cationic polymer that readily binds highly anionic substrates, such as DNA and other negatively charged molecules and it works as a carrier vector.

1. Dilute 4µl PEI per µg of DNA into 1/10 of the final volume of serum-free DMEM (1ml for 10 mm plate). Mix gently and incubate 5 min at room temperature (RT).
2. Add desired µg of DNA, mix and incubate 20min at RT. Add the solution to the culture plate gently.
3. Overnight (O/N) after transfection, change the medium to DMEM plus 10% FBS.
4. Analyse 48h after transfection.

MM3. CELL INFECTION

Lentivirus production

To produce virus, HEK293T cells were transfected according to cell transfection protocol (see above). Plasmid used are:

- 10 µg of the DNA of interest
- 7 µg pCMV-dR8.2 (packing plasmid) [Addgene, Ref. 8455]
- 3 µg pMD2.G (envelop plasmid) [Addgene, Ref. 12259]
- 1 µg pCS2EA (GFP vector to control transfection efficiency]

48h after transfection, viral supernatants are collected and filtered using a 45 µm filter and directly used or concentrated by ultracentrifugation (20000 rpm for 3h at 4ºC) and storage at -80ºC.

Cell infection and selection

Cell infection with viruses carrying plasmids described above was performed as follows:

- Plate the target cells in a 6-well plate, 24h prior to viral infection.
- Add virus-containing media or 100-200 µL of concentrated virus plus 10 µg/µL Polybrene [Sigma, Ref. H9268].
- After 24h remove medium and add fresh medium.
- Add selection with specific antibody, usually puromycin (1.25 µg/mL) or Hygromycin (800 µg/µL). Culture the cells with the antibiotic selection for 3-5 days.

MM4. CRISPR-Cas9 GENE MODIFICATION

The CRISPR-Cas9 (Clustered Regularly Interspaced Short Palindromic Repeats) is a nuclease system originally used by bacteria as a defence system against external DNA, which recognizes the CRISPR

DNA sequences in the genome of the bacteria and the Cas9 is the enzyme that uses these sequences to perform a double-strand break (DSB) in the DNA. This system has been optimized to use it in genome editing and knock-out (KO) cell line generation.

For introduce this system in mammalian cell lines, we used the plasmid *lentiCRISPRv2* [Addgene, Ref. 52961], designed by Zhang Lab[268]. This plasmid has the Cas9 coding sequence and a cloning site to introduce the single-guide RNA (sgRNA), called sgRNA scaffold. The sgRNA of 20 bp is designed as near as TSS of the gene as possible and next to a 3' PAM sequence (NGG), which is used by the Cas9 enzyme to bind to the DNA and perform the DSB. This normally causes changes in the coding frame which leads to aberrant proteins or premature STOP codons, resulting in the impossibility to generate the targeted protein from the altered DNA. The sgRNAs for NEMO/IKBKG gene were designed using Benchling [RRID:SCR_013955] (**Table MM1**) and ordered from Sigma, adding restriction enzyme sites for Esp3I [ThermoFisher, Ref. ER0451] (CACCG at 5' in the Forward primer and CAAA at 5' in the reverse one). In order to clone the sgRNAs into the different plasmids:

- Digest and dephosphorylate 5 µg of plasmid with Esp3I restriction enzyme and FastAP (Alkaline Phosphatase) [ThermoFisher, Ref.EF0651] for 30 min at 37ºC.
- Purify the 11 kb fragment and discard the 2 kb fragment using the GFX PCR DNA and Gel Band Purification Kit [GE Healthcare, Ref.28903471].
    - Run all the digestion reaction in 0,7% Agarose gel.
    - Cut the 11 kb band and add 500 µL of Capture Buffer.
    - Incubate 15-30 min at 60 ºC until agarose is completely liquid.
    - Purify the DNA using the GFX columns.
    - Elute in 50 µL of Elution Buffer Type 6.
- In parallel, phosphorylate and anneal each pair of oligos using the T4 Polynucleotide Kinase (PNK) enzyme.
    - Use 1 µL of each oligo (stock 100 µM), 1 µL of 10x T4 Ligation Buffer [New England Biolabs (NEB)], 6.5 µL ddH_2O and 0.5 µL T4 PNK [NEB, Ref. M0201S].
    - Leave 37ºC for 30 min.
    - 95º for 5 min.
    - Lower the temperature to 25ºC at 5ºC/min
    - Dilute the phosphorylated and annealed oligos 1/200.
- Ligate the oligos with the digested plasmid

- 50 ng of digested plasmid, 1 µL of annealed oligos, 1 µL of 10x T4 Ligase Buffer [NEB], ddH20 up to 10 µL, 1 µL of T4 Ligase [NEB, Ref. M0202S].
- Incubate at RT for 10 min.

- Transform the ligation reaction into XL1 Blue bacteria (perform all steps under the hood).
  - Thaw bacterial glycerol stock on ice (100 µL).
  - Mix the ligation reaction with the bacteria.
  - Incubate 30 min on ice.
  - Add 1 mL of LB (without antibiotic) and incubate 20-30 min at 37 ºC.
  - Seed 200 µL into LB-agar plate supplemented with Ampicillin and incubate at 37 ºC O/N.
- Pick some colonies and extract plasmid DNA.
- Sequence plasmids by Sanger sequencing using U6-promoter forward primer (upstream of the sgRNA).

Table MM1. sgRNA used for NEMO KO generation.

Target	Specie	Forward	Reverse
CRISPR NEMO sgRNA	Human	CACCGTGGGCGAAGAGTCTCCTCTG	AAACCAGAGGAGACTCTTCGCCCAC

Using CRISPR-Cas9 technology, viral production and cell infection procedures HEK293T and Caco2 NEMO KO cells lines were obtained. After puromycin selection, the pool of cells was plated as single cells in 96-well plates to isolate clones. Cell sorting was performed on FACS Aria [BD Biosciences]. DAPI staining [Molecular Probes] was used to exclude dead cells. All data were analyzed with FlowJo software [Tree Star]. Individual cells were placed in separated wells and allowed to expand up to have enough cells to get cell lysates to isolate genomic DNA and total proteins.

MM5. CELL LYSATES

Lysates from cells were obtained for posterior proteomic analyses. Depending on the cell fractionation desired different lysis buffers and lysis protocols are used.

1- Soluble/Insoluble extracts**:** by this method the cytoplasmatic and nuclear soluble proteins and the chromatin insoluble proteins will be separated.
   - Remove the medium and wash cells with PBS. Discard supernatant.

- Lysate cells with ice-cold CoIP lysis buffer (PBS plus 0.5% Triton X-100, 1mM EDTA, 100mM NA-orthovanadate (Na_3VO_4), 0.25mM phenyl-methylsulfonylfluoride (PMSF) and complete protease inhibitor cocktail [Roche, Ref.11836153001]. For adherent cells, scrape cells from the plate and recover the sample in an eppendorf tube. For suspension cells, directly add the lysis buffer to the pellet of cells (previously centrifugated at 300 rcf for 5 min) and resuspend.
- Incubate 20 min on ice.
- Centrifuge at maximum speed for 10 min at 4ºC.
- Recover the supernatant (soluble extract), keep 5 µL for measuring the protein concentration by Bradford and add the adequate volume of 6X Loading Buffer (50mM Tris-HCl pH 6.8, 1.4M β-mercaptoethanol (β-ME), 2% SDS, 0.1% bromophenol blue, 10% glycerol in H_2O).
- Resuspend the pellet (chromatin/insoluble extract) in PBS with 1% SDS and sonicate 2-3X for 10 seconds with 10% amplitude with a Digital Sonifier [Brandson].
- Add 6X Loading buffer and boil at 95ºC for 10 min.
- Keep the samples at -20ºC.

2- Cytoplasm/Nuclear fractions**:** by this method proteins from the cytoplasm and the nucleus are separated. Nuclear fraction will include soluble and insoluble proteins.
    - Lysate the cells with ice-cold Buffer A pH 7.9 (10 mM Hydroxyethyl piperazineethanesulfonic acid (HEPES) [Sigma, Ref. H-3375], 1.5 mM $MgCl_2$, 10mM KCl,0.5 mM DTT, 0.05% NP40 and complete protease inhibitor cocktail.
    - Incubate on ice for 20 min.
    - Centrifuge at 1000 rcf for 10 min at 4ºC.
    - Recover the supernatant (Cytoplasm fraction) and wash pellet with Buffer A (two times the amount used at the beginning) and centrifuge again.
    - Discard supernatant and resuspend the pellet (nuclear fraction) in PBS plus 1% SDS and sonicate 2-3X 10 sec with 10% amplitude.
    - Add 6X Loading Buffer to the samples and boil at 95ºC for 10 min.
    - Keep the samples at -20ºC.

MM6. WESTERN BLOT

Western blot (WB) is a common method used in molecular biology to detect specific proteins from cell lysates. Briefly, denatured proteins are separated by gel electrophoresis based on their molecular weight and transferred to a membrane where they will be detected using specific antibodies. For protein visualisation, membranes are incubated with secondary antibodies conjugated to HRP that catalyse the reaction to generate a light signal.

1. Carry out protein separation using standard SDS-polyacrylamide gel electrophoresis (SDS-PAGE) at 120V.
2. Transfer the proteins to a Polyvinylidene difluoride (PVDF) membrane [Millipore, Ref. IPVH00010] at 400mA for 1h.
3. Block the membrane with 5% non-fat milk in Tris buffered saline plus Tween20 (TBS-T) buffer (50mM Tris-HCl pH 8.0, 150 mM NaCl, 0.05% Tween 20 [VWR, Ref. 8.22184], in H_2O) rocking 1h at RT.
4. Incubate the membrane with the primary antibody in blocking solution (**Table MM2**) rocking O/N at 4ºC.
5. Wash 6X in TBS-T buffer rocking 5 min at RT.
6. Incubate the membrane with the secondary antibody (HRP-conjugated) in blocking solution (**Table MM2**) rocking 1h 30min at RT.
7. Wash 6X in TBS-T buffer rocking 5 min at RT.
8. Peroxidase activity was visualised incubating the membranes with ECL solution [Biological Industries, Ref. 20-500-120] or [GE Healthcare, Ref. RPN2232], that contains a chemiluminescent HRP substrate.
9. Develop the chemiluminescent signal in an autoradiography film [GE Healthcare, Ref. 28906844].

Table MM2. Antibodies used in WB.

Antibody	Company	Reference	Specie	Dilution
IKKα	Abcam	ab32041	Rabbit	1:1000
p-IKK (Ser176/180)	Cell Signalling	#2697	Rabbit	1:1000
IKKβ	Abcam	ab32135	Rabbit	1:1000
NEMO	Santa Cruz	sc-8338	Rabbit	1:1000
p-ATM (Ser1981)	Merck Millipore	05-740	Mouse	1:1000
ATM	Abcam	ab199726	Rabbit	1:1000
p-ATR (Ser428)	Cell Signalling	#2853	Rabbit	1:1000
ATR	Cell Signalling	#2790	Rabbit	1:1000
DNA PKc	Cell Signalling	#12311	Mouse	1:1000
p-Chk1 (Ser345)	Cell Signalling	#2348	Rabbit	1:1000
p-Chk2 (Thr68)	Cell Signalling	#2661	Rabbit	1:1000
Chk1	Cell Signalling	#2360	Mouse	1:1000
PARP1	SN	-	Mouse	1:500
ELKS	Santa Cruz	sc-135215	Rabbit	1:1000
yH2A.X (Ser139)	Cell Signalling	#2577	Rabbit	1:1000
p-ERK1/2 (Thr202/Tyr204)	Cell Signalling	#4370	Rabbit	1:1000
ERK1/2	Cell Signalling	#9102	Rabbit	1:1000
p-BRAF(Ser445)	Cell Signalling	#2696	Rabbit	1:1000
BRAF	Cell Signalling	#14814	Rabbit	1:1000
Lamin B	Santa Cruz	sc-6216	Goat	1:1000
PP1	Santa Cruz	sc-7482	Mouse	1:10000
Histone H3	Abcam	ab1791	Rabbit	1:5000
Tubulin-α	Sigma Aldrich	T6074	Mouse	1:10000
Polyclonal Goat anti-Rabbit Immunoglobulins/HRP	Dako	P0448	Rabbit	1:2000
Polyclonal Rabbit anti-Mouse Immunoglobulins/HRP	Dako	P0260	Mouse	1:2000
Polyclonal Rabbit anti-Goat Immunoglobulins /HRP	Dako	P0449	Goat	1:2000
Veriblot for IP detection Reagent HRP	Abcam	ab131366	Rabbit	1:2000
Monoclonal Rat anti-Mouse Immunoglobulins /HRP	Abcam	ab131368	Mouse	1:2000

MM7. BioID METHOD AND BIOTIN IMMUNOPRECIPITATION

Proximity-dependent biotinylation (BioID) screen are excellent tools to capture *in cellulo* interactomes for a large variety of baits, including transient and weak affinity interactions, as well as localization-specific proximity components[269,270]. This identification method is based on the fusion of a *E. coli* Biotin Ligase (BirA) with a bait protein (IKKα), that after biotin addition will biotinylated the proteins that are close to or interact with our protein of interest. BirA catalyzes the formation of biotinoyl-5'-AMP that reacts with accessible amine groups of exposed lysine residues. Thus, proteins that are proximal or interact with the bait will be irreversibly biotinylated. Then, these biotinylated proteins can be precipitated and identify by different proteomic techniques.

BirA-IKKα plasmid encoding IKKα protein sequence in the C-terminus of BirA (R118G) sequence was obtained from Protein Technologies unit form CRG by subcloning IKKα coding sequence into pcDNA3.1-mycBioID vector [Addgene, Ref. 35700] (**Figure MM1**).

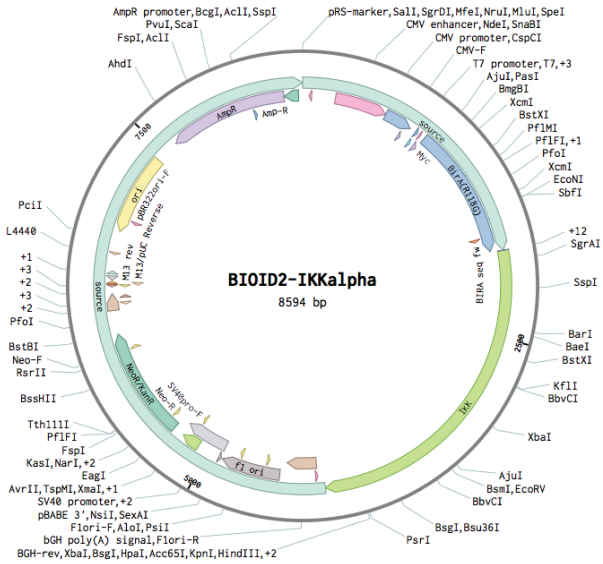

Figure MM1. BioID plasmid. BirA-IKKα plasmid encoding IKKα protein sequence in the C-terminus of BirA (R118G) sequence. Created with Benchling.com.

Biotin Immunoprecipitation (Biotin IP)

- Seed 3x10^6 HEK293T cells carrying BirA-IKKα plasmid per condition.
- Treat with 50µM Biotin O/N

- Perform cell lysis as explained above and from each sample separate 100 µL for the input.
- Capture the biotinylated proteins adding 100µL Streptavidin Sepharose beads [Cytiva, Ref. 17511301] (previously blocked with 10% BSA 100 mg/mL and washed with lysis buffer).
- Incubate with rotation at 4ºC for 2h.
- Spin down the beads by centrifuging them for 2 min at 300 rcf at 4ºC. Remove the supernatant.
- Wash 5X with 500 µL lysis buffer, centrifuging between washes.
- After the final wash, remove the supernatant, add 100-150 µL 1x Loading buffer and boil 10 min 95ºC.

MM8. MASS SPECTOMETRY

Mass spectrometry (MS) is technique that allows us to distinguish chemical entities with different mass-to-charge ratio. It is used in proteomics for the characterization and sequencing of proteins. This permits the study of cellular processes involving proteins such as cell signalling processes, structure of protein complexes or post-translational modifications. Usually, components are first separated by liquid chromatography (LC) following coupled MS (LC-MS/MS) to enhance detection.

Cell lysates and Biotin Immunoprecipitation

Total lysates from HEK293T cells carrying BirA-IKKα plasmid, and pretreated with 50µM Biotin O/N, were obtained lysing cells with CoIP lysis buffer, sonicating 3X for 15 sec at 10% amplitude and then, centrifugating them at 1000 rcf for 10 minutes. Precipitation of biotinylated proteins was performed incubating with Streptavidin Sepharose beads for 2h and apart from 5X washes with CoIP lysis buffer, 3X more washes with PBS. As a technical control HEK293T cells transfected with empty BirA plasmid were used.

Sample digestion and phosphopeptide enrichement

- Add 10 mM solution of DTT [Sigma, Ref. D9163] and let the reaction proceed for 1 hour at 37ºC.
- Prepare 20 mM IAM (Iodoacetamide) [Sigma, Ref. I1149] by mixing 100 µL 100 mM IAM with 400 µL 200 mM ABC. Add the appropriate volume of 20mM IAM to the sample and alkylate for 30 minutes at room temperature in the dark.

- Dilute samples with 200 mM ABC to have samples at 2M Urea before adding the endoprotease LysC. Dissolve a vial of LysV (10UA) [Wako, Ref. 129-02541] in 1 mL of TEAB 50 mM [Sigma, T7408] to have a solution of 2,4 µg/ µL of LysC.
- Add the required amount of endoprotease LysC in the sample to have a ratio 1:10 ratio enzyme:protein (w:w). You can dilute the enzyme with the appropriate volume of 200 mM ABC.
- Digest O/N at 37ºC at 650 rpm in the thermos-mixer.
- Dilute samples with 200 mM ABC to have samples at less than 1M Urea before adding sequence-grade trypsin [Promega, Ref. V5111].
- Add the required amount of sequence-grade trypsin in the sample to have a 1:10 ratio enzyme protein (w:w). You can dilute the enzyme with the appropriate volume of 200 mM ABC.
- Stop the reaction by adding formic acid (10% of final total volume) [Merck, Ref. 1.00264.0100].
- Enrich sample in phosphopeptides using Titanium Dioxide (TiO_2) beads [Titansphere, 5 µM, GL sciences Inc.].
- Clean up the sample with Hypersep C18 columns [Thermo, Ref. 60108-305]:
    - *Column conditioning*: Activate the selected columns with methanol 100%
    - *Column equilibration:* Equilibrate the selected columns with 5% formic acid in water.
    - *Sample loading:* Acidified samples are slowly loaded twice into the selected columns.
    - *Column wash*: Wash the selected columns with 5% formic acid in water.
    - Sample elution: Elute the sample from the selected columns with 5% formic acid in a 1:1 solution acetonitrile:water (v/v).
    - Evaporate the solvent of the eluted sample to dryness using a speed-vac system.
    - For mass spectrometric analysis redissolve the sample in 0,1% formic acid in water.
- Evaporate the solvent of the samples with a speedvac.
- Dissolve the samples in 0,1% formic acid in water to a final concentration of 1 mg/mL.

<u>Sample Injection</u>

- 45% of each sample was injected in an Orbitrap Eclipse with a 90 min gradient using a 2 cm Trap-column and 122 cm 3 µm column. Each sample was injected twice with the acquisition methods: DDA_TOP20_CID and DDA_TOP20_MSA. To avoid carry over, BSA runs were added

between the samples. BSA controls were included both in the digestion and LCMSMS analysis for quality control.

Data analysis

The data has been searched using the search algorithm Mascot v2.6 (www.matrixscience.com) against a SP_Human (UniProt, February 2020) database. Protein/peptide identification was obtain using the Proteome Discovered software v2.4. The protein-protein interactions have been scored with the Significance Analysis of INTeractome (SAINT) software[271], that allows to select bona fide interactions and remove nonspecific interactions in an unbiased manner. Peptides have been filtered based on false discovery rate (FDR) and only peptides showing an FDR lower than 5% have been retained. Protein network was done using cytoscape software (www.cytoscape.org).

MM9. CO-IMMUNOPRECIPITATION

Co-Immunoprecipitation (Co-IP) assay is widely used technique to identify physiologically relevant protein-protein interactions by using specific antibodies to indirectly capture proteins that are bound to a specific target protein. The immune complex formed by the specific antibody and target protein is precipitated on a beaded support to which an antibody-binding protein is immobilized (Protein A or G). Then the precipitated proteins be analysed by WB. Protein-protein interactions can be strengthened by crosslinking the binding partners.

1. Use 3 x 10^6 cells per condition.
2. Remove the medium and wash cells with PBS
3. Crosslink proteins by using the reversible crosslinker DSP (1mM) [Thermo scientific, Ref. 22586] for 10 min at RT
4. Lysate cells with 1 mL ice-cold lysis buffer following the protocol described above.
5. From each fraction separate 100-150 µL as the input.
6. Add 2-5µg of specific antibody or unspecific IgG and leave rotating O/N at 4ºC (**Table MM3**).
7. Add 100-150 µL Sepharose A beads [Cytiva, Ref. 17078001] (previously hydrated and blocked with lysis buffer with 10% BSA 100 mg/mL).
8. Incubate rotating 2h at 4ºC.
9. Centrifuge 300 rcf for 2 min. Discard the unbound fraction.
10. Wash 5X with lysis buffer, centrifuging between washes at 1200 rpm for 2 min.
11. Add 100-150 µL 1x Loading Buffer and boil 10 min 95ºC. Store at -20ºC.

Table MM3. Antibodies used in Co-IP experiments.

Antibody	Company	Reference	Specie
IKKα(p45)	Millipore	MABF222	Mouse
Mouse IgG	Sigma	I8765	Mouse

MM10. SIZE EXCLUSION CHROMATOGRAPHY ASSAY

Size exclusion chromatography (SEC) assay separates molecules based on their size by filtration through a gel, which consist of spherical beads containing pores of a specific size distribution. Separation occurs when molecules of different sizes are included or excluded from the pores within the matrix. Small molecules diffuse into the pores and their flow through the column is retarded according to their size, while large molecules do not enter into the pores and are eluted faster. Consequently, proteins and protein complexes separate based on their size as they pass through the column and are eluted in order of decreasing molecular weight (MW).

1. Lysate cells with 200 µL ice-cold lysis buffer following the protocol described above.
2. Load the lysates on Superdex200 gel filtration column [Cytiva, Ref. 17104301], previously packaged and washed with PBS.
3. Allow the solution enter into the matrix and leave between 5-10 drops to pass before start collecting.
4. Collect one drop per fraction (For Biotin IP 2 drops per fractions were collected).
5. Add 20 µL 6x SDS-Laemmli buffer and boil 10 min 95ºC
6. Store at -20ºC.

MM11. IMMUNOFLUORESCENCE

Immunofluorescence (IF) is used for a direct visualization of protein expression and localization. Proteins are detected using specific antibodies and then a secondary antibody with a conjugated fluorochrome is used to detect protein levels. For adherent cell lines, cells are cultured in a glass coverslip and all the steps are performed in the same coverslip and mounted on a slide in the last step. However, for suspension cells in order to obtain a monolayer of cells in a slide a cytospin has to be performed before IF steps.

1. For adherent cells seed $1x10^6$ cells per condition and for suspension cells take $1x10^5$ cells per condition (final volume 150-200 µL).

Table MM4. Antibodies used in IF and IHC experiments.

Antibody	Company	Reference	Specie	Dilution
p-ATM (Ser1981)	Merck Millipore	05-740	Mouse	1:500
ATM	Abcam	ab199726	Rabbit	1:500
p-53BP1(Ser1618)	Cell Signalling	#6209	Rabbit	1:500
p45-IKKα	SN	-	Mouse	1:100
γH2A.X (Ser139)	Cell Signalling	#2577	Rabbit	1:500
γH2A.X (Ser139)	Upstate	05-636	Mouse	1:500
Ki-67	Novocastra	NCL-Ki67-MM1	Mouse	1:500
Alexa Fluor 488 donkey-anti-rabbit IgG	Invitrogen	A21206	Donkey-anti-rabbit	1:1000
Alexa Fluor 488 donkey-anti- mouse IgG	Invitrogen	A21202	Donkey-anti-mouse	1:1000
Alexa Fluor 647 donkey-anti-rabbit IgG	Invitrogen	A31573	Donkey-anti-rabbit	1:1000
Alexa Fluor 647 donkey-anti- mouse IgG	Invitrogen	A31571	Donkey-anti-mouse	1:1000

2. Cytospin of suspension cells:
    - Mount the slide, the paper and the cuvette in the metal holder.
    - Add up to 200 µL of cells into each cuvette.
    - Centrifuge at 500 rpm for 3 min.
    - Extract the slide, paper and cuvette without disturbing cell monolayer.
3. For adherent cells, remove the medium and wash with PBS.
4. Fix the cells with Paraformaldehyde (PFA) 4% [Sigma, Ref. P6148, 4% in PBS] for 30 min at 4ºC.
5. Wash 3X with PBS rocking 5 min at RT.
6. Permeabilization and blockage with 4% milk and 0.3% Triton X-100 [Surfactant Amps, Thermo Scientific, Ref. 28340] in PBS for at least 1h at 4ºC.
7. Incubate with the appropriate dilutions of primary antibodies in the same permeabilization solution and leave O/N at 4ºC (**Table MM4**).
8. Wash 5X with PBS.
9. Incubate with the secondary antibodies, diluted in PBS plus 4% milk for 1h30min at RT (**Table MM4**).
10. Was 5X with PBS.

11. Mount in 4,6-diamino-2-phenilindole (DAPI) Fluoromount-G [Southern Biotech, Ref. 0100-20] onto a slide.
12. Images were taken in an SP5 upright confocal microscope [Leica], using the Leica Application Suite software.

MM12. RNA ISOLATION

Total RNA from cells was extracted with the RNeasy Mini Kit [Qiagen, Ref. 74106], following manufacturer's instructions:

1. Lysate cells with 350 µL RLT buffer plus 3.5 µL β-mercaptoethanol.
2. Homogenise with a 21G needle.
3. Add 1 volume of 70% ethanol and transfer it to a RNeasy MinElute spin column.
4. Centrifuge at 8000 rcf for 20 sec.
5. Add 350 µL of RW1 Buffer. Centrifuge at 8000 rcf for 20 sec.
6. Add 10 µL of diluted DNase I. Incubate for 15 min at RT.
7. Add 350 µL of RW1 Buffer. Centrifuge at 8000 rcf for 20 sec.
8. Add 500 µL of RPE Buffer. Centrifuge at 8000 rcf for 2 min.
9. Centrifuge at 20000 rcf for 5 min and discard the supernatant.
10. For elution, add 15 µL of H_2O. Centrifuge at 20000 rcf for 1 min.
11. RNA concentration is quantified with a NanoDrop spectrophotometer [Thermo Scientific]

MM13. RT-qPCR

Quantitative real time polymerase chain reaction (qRT-PCR) is a technique used to amplify and simultaneously quantify specific DNA regions. First, complementary DNA (cDNA) has to be synthesised from RNA sample by retrotranscription, using the Transcriptor First Strand cDNA Synthesis Kit [Roche, Ref. 04897030001].

1. Mix 2 µg of extracted RNA (see above) with H_2O up to 11 µL.
2. Add 2 µL of anchored-oligo(dT)18 primer.
3. Denature the template-primer mixture by heating the tube for 10 min at 65ºC in a block cycler with a heated lid. This step ensures denaturation of RNA secondary structures.
4. Cool the tube on ice immediately.
5. Add 7 µL of a mix containing (x1 reaction): 4 µL of buffer, 2 µL of dNTPs, 0.5 µL RNase inhibitor and 0.5 µL Transcriptor Reverse Transcriptase.

6. Incubate at 30 min at 55ºC in the block cycler.
7. Inactivate Transcriptor Reverse Transcriptase by heating to 85ºC for 5 min and keep at 4ºC.
8. Dilute the sample 1:20 with H_2O and store at -20ºC.

After cDNA synthesis, qRT-PCR was performed in the LightCycler480 system, using a SYBR Green I Master Kit [Roche, Ref. 04887352001]. Samples were normalised to the mean expression of the housekeeping genes TBP, GAPDH, ACTB. Primer used are listed in the **Table MM5**.

1. Prepare the mix containing (x1 reaction): 5 µL of SYBR Green I Master Kit, 2 µL of H_2O, 0.5 µL (10 µM) of forward primer and 0.5 µL of reverse primer (10 µM).
2. Add 8 µL of the mix to a 384-wells plate.
3. Add 2 µL of diluted cDNA.
4. Seal the plate and centrifuge at 150 rcf for 1 min.
5. Perform the RT-qPCR in LightCycler 480 machine [Roche].

Table MM5. Primers used for RT-qPCR.

Target	Specie	Forward	Reverse
ATM	Human	CATTTTGATGAGGTGAAGTCCATTG	CGTCATCAATAACTCCACCACAATC
ATR	Human	CCGCAAAAGGAGATTTGGTA	TTCGGAAGTGCTGTCATCTG
DNA PKc	Human	CATGGAAGAAGATCCCCAGA	TGGGCACACCACTTTAACAA
Chk1	Human	TCTGCTCCTCTAGCTCTGCT	TGGGAGACTCTGACACACCA
Chk2	Human	CTGTTGGGACTGCTGGGTAT	CGTAAAACGTGCCTTTGGAT
53BP1	Human	CTTTAGCCGCCAGTCTTCAC	CTTGGGAACGTGGCTGTTAT
Rad51	Human	CGACTCTCCCTGTCTTCCTG	TTTCCCGGAAGCTTTATCCT
NBS1	Human	GAGGCTGGCCTCTACATCAC	GAGGCTGGCCTCTACATCAC
MRE11	Human	CCGCGGAATTCAGGTTTACG	CAGGCCGATCACCCATACAA
Rad50	Human	CCTTGCTTCGGCCTCAGTTA	TTGTGTCTGACGTACCTGCC
PARP1	Human	CCGCAAAAGGAGATTTGGTA	TTCGGAAGTGCTGTCATCTG
CDK12	Human	AACAGTGGACAGCCCAAAAC	GACTGACCGACTGCCTTCTC
P53	Human	CTTTGAGGTGCGTGTTTGTG	GGGCAGTGCTCGCTTAGT
TBP	Human	TGCCCGAAACGCCGAATATAATC	GTCTGGACTGTTCTTCACTCTTGG
GAPDH	Human	GTCATCCCTGAGCTGAACG	CTCCTTGGAGGCCATGTG
ACTB	Human	GCACCACACCTTCTACAATGAGC	TAGCACAGCCTGGATAGCAACG

MM14. COMMET ASSAY

One method to analyse DNA-damage is by comet assay, or single cell gel electrophoresis assay, which is based on the capacity of denatured and damaged DNA fragments to migrate when performing an electrophoresis. Conversely, intact DNA migrates slower and stays inside the nucleus. Analysis of the size and shape of DNA "tail" reflects the quantity of DNA-damage in the cells. Comet assays were performed using the Comet Assay Kit [Trevigen, Ref. 4250-050-K]. The alkaline assay was used because is more sensitive and can detect both single and double-stranded breaks and other types of DNA-damage, like DNA adducts.

1. Use 10-12,5 x10^3 cells per condition.
2. Combine 35 µL of cells diluted in PBS with 250 µL molten LMAgarose at 37ºC and pipette 60 µL onto CometSlide.
3. Keep the slides at 4ºC for 30 minutes.
4. Immerse slides in 4º Lysis Solution O/N
5. Immerse slides in Alkaline Unwinding Solution for 1h at 4C.
6. Perform electrophoresis at 21V for 30 minutes immersing slides in 4ºC Alkaline Electrophoresis Solution.
7. Was with dH_2O twice and with 70% ethanol, 5 min each.
8. Dry samples at 37ºC until the LMAgarose is completely gone.
9. Stain DNA with 100 µL of diluted SYBR Safe for 30 min.
10. Wash with dH_2O.
11. Allow slides to dry at 37ºC.
12. 25 pictures of every replicate were taken using a Nikon Eclipse Ni-E epifluorescence microscope and tail moment was calculated using the OPENCOMET plugin for ImageJ.

MM15. VIABILITY ASSAYS

Viability assays have been used in this study for analysing the dose-response to drugs of different cell lines. The number of viable cells has been measured by analysing the ATP present in the medium, which allows identifying the quantity of metabolically active cells in culture.

1. 5000-10000 cells were plated in 96-well plates with 100 µL of complete medium.
2. Growing cells were treated with increasing concentrations of different treatments (see MM1), in monotherapy or in combination at the indicated concentration for 72h or 1 week.

To study the ability of cells to recovery from damage, after treatment, drug washout was performed and cells were leave with fresh complete medium for 72h.

3. Cell viability was measured using the CellTiter-Glo 3D Cell Viability Assay [Promega, Ref. G7571].
    - Equilibrate the plate and CellTiter Glo Reagent at RT for approximately 40-45 min.
    - Add 15 μL of CellTiter-Glo Reagent to every well.
    - Mix contents for 5 min on an orbital shaker to induce cell lysis.
    - Allow the plate to incubate at room temperature for 25 min.
    - Record luminescence (measurement of 1 second per well) in an Orion II multiplate luminometer.

MM16. ANNEXIN V BINDING ASSAY

An early marker of apoptosis is phosphatidylserine (PS), which is transported from the inner to the outer part of the plasma membrane when pro-apoptotic signals are released. It has been demonstrated that annexin V can specifically bind to PS. For this reason, for analysing increase of apoptosis in cells under certain conditions the annexin V binding assay can be used. Apoptosis in treated cells was determined by flow cytometry using the standard Annexin V Apoptosis Detection Kit APC [Thermo Fisher, Ref. 88-8007].

1. Use $1x10^6$ cells per condition.
2. Wash cells with PBS.
3. Wash cells with 1X Binding Buffer (Prepared from 10x Binding buffer: 0.1M HEPES pH7.4, 1.4M NaCl, 10mM $MgCl_2$ in ddH_2O) plus 2.5mM $CaCl_2$ and centrifuge at 500 rcf for 5 min at RT.
4. Resuspend in 200 μL of 1X Binding Buffer and incubate 15 min 5 μl of fluorochrome-conjugated Annexin V [BD pharmingen, Ref. 556422], in the dark at RT.
5. Wash cells in 1 mL of 1X Binding Buffer and centrifuge at 500 rcf for 5 min at RT.
6. Resuspend in 200 μL of 1X Binding Buffer and add 5 μL of Propidium Iodide [Thermo Fisher, Ref.P3566], for staining the DNA content.
7. Incubate 10 min at RT in the dark.
8. Analysis of the cells in the LSRFortessa analyser [BD Biosciences].

MM17. CELL CYCLE ANALYSIS

The study of cell cycle distribution by flow cytometry permits to estimate the percentages of a cell population in the different phases of the cell cycle. Staining the total DNA with different fluorescent dyes, such as DAPI, is one of the most direct way of staging the cells based on DNA content. Cell cycle was analyzed by flow cytometry using a standard Cell Permeabilization Kit [Life Technologies, Ref. GAS004] for the detection of intracellular antigens:

1. Use $1x10^6$ cells per sample.
2. Trypsinisize adherent cells and centrifuge at 150 rcf for 5 min at RT.
3. Wash cells with PBS.
4. Add 100 μL of Fixation medium (Reagent A) and incubate for 15 minutes at room temperature.
5. Wash 2X with PBS and centrifuge at 500 rcf for 5 min at RT.
6. Add 100 μL of Permeabilization medium (Reagent B) and incubate for 25 minutes at room temperature.
7. Wash 2X with PBS and centrifuge at 500 rcf for 5 min at RT.
8. Resuspend in PBS with DAPI, for staining the DNA content, and incubate at least 1h.
9. Analyse the cells in the LSRFortessa analyser [BD Biosciences]

MM18. CRYTAL VIOLET STAINING

Crystal violet staining is widely used for visualization of cell colonies. The amount of crystal violet staining is directly proportional to the cell biomass that is attached to the plate. It is a quick and reliable assay which relies on the detachment of adherent cells from cell culture plates during cell death.

1. Gently aspirate supernatant of cells in a 12-well culture plate.
2. Rinse once with 1 mL PBS
3. Fix with ice-cold 100% methanol for 10 minutes (keep in freezer)
4. Gently cover the cells with 0.5% crystal violet solution in 25% methanol. Incubate for 10-15 minutes at RT.
5. Remove the crystal violet and wash cells with water several times.
6. Allow the cells to dry at RT.

MM19. PARAFFIN EMBEDDING OF TUMOR SAMPLES

For long-term conservation of samples and to perform immunohistochemistry and immunofluorescence analysis, samples have to be paraffin embedded.

1. Collect the tissues from the organs of interest in ice-cold PBS and place them in a cassette.
2. Fix in 4% PFA rocking O/N at RT. Wash x2 in PBS 15 min rocking at RT.
3. Wash in 25% and 50% ethanol rocking 15 min each at RT.
4. Wash in 75% ethanol rocking O/N at 4ºC.
5. Wash in 90% ethanol rocking 30 min at RT.
6. Wash x3 in absolute ethanol and xylene rocking 1 h each at RT.
7. Place tissue in embedding moulds and incubate in paraffin 1 h at 65ºC.
8. Change paraffin and incubate O/N at 65ºC.
9. Change paraffin and cool down at -20ºC.
10. Unmould the block and store it at 4ºC.

MM20. IMMUNOHISTOCHEMISTRY

Immunohistochemistry (IHC) combines histological, immunological and biochemical techniques for the identification of specific tissue components by means of a specific antigen/antibody reaction tagged (directly or most commonly indirectly) with a visible label. IHC allows us to visualize the distribution and localization of specific cellular components within cells and in the proper tissue context. Starting material is usually 2,5 or 4µm paraffin sections.

1. Dewax the slides heating them at 65ºC, for 2 h or O/N if they have been re-paraffined, to melt all the paraffin.
2. Rehydration battery: xylene I and II 15 min each, absolute ethanol I and II, 96%, 70% and 50% ethanol 10 min each and distilled water for 10min.
3. Antigen retrieval: citrate-based antigen retrieval (sodium citrate pH 6.0) was used, at 100ºC for 20 min without pressure. Then, retain in buffer 1h allowing cooling down.
4. Wash x3 with PBS rocking 5 min at RT.
5. Blockage of endogenous peroxidase activity with 1.5% H_2O_2 [Sigma, Ref. H1009] for 20 min.
6. Wash x3 with PBS rocking 5 min at RT.
7. Permeabilization and blockage with 0.3% Triton X-100, 1% BSA in PBS for 1 h.
8. Incubate the appropriate dilutions of the primary antibodies in PBS containing 0.05% BSA,

O/N at 4°C (**Table MM4**).

9. Wash x3 with PBS 5 min at RT.
10. Incubate with the secondary antibodies, using the Envision+ System HRP Labelled Polymer anti-Rabbit [Dako, Ref. K4003] or anti-Mouse [Dako, Ref. K4001] for 90 min at RT.
11. Wash x5 with PBS 5 min at RT.
12. Develop the samples with 3,3'-diaminobenzidine (DAB) [Dako, Ref. K3468] for the appropriate time, wash x5 in PBS 5 min at RT and counterstain with haematoxylin [Merck, Ref. 1092530500] and mount with DPX [Merck, Ref. 1.01979.0500]
13. Images were obtained with an Olympus BX61 microscope.

MM21. HAEMATOXYLIN AND EOSIN STAINING

Haematoxylin and eosin (HE) staining is widely used for correct visualisation of cell structures. Cell nucleus is stained by haematoxylin (dark-purple) and cytoplasm by eosin (pink), although other cell structures can also be stained, such as components from the extracellular matrix. With this objective, tissue paraffin embedded samples were sectioned appropriately and stained with HE.

1. Dewax the slides heating them at 65ºC, for 2 h or O/N if they have been re-paraffined, to melt all the paraffin.
2. Rehydration battery: xylene I and II 15 min each, absolute ethanol I and II, 96%, 70% and 50% ethanol 10 min each and distilled water for 10min.
3. Staining with haematoxylin for 30 sec [Merck, Ref. 1092530500]. Wash with tap water for 5 min.
4. 80% ethanol 0.15% HCl for 30 sec. Wash with distilled water for 30 sec.
5. Ammonia water [NH_3(aq)] 0.3% for 30 sec. Wash with distilled water for 30 sec.
6. 96% ethanol for 5 min.
7. Counterstaining with eosin for 3 sec [Bio-Optica, Ref. 05-10003/L].
8. Wash x3 with absolute ethanol 1 min each.
9. Dehydration battery: absolute ethanol I and II 5 min each and xylene I and II 5 min each.
10. Mount in DPX [Merck, Ref. 1.01979.0500].
11. Images were obtained with an Olympus BX61 microscope.

MM22. ANIMALS

Animal models or model organisms are widely used in biomedical research to investigate human diseases or biological processes. The classical vertebrate model is the house mouse (*Mus musculus*), which shares around 95% of its genome with humans. Mice can be genetically manipulated to mimic human diseases or conditions and can be inbred to maintain uniformity within strains, allowing for more accurate and repeatable experiments. They have an accelerated lifespan, and an entire life cycle can be studied within 2-3 years. They are cost-effective and efficient research tool: they are small, reproduce quickly and are relatively easy to house and transport. Sacrifice of adult mice was done using exposure to CO_2. In all procedures, animals were kept under pathogen-free conditions and all animal work was conducted according to the guidelines from the Animal Care Committee at the Generalitat de Catalunya. These studies were approved by the Committee for Animal Experimentation at the Institute of Biomedical Research of Bellvitge (Barcelona).

For *in vivo* experiments, fragments of human BRAF V660E mutant malignant melanoma tumor obtained with the informed consent of the patient and following all recommendations of Hospital del Bellvitge Ethics Committee, the Spanish regulations, and the Helsinki declaration's Guide were transplanted and expanded in nude mice as orthoxenografts. To perform drug testing, equivalent pieces of individual tumors were implanted orthotopically as skin patches. When tumors started growing, animals were randomly ascribed to the different groups of treatment. Temozolomide (40 mg/kg) was administered intraperitoneally in 20% DMSO and Vemurafenib (75 mg/kg) was administered orally, and in the double treatment Temozolomide was given 1 hour after Vemurafenib. Animals were treated every day (expect the weekend) for 21 days and tumors measured every 2-3 days. At day 21 animals were euthanized and tumors collected, photographed and measured.

MM23. BIOINFORMATIC ANALYSIS

Transcriptomic dataset corresponding to colorectal cancer (CRC) patients GSE39582[272] was downloaded from GEO[273] (v2.62.2) repository as series matrix. GSE39582 raw cel files were processed using RMA normalization method as implemented in Bioconductor R package affy[274]. Annotation of Affymetrix microarray was performed using Bioconductor R package hgu133plus2.db (v3.13.0). This dataset included 562 patients with disease-free survival and stage clinical data.

Expression data of 329 CRC patients with available clinical data from the TCGA Portal was downloaded from the open-access resource CANCERTOOL[275].

Association of the gene expression with relapse was assessed in the cancer transcriptomic data sets using a Kaplan-Meier estimates and Cox proportional hazard models. Patients were classified into two subgroups according to a cutoff point obtained using the survminer (v.0.4.9) package for each group of patients. A standard log-rank test was applied to assess significance between subgroups. This test was selected because it assumes the randomness of the possible censorship. All the survival analyses and graphs were performed with R using the survival[276] (v.3.3-1) and survimer packages and a p-value<0.05 was considered statistically significant.

MM24. QUANTIFICATION AND STATISTICAL ANALYSIS

Statistical parameters, including number of events quantified, standard deviation and statistical significance, are reported in the figures and in the figure legends. GraphPad Prism 6 software was used for statistical analysis and p-value<0.05 is considered significant. Statistical significance among groups was determined by Student's t-test (data fitting normal distribution) or Mann Whitney U test (data not fitting normal distribution) for two-group comparison or one-way ANOVA with Tukey's correction for multiple comparison testing.

RESULTS

RESULTS: PART I

R1. ATM is in a complex with IKKα under basal conditions.

Previous studies from our group identified a truncated form of IKKα, IKKα(p45), localized in the nuclear compartment of CRC cancer cells that promotes tumor growth. This truncated form of IKKα is phosphorylated and activated in response to damage and regulates DNA damage response (DDR) pathway activation through direct ATM phosphorylation[211]. However, the mechanisms regulating the role of IKKα in response to damage remains unexplored.

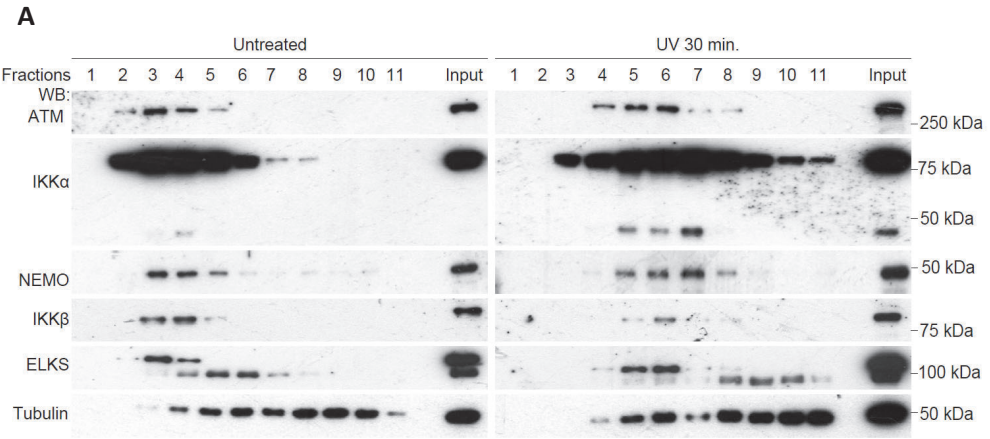

Figure R1. IKKα associates with ATM in CRC cells. (A) Soluble extracts from CaCo2 cells untreated (left panel) or 30 minutes after UV treatment (right panel) were obtained and loaded on a Superdex200 column. One drop per fraction was collected and analyzed by western blot with the indicated antibodies.

We addressed this issue by studying the interactome of IKKα in CRC cells under basal conditions and following DNA damage. We first obtained protein lysates from CaCo2 cells untreated or exposed to UV light and analyzed them by Size-exclusion chromatography. In basal conditions, IKKα, IKKβ, NEMO and the IKK-related protein ELKS were identically eluted in fractions 3 and 4 (**Figure R1A, left panels**), likely corresponding to the canonical IKK complex. However, upon UV treatment, whereas full-length IKKα and IKKα(p45) continue coeluting with NEMO and ELKS in fractions 4-7, the coelution of them with IKKβ were restricted to fraction number 6 (**Figure R1A, right panels**). These results indicate that there is a change in the composition of IKKα containing complexes upon damage.

Unexpectedly, the DDR element ATM was coeluting with IKKα (full-length and IKKα(p45)) NEMO and ELKS not only after damage but also in basal conditions, suggesting that ATM might be in a complex with IKKα previous to damage. This observation is in agreement with the notion that IKKα participates in a cellular response together with ATM that requires a rapid activation upon damage.

Nevertheless, the coelution on the Size-exclusion chromatography does not indicate the interaction between proteins. To directly study the interactome of IKKα, we use the novel BioID identification method. This method is based on the fusion of a Biotin Ligase (BirA) protein with a target protein, that in presence of biotin, will biotinylated proteins that are close to or interact with the protein of interest, in this case IKKα. Then these biotinylated proteins can be identified by different proteomic techniques[277].

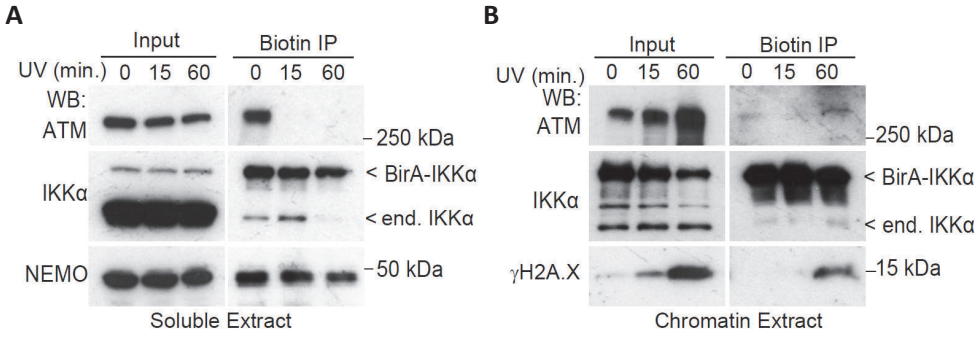

Figure R2. IKKα interacts with ATM previous to damage and translocates to the chromatin upon UV exposure. Immunoprecipitation of biotinylated proteins from soluble extract **(A)** and chromatin extract **(B)** of HEK-293T cells transfected with BirA-IKKα plasmid, pretreated with Biotin (50μM, O/N) and treated with UV light (130mJ) as indicated. WB analysis demonstrated the presence of endogenous IKKα (85kDa) and BirA-IKKα fusion protein (120kDa) in the precipitates.

We transfected HEK293T cells transfected with the fusion protein BirA-IKKα (**Figure MM1**) and treated them with Biotin (50μM) O/N. To identify elements involved in the response of IKKα to damage, we performed biotin immunoprecipitations in cells untreated and exposed to UV light (130 mJ) for 15 or 60 minutes and analyzed by western blot (WB) for the presence of candidate interactors.

In previous work, our group demonstrated that the direct interaction of IKKα with ATM increase in early timepoints after damage, as ATM is a direct substrate of active IKKα(p45) and its activation induces DDR[211]. However, we here observed that ATM and IKKα coelute also in basal conditions,

suggesting that they form a constitutive complex that is activated in response to damage. By WB analysis of the precipitates from soluble cell lysates, we confirmed the direct interaction of ATM and IKKα in basal conditions. Interestingly, after exposure to UV light, the biotinylated ATM was undetectable in these precipitates (**Figure R2A**). As ATM functions activating DNA damage response pathway and regulating cell cycle, it seems unlikely that biotinylated ATM was lost due to degradation. Therefore, we precipitated biotinylated proteins from the chromatin extracts. We found that the levels of biotinylated ATM increase after UV treatment in a time dependent manner (**Figure R2B**), suggesting that the ATM that interacted with IKKα translocated to the chromatin fraction upon damage. Furthermore, our results further confirmed that IKKα interacts with histones, and in particular with γH2A.X (a marker of DNA damage), in response to damage, supporting its function in DNA repair. We confirmed these results obtained by BioID by co-immunoprecipitation assays (Co-IP) with the antibody targeting IKKα(p45) in CaCo2 cells untreated or exposed to UV light (**Figure R3A**).

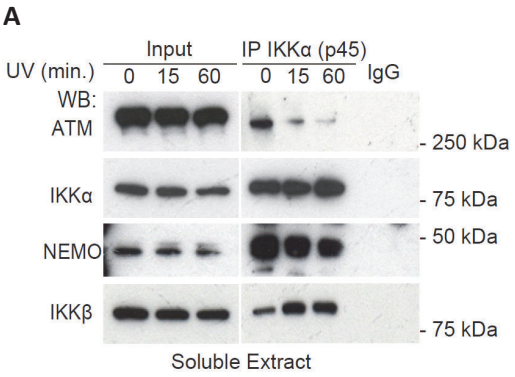

Figure R3. IKKα interaction with ATM in basal conditions in CRC cells. (A) Co-immunoprecipitation assay with the anti-IKKα(p45) antibody from CaCo2 cells treated as indicated with UV light (130 mJ).

To gain further insight of ATM- IKKα complex, we combined the BioID method with the Size-exclusion chromatography technique. We confirmed that IKKα and ATM interaction in untreated cells takes place in the context of the macromolecular complex that eluted in fractions 3 to 6 (**Figure R4A, left panels**). Moreover, it could be observed that in cells exposed to UV there is a considerable reduction in the levels of interacting ATM and IKKα in these soluble lysates (**Figure R4A, right panels**), which is in accordance with the concept that this ATM- IKKα complex functions in repairing damaged-chromatin.

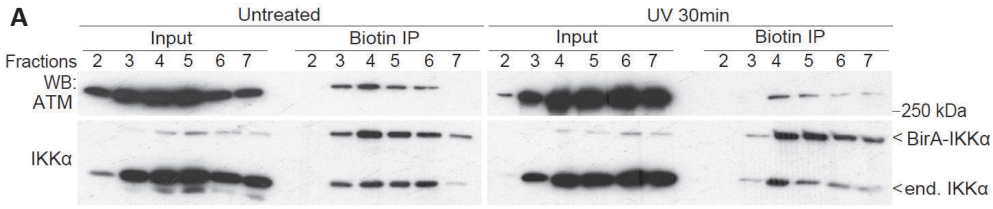

Figure R4. IKKα forms a complex with ATM. (A) Soluble extracts from untreated (left panel) or UV treated (right panel) HEK293T BirA-IKKα, pre-treated with Biotin (50µM, O/N), were fractionated in Superdex200 column. Two drops per fraction were collected and precipitated with Streptavidin beads.

R2. IKKα interactome in response to damage.

To further study the interactome of IKKα in response to cellular damage, we performed an unbiased Liquid Chromatography Mass spectrometry (LC-MS) of biotin immunoprecipitates from cells expressing BirA-IKKα, untreated or treated with UV light. As a control we used cells transfected with empty BirA plasmid.

The results of LC-MS analysis revealed that in basal conditions the most significant IKKα interactors are members of NF-κB pathway (such as IKKβ/IKBKB, NEMO/IKBKG, NFKB2/p100 and NFKB1/p105) or Hsp90/Cdc37 chaperone. Notably, ATM was also identified in the analysis as significant IKKα interactor in basal conditions, consistent with previous results. However, after UV treatment the interaction between IKKα and most of NF-κB members decreased and new possible interactors appeared, including different members of DDR pathway such as PARP1, RAD51, POLD2, POLDIP2 or APEX1 (**Figure R5A**). Therefore, LC-MS analysis revealed that the interactome of IKKα in basal conditions and in response to damage is different, further supporting an NF-κB-independent IKKα role in DNA damage repair.

Although the interaction of IKKα and most NF-κB members is reduce upon damage, LC-MS data showed that the interaction between IKKα and NEMO was maintained stable after exposure to UV light, which was confirmed by WB (**Figure R2A** and **R3A**). Interestingly, NEMO is localized at the crossroad of the different nodes (untreated, UV 15 min and UV 60 min) in the IKKα interactors network suggesting that it may play a role in the transfer from NF-κB-related IKKα complexes to DDR-related complexes (**Figure R5B**). Supporting the possibility that NEMO might play a role in defining IKK substrate specificity, it was previously found that NEMO is required for directing IKKβ

function towards IκBα[278]. Thus, we studied whether NEMO was regulating IKKα activity in response to damage.

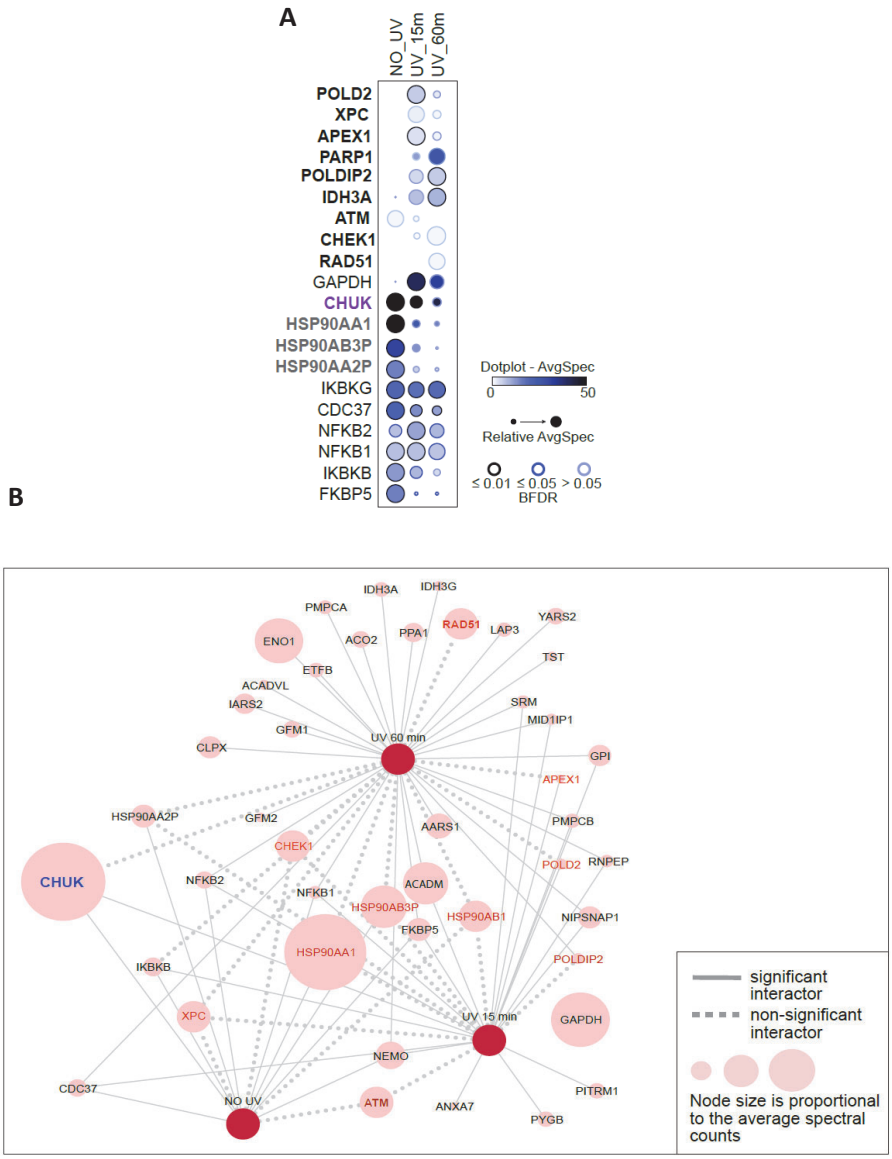

Figure R5. IKKα interactome in response to damage. (A) Representation of the results obtained in the mass spectrometry analysis of streptavidin precipitates from HEK-293T cells expressing the fusion protein BirA-IKKα. **(B)** Network of selected proteins identified as putative IKKα interactors in cells untreated or treated for 15 or 60 minutes with UV light.

R3. NEMO regulates chromatin association of IKKα and IKKα -interacting ATM

Since the interaction between NEMO and IKKα was stable upon treatment and NEMO coeluted with IKKα and ATM in the size exclusion chromatography assay, we propose NEMO as a possible element of the ATM-IKKα complex. NEMO was found to exert a central role in the activation of the NF-κB pathway in response to damage via ATM and PARP1 [182]. However, it is not known whether NEMO is involved in damage response independently of NF-κB. To study this possibility, we generated NEMO *Knock-Out* (KO) cell lines using CRISPR-Cas9 system and tested if the absence of NEMO produces deregulations in damage response.

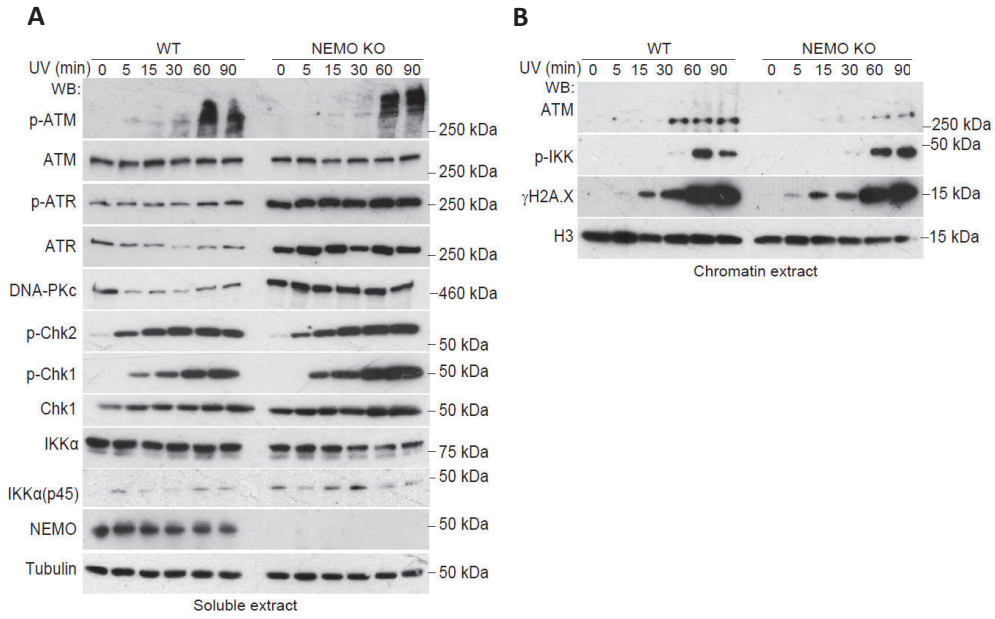

Figure R6. Normal DDR activation, but defective ATM chromatin accumulation in NEMO deficient cells. WB analysis of soluble **(A)** and chromatin **(B)** extracts from Caco2 NEMO WT and NEMO KO cells exposed to UV light (130 mJ) and collected at the indicated time points.

Comparative analysis of WT and NEMO KO CaCo2 cells exposed to different damaging agents such as UV light (**Figure R6A**) revealed that NEMO-deficient cells displayed proper activation of different DDR elements, as indicated by the increase of phosphorylated ATM, Chk1, Chk2 and γH2A.X upon time. γH2A.X is the phosphorylated form of H2A.X downstream PIKK kinases and it is considered a marker of DNA damage. It should be noticed that NEMO KO cells do have increased levels of ATR and DNA PKc, raising the possibility that they might have some DDR alterations. Indeed, by RT-qPCR

analysis we found upregulation of several DDR genes in NEMO KO cells in basal conditions, but in general there were not significant differences in their activation in response to treatment (**Figure R7A**).

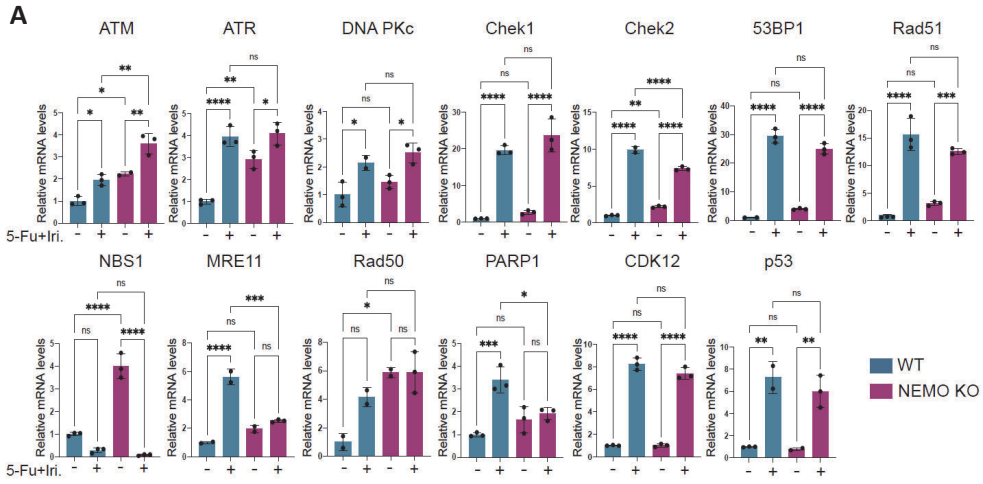

Figure R7. The expression of DDR key genes is induced upon treatment in CRC cells. (A) RT-qPCR analysis of normalized expression of selected DDR genes in untreated or 5-Fu+Irinotecan (50µg/mL + 20µg/mL, O/N) treated Caco2 NEMO WT and NEMO KO cells.

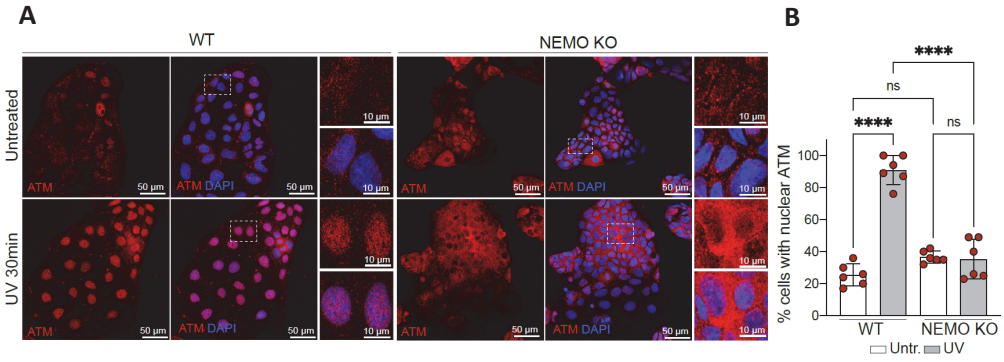

Figure R8. Defective nuclear accumulation of ATM in NEMO deficient CRC cells in response to damage. (A) Representative images of ATM staining in NEMO WT and NEMO KO Caco2 cells exposed to UV light (130 mJ, 30 min). **(B)** Quantification of the percentage of positive cells displaying nuclear ATM.

Although ATM activation by damage was apparently normal in NEMO KO cells, we observed that the chromatin levels of ATM were significantly reduced in NEMO-deficient cells (**Figure R6B**). Remarkably, immunofluorescence analysis of cellular ATM distribution showed that whereas in WT

cells the majority of ATM is translocated to the nucleus in response to damage, in NEMO KO cells most of ATM was accumulated in the cytoplasm (**Figure R8A** and **R8B**), suggesting that NEMO might be involved in the nuclear localization of ATM.

To further study this failure in nuclear translocation or retention of ATM, cells were treated with the CRM1/exportin 1 inhibitor Leptomycin B, that prevents the export of proteins by binding to CRM1. Pretreatment of cells with leptomycin B leads to nuclear ATM accumulation upon damage specifically in NEMO WT cells. In contrast, NEMO KO cells did not show any detectable increase in nuclear ATM accumulation upon damage, indicating that NEMO deficiency inhibits nuclear shuttling of ATM (**Figure R9A** and **R9B**).

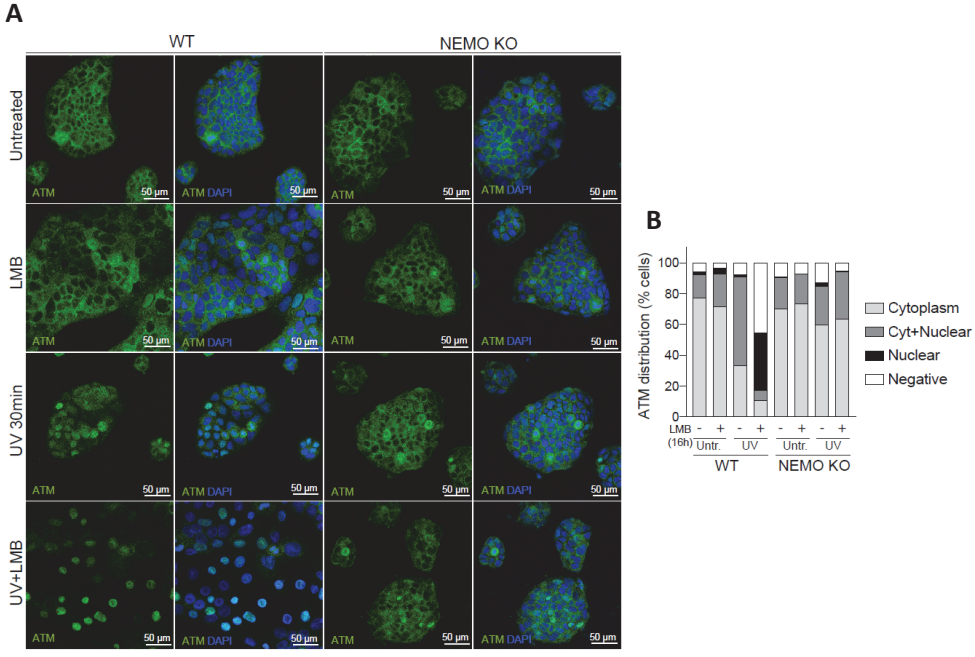

Figure R9. Defective nuclear translocation of ATM in NEMO deficient CRC cells in response to damage (A) Representative images of ATM staining in NEMO WT and NEMO KO CaCo2 cells pre-treated with Leptomycin B for 16 hours (5µg/µL) and then left untreated or exposed to UV light for 30 minutes (130mJ). **(B)** Quantification of the percentage of cells showing the indicated subcellular distribution of ATM.

A more extensive analysis of active ATM cellular localization revealed that UV-treated NEMO KO cells showed significantly reduced percentage of cells positive for nuclear p-ATM and contained cytoplasmic activated ATM (**Figure R10A** and **R10B**). This decrease in nuclear p-ATM correlates with fewer cells positive for the DNA damage marker γH2A.X (**Figure R10C**). Interestingly, in the few

NEMO KO cells displaying nuclear p-ATM, this protein does not colocalize with γH2A.X indicating a defect in the recognition of DNA damage sites by ATM (**Figure R10A** and **R10D**).

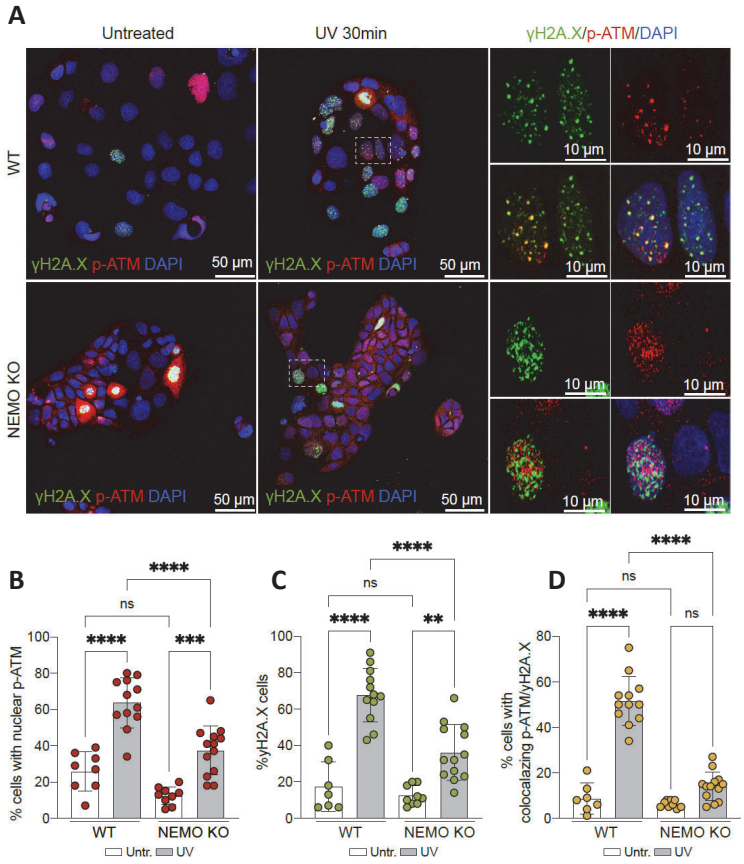

Figure R10. Active ATM fails to detect DNA damage sites in NEMO deficient CRC cells upon UV exposure. (A) Double immunofluorescence analysis of p-ATM and γH2A.X in CaCo2 WT and NEMO KO cells exposed to UV light (130 mJ, 30 min). **(B-D)** Quantification of the percentage of cells positive for nuclear p-ATM **(B),** positive for γH2A.X **(C)** and percentage of cells with co-localizing p-ATM and γH2A.X **(D)**.

When comparing different damaging agents, we found that NEMO-deficient cells treated with chemotherapy (CT), which produces damage directly in the DNA, showed a higher percentage of p-ATM and γH2A.X double positive cells compared to NEMO KO cells treated with UV light (**Figure R11A** and **R11C**), even though the percentage of p-ATM positive cells was comparable (**Figure R10B** and **R11B**). Notably, the number of colocalizing p-ATM/γH2A.X dots in these double positive cells was significantly reduced in NEMO KO cells compare to the WT cells (**Figure R11D**). Similar results were obtained from the analysis of the ATM-downstream element 53BP1 (**Figure R12A, R12B** and

R12C), indicating a failure in the recruitment of DDR elements to the sites of damage in the absence of NEMO.

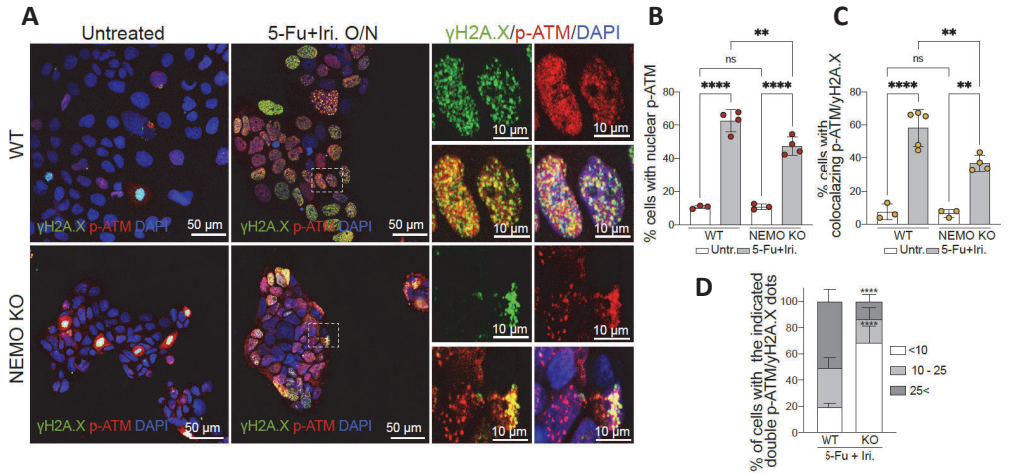

Figure R11. p-ATM fails to localize DNA damage sites in the absence of NEMO upon chemotherapy treatment. (A) Representative images of p-ATM and γH2A.X double IF staining in cells treated with 5-Fu+Iri. combination (50μg/mL + 20μg/mL, O/N). **(B and C)** Quantification of the percentage of cells treated with chemotherapy displaying nuclear p-ATM **(B)** or colocalizing p-ATM and γH2A.X **(C)**. **(D)** Quantification of the number of p-ATM/γH2A.X colocalizing foci per nucleus in treated cells.

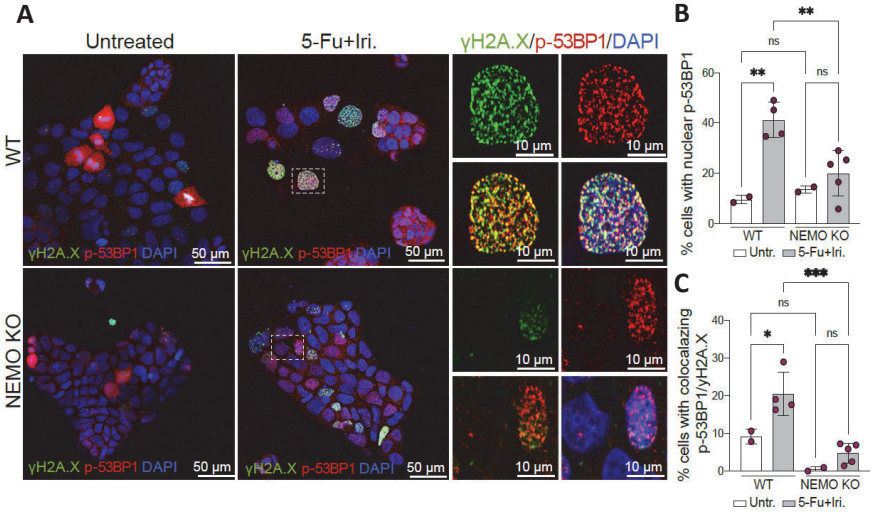

Figure R12. Failure in the recruitment of DDR elements to damage sites in NEMO deficient CRC cells upon treatment. (A) Double IF analysis of p-53BP1 and γH2A.X in Caco2 WT and NEMO KO cells treated for 16 hours with 5-Fu+Iri (50μg/mL + 20μg/mL). **(B and C)** Quantification of the percentage of cells positive for nuclear p-53BP1 **(B)** and cells with colocalizing p-53BP1 and γH2A.X **(C)**.

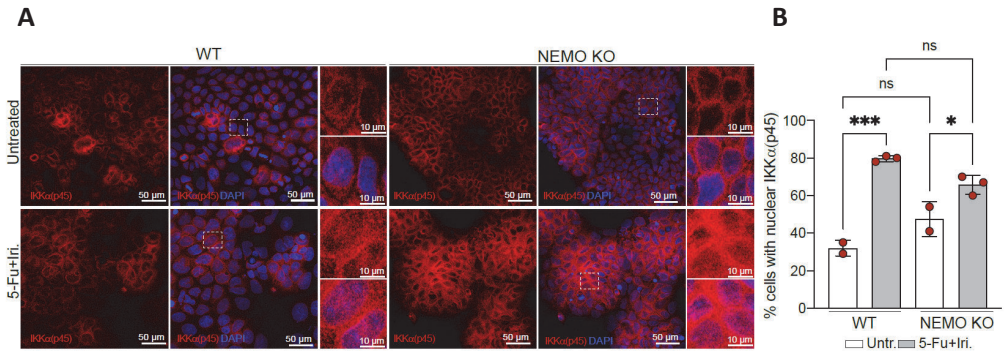

Figure R13. Cellular distribution of IKKα(p45) upon treatment. (A) Representative images of IKKα(p45) staining in NEMO WT and NEM KO CaCo2 cells untreated or exposed to chemotherapeutic combination 5-Fu+Iri. (50μg/mL + 20μg/mL, O/N). **(B)** Quantification of percentage of cells positive for nuclear IKKα(p45).

Similar to ATM, we detected increased levels of cytoplasmatic IKKα(p45) in both untreated and CT-treated NEMO KO cells (**Figure R13**). This is in agreement with the WB data in **Figure R6A** in which we observe that NEMO KO cells have slightly more IKKα(p45). However, neither nuclear translocation of IKKα(p45) nor p-IKK accumulation in the chromatin extracts upon damage (**Figure R6B**) were observed in NEMO KO cells, suggesting that NEMO is not necessary to its activation.

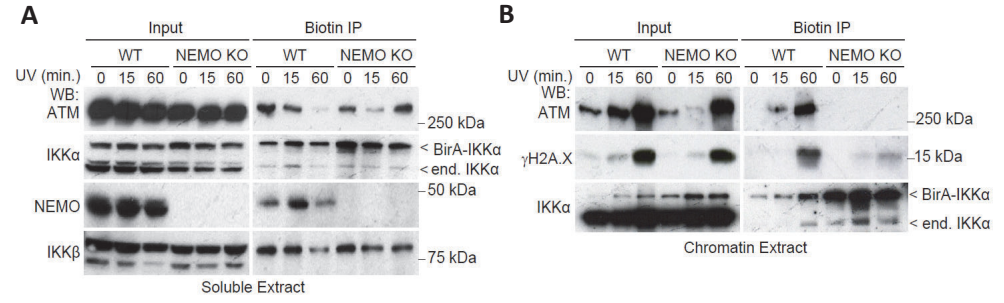

Figure R14. NEMO regulates ATM-IKKα complex translocations to DNA damage sites. Immunoprecipitation of soluble **(A)** and insoluble **(B)** biotinylated proteins from WT and NEMO KO HEK-293T cells expressing BirA-IKKα plasmid, pretreated with Biotin and treated with UV light as (130 mJ) indicated.

Altogether, these results indicate that NEMO has a role in regulating nuclear localization of ATM and IKKα, but they do not prove that NEMO is regulating IKKα activity towards ATM and DDR. To formally test this possibility, we conducted a biotin immunoprecipitation from WT and NEMO KO expressing BirA-IKKα. WB analysis of the precipitates indicate that the fraction of ATM that interacted and was biotinylated by IKKα was the one that translocates to the chromatin upon

damage in a NEMO-dependent fashion (**Figure R14A** and **R14B**). Of note, the levels of biotinylated γH2A.X were also significantly reduced in NEMO KO cells compared to WT cells, suggesting that neither active IKKα(p45) nor IKKα-associated ATM were recruited to sites of damaged DNA in the absence of NEMO (**Figure R14B**). Together these data suggest that NEMO regulates the translocation of the ATM-IKKα complex to chromatin, being necessary for the recognition of damage sites.

R4. NEMO-deficient cells are unable to repair DNA damage efficiently and are more sensitive to damaging agents.

The actual possibility that NEMO facilitated the recognition of damaged DNA by the ATM-IKKα complex and the subsequent recruitment of the DDR machinery (i.e. 53BP1) suggested to us that NEMO deficient cells would not repair DNA damage correctly. To investigate this possibility, we measure the total DNA damage in WT and NEMO KO cells treated with CT at different time points by Comet Assay. CaCo2 NEMO-deficient cells exhibited higher amount of DNA damage, even in basal conditions, that increased significantly for at least 72h, a time point when WT cells have already repaired the damage (**Figure R15A**).

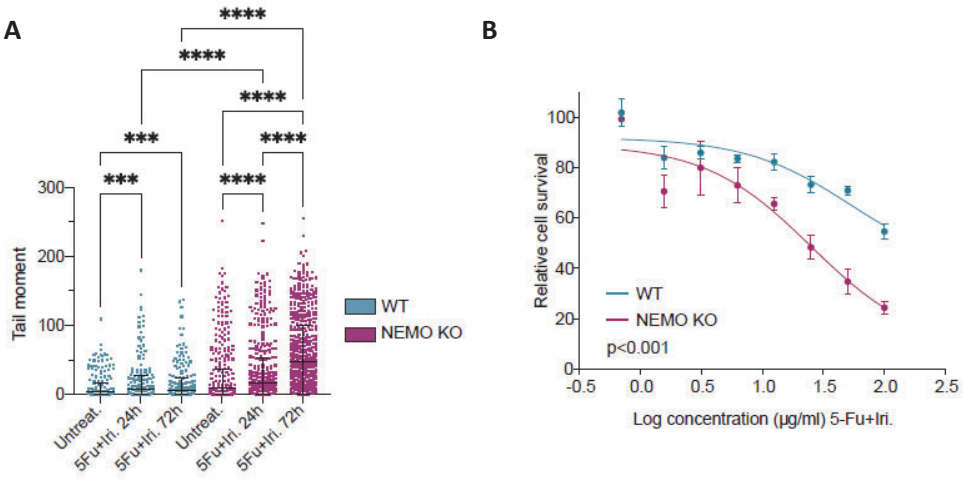

Figure R15. NEMO deficient CRC cells present higher amount of DNA damage and are more sensitive to chemotherapy treatment. (A) Comet assay of Caco2 WT and NEMO KO cells, treated with chemotherapy combination 5-Fu+Iri. (10 µg/mL + 4 µg/mL). Tail moment was measured 24h or 72h after treatment. **(B)** Dose-response curves of Caco2 WT and NEMO KO cells treated with 5-Fu+Iri. as indicated for 72h.

We anticipated that this lower capacity of NEMO-deficient cells to repair DNA damage could related with higher sensitivity to damaging treatments. As anticipated, dose-response curves of 5-FU+Iri. demonstrated that NEMO KO cells were more sensitive to CT than WT cells (**Figure R15B**). We also studied the apoptosis in these cells by flow cytometry analysis of Annexin V binding and Propidium Iodide (PI) incorporation. In our analysis, the proportion of both apoptotic (Annexin V positive) and dead cells (PI positive) increased upon UV treatment, decreasing cell viability, but without significant differences between WT and NEMO KO cells (**Figure R16A**). However, we observed a tendency of a larger apoptotic population in NEMO-deficient cells even in basal conditions (**Figure R16B**).

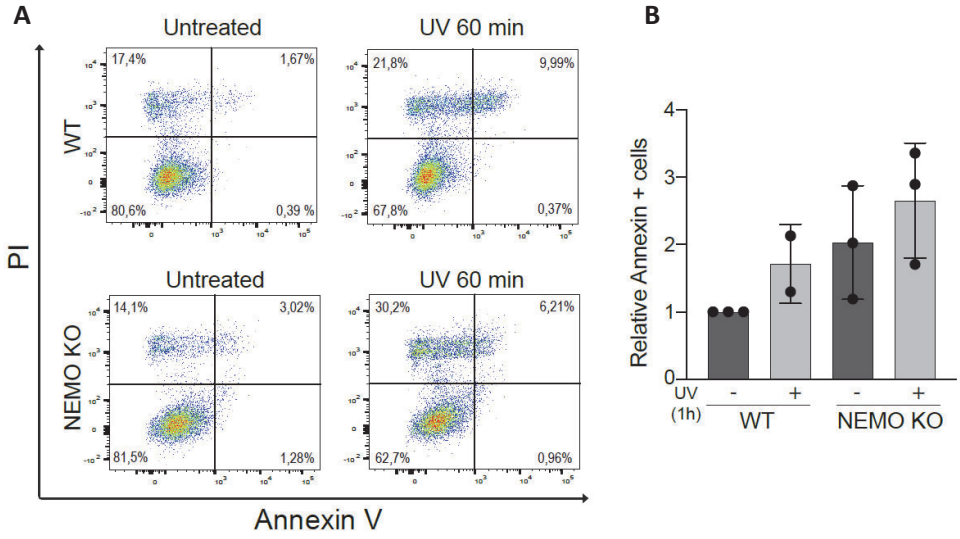

Figure R16. NEMO deficiency does not produce significant increase in apoptosis. (A) Cytometry analysis of Annexin V binding in CaCo2 WT and NEMO KO cells, untreated or exposed to UV light (130 mJ) for 1h. **(B)** Quantification of Annexin V positive cells relative to untreated CaCo2 WT cells.

We also studied the possibility that NEMO deficiency was affecting proliferation of CRC cells. Crystal violet staining of CaCo2 cells seeded at the same concentration and maintained in culture for 72 hours suggested that NEMO KO cells grow differently compared to WT cells (**Figure R17A**). By IF of Ki67 staining, a marker of proliferation, we detected that NEMO KO cells have three times less Ki67 positive cells. In untreated WT cells, the proportion of positive Ki67 cells is almost 80%, but this percentage was reduced to 20% in NEMO-deficient cells (**Figure R17B** and **R17C**). Of note, these percentages do not change upon 24h of CT treatment. Moreover, whereas these proliferative cells were distributed randomly in Caco2 WT colonies, in NEMO KO colonies Ki67 positive cells were

mainly found in the centre of the colonies. Nevertheless, by flow cytometry analysis, we did not detect any alteration in cell cycle distribution in NEMO deficient cells, just a slight accumulation of NEMO KO cells in G0 phase (**Figure R17D**).

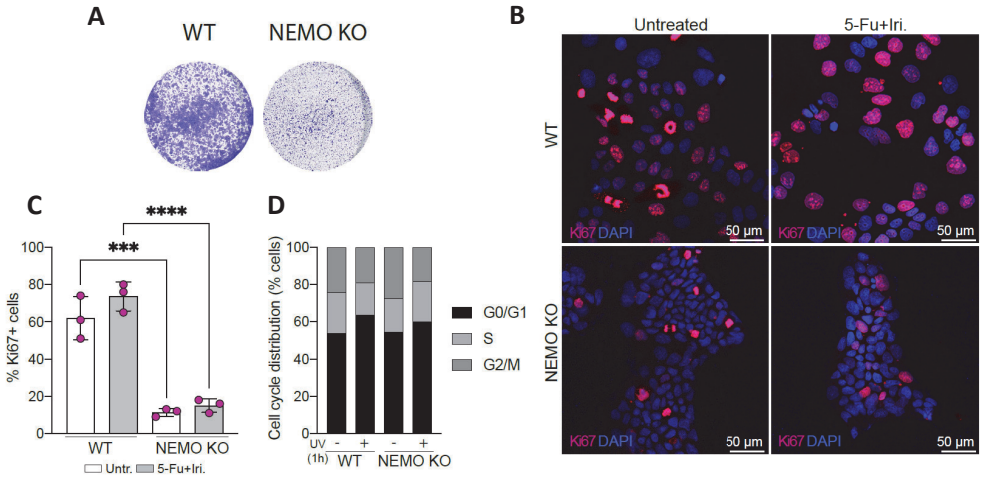

Figure R17. NEMO deficiency slows down cell proliferation but does not affect cell cycle distribution. (A) Representative image of crystal violet staining of Caco2 WT and NEMO KO cell colonies. $1x10^5$ cells were seeded and leaved growing for 72h. **(B)** Representative images of Ki67 staining in Caco2 WT and NEMO KO cells untreated or treated with chemotherapy 5-Fu+Iri. (50µg/mL + 20µg/mL, O/N). **(C)** Quantification of Ki67 positive cells. **(D)** Quantification of cell cycle distribution analyzed by flow cytometry showing DAPI incorporation of Caco2 WT and NEMO KO cells untreated or exposed to UV light.

R5. IKKα-ATM complex requires PARP1 to be recruited to DNA damage sites

NF-κB activation by genotoxic stresses requires sequential modifications of nuclear NEMO, for which the SUMO-1 ligase PIASy and ATM have been implicated. Apart from them, previous studies have demonstrated that PARP1 is also required for DNA damage induced NF-κB pathway activation, being its PARylation activity required for the recruitment of PIASy and ATM to NEMO[187]. PARP1 also acts a DNA damage sensor, promoting the recruitment and activation of repair elements to the sites of damage. We studied the activation and nuclear translocation of ATM in PARP WT, PARP1 KO and PARP2 KO SU-DHL-10 cells (B cell lymphoma cell line, provided by Jose Yelamos lab) treated with chemotherapeutic agent Doxorubicin (6h).

WB results showed that ATM activation is not PARP dependent, even though PARP1 KO cells seem to have some defect in ATM phosphorylation, as indicated by the reduction in the upper p-ATM band (**Figure R18A**). Interestingly, defective chromatin recruitment of active ATM was observed specifically in PARP1 KO cells (**Figure R18B**). In addition, IF analysis of p-ATM and γH2A.X confirmed a strong reduction in the number of cells displaying nuclear p-ATM in PARP1 KO cells upon damage, which seems to accumulate perinuclear (**Figure R19A** and **R19B**). Indeed, even though H2A.X phosphorylation was PARP-independent (**Figure R19C**), p-ATM and γH2A.X colocalization was abolished in PARP1 deficient cells (**Figure R19D**).

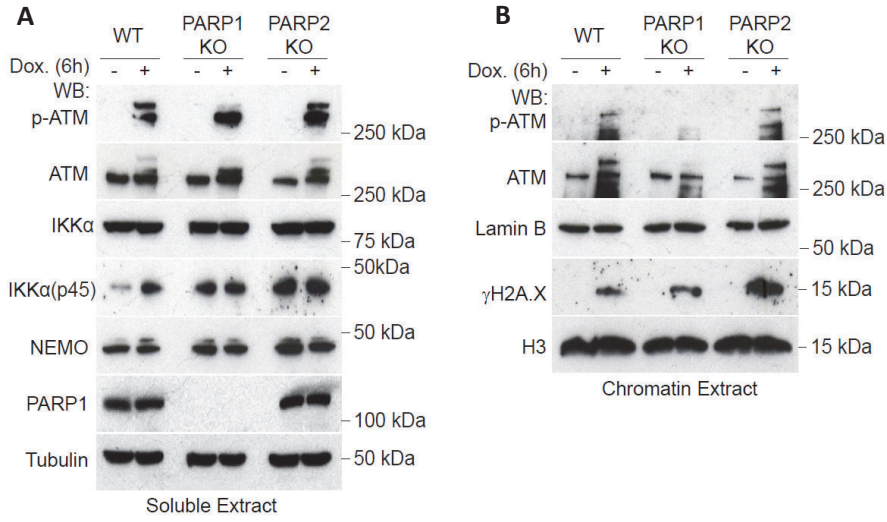

Figure R18. PARP1 is required for proper p-ATM activation and chromatin accumulation. WB analysis of soluble **(A)** and chromatin **(B)** extracts from SU-DHL-10 WT, PARP1 KO and PARP2 KO cells exposed to doxorubicin treatment (2μg/mL) for 6 hours.

Our initial mass spectrometry analysis of biotinylated proteins in the BioID-IKKα system led to the identification of PARP1 as a new IKKα interactor induced by damage (**Figure R5A** and **R20A**). Based on that observation, we hypothesized that PARP1 may also be involve in the regulation of the ATM-IKKα complex, allowing the recognition of DNA damage sites. Interestingly, using BioID method, we observed that NEMO deficiency precluded the damage-induced association of IKKα with PARP1 in the chromatin (**Figure R20B**). This defect in the IKKα-interacting PARP1 chromatin translocation in the absence of NEMO correlates with the recognition failure of DNA damage sites by ATM and IKKα.

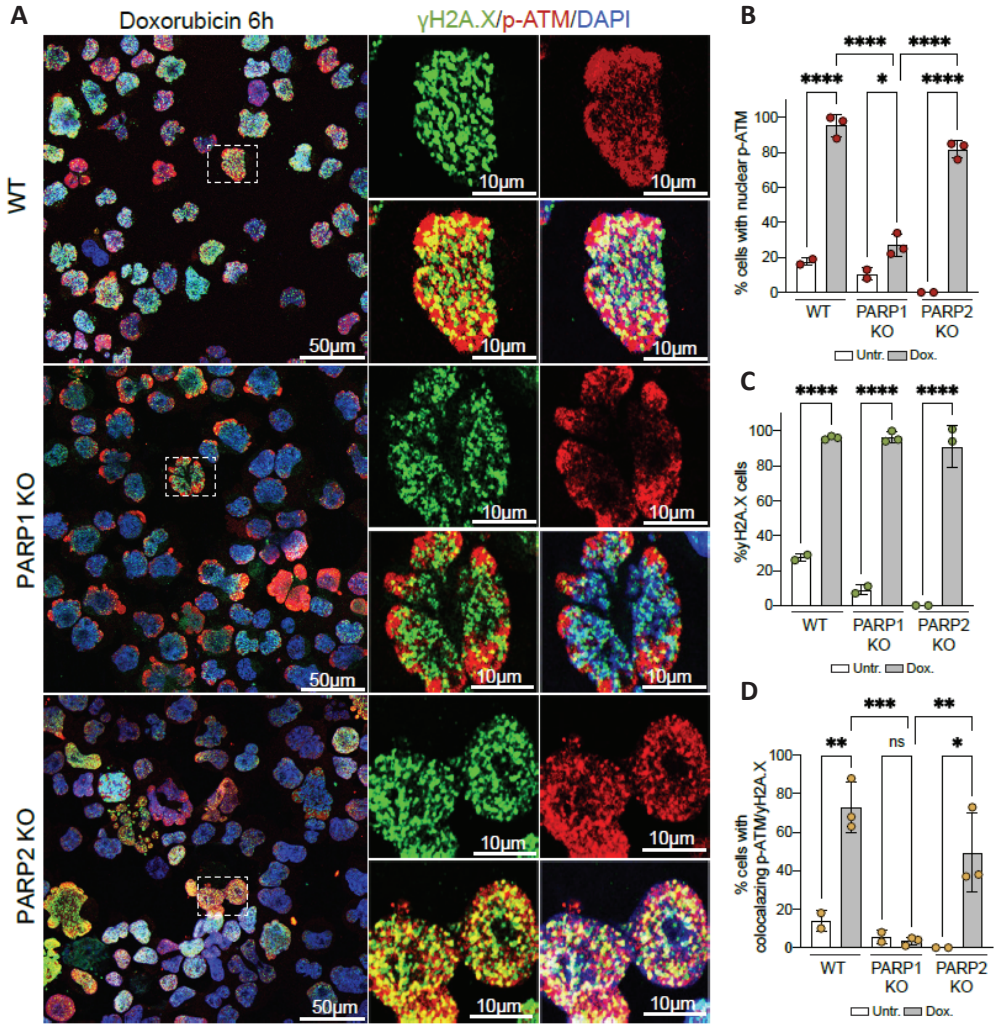

Figure R19. Active ATM fails to detect DNA damage sites in PARP1 deficient cells upon chemotherapy treatment. (A) Double immunofluorescence analysis of p-ATM and γH2A.X in SU-DHL-10 WT, PARP1 KO and PARP2 KO cells treated with doxorubicin (2μg/mL) for 6 hours. **(B-D)** Quantification of the percentage of cells positive for nuclear p-ATM **(B),** positive for γH2A.X **(C)** and percentage of cells with co-localizing p-ATM and γH2A.X **(D)**.

To study whether PARP1 activity was required for ATM recruitment DNA damaged-sites, we used the PARP inhibitor Olaparib. PARP inhibitors trap PARP1 at DNA lesions and disrupt its catalytic cycle, blocking its PARylation activity and leading to replication fork progression and consequent DSB formation. By IF we determined the levels of nuclear p-ATM in Caco2 WT and NEMO KO cells,

treated with 5-FU+Iri. alone or in combination with Olaparib. We found that inhibition of PARP activity did not affect the subsequent activation and accumulation of phosphorylated ATM in the nucleus induced by CT (**Figure R21A** and **R21B**). However, treatment with Olaparib significantly reduces the proportion of WT cells with colocalizing p-ATM/γH2A.X to the levels of CT-treated NEMO KO cells. The effect of Olaparib in p-ATM recruitment to damaged sites was attenuated in NEMO-deficient cells, which already showed reduced p-ATM/γH2A.X colocalization (**Figure R21C**).

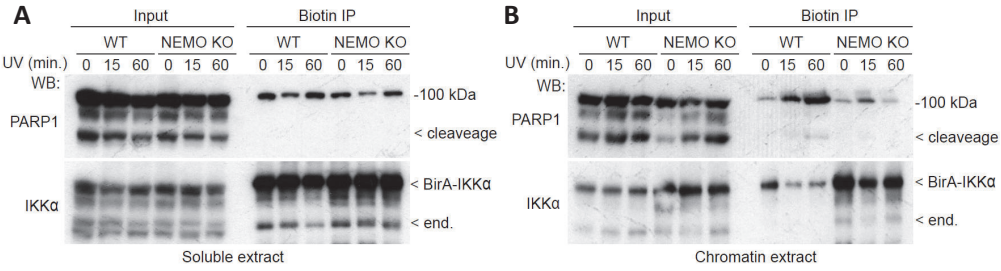

Figure R20. IKKα-interacting PARP1 requires NEMO to accumulate in damage sites. Immunoprecipitation of soluble **(A)** and insoluble **(B)** biotinylated proteins from WT and NEMO KO HEK-293T cells expressing BirA-IKKα plasmid, pretreated with Biotin and treated with UV light as (130 mJ) indicated.

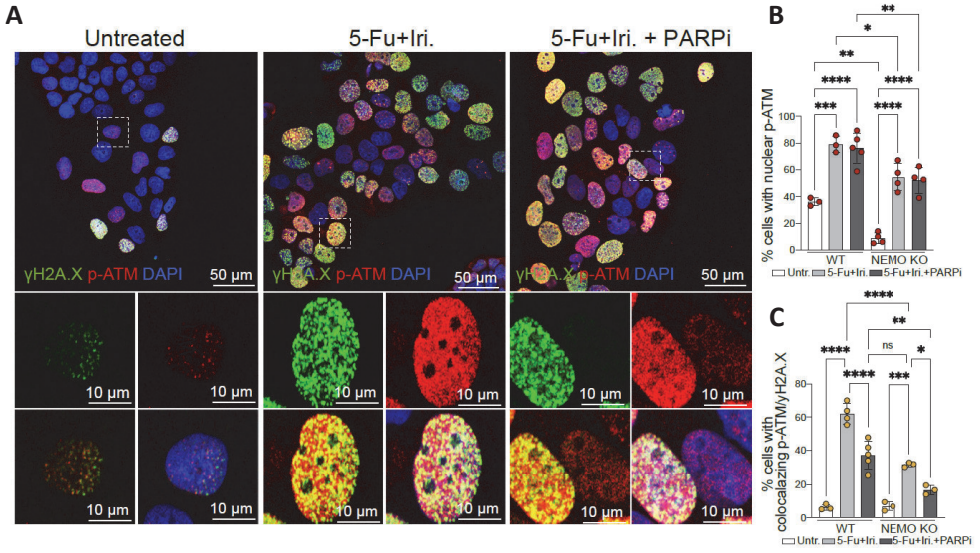

Figure R21. PARP inhibition reduces pATM/γH2A.X colocalization in CRC cells. (A) Representative images of p-ATM and γH2A.X double IF staining in CaCo2 WT cells treated with 5-Fu+Iri. (50μg/mL + 20μg/mL, O/N) alone or in combination with PARP inhibitor Olaparib (10μM, O/N). **(B and C)** Quantification of the percentage of CaCo2 WT and NEMO KO cells treated with the combination treatment displaying nuclear p-ATM **(B)** or colocalizing p-ATM and γH2A.X **(C)**.

In agreement with these results, PARP inhibition led to a significant accumulation of DNA damage upon CT treatment in NEMO WT CaCo2 cells, which was comparable to the levels observed in single agent-treated and double agent-treated NEMO-deficient cells (**Figure R22A**). Indeed, combination treatment of CT with Olaparib did not generate additional damage to NEMO KO cells. These observations indicate that NEMO-dependent PARP1 functions are involved in the recognition of damaged DNA by active ATM and correct DNA repair.

All together, these data demonstrate that NEMO and PARP1 are crucial regulators of the ATM-IKKα complex function in response to damage and that, in absence of these enzymes, the ATM-IKKα complex fails to recognize the DNA damage sites in the chromatin, thus precluding the subsequent recruitment of additional DDR elements and compromising DNA repair.

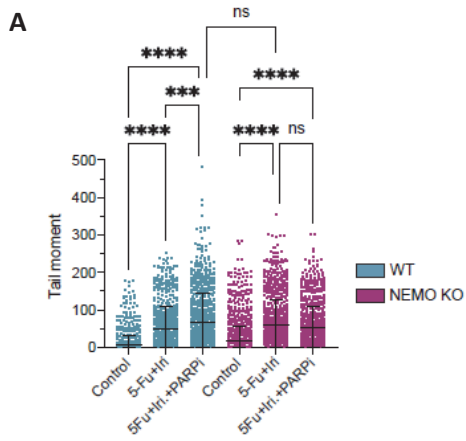

Figure R22. PARP activity inhibition increased DNA damage in CRC cells. (A) Comet assay of CaCo2 WT and NEMO KO cells, treated with 5-Fu+Iri. alone (10µg/mL + 4µg/mL) or in combination with PARP inhibitor Olaparib (2µM). Tail moment was measured after 72h of treatment.

R6. High levels of NEMO are predictive of poor prognosis in CRC patients.

Finally, we studied whether NEMO expression levels could provide information on the prognosis of CRC patients. Bioinformatic analysis of CRC public datasets Marisa (n=562, p<0.0001) and TCGA (n=329, p=0.011) demonstrated that NEMO/IKBKG levels were sufficient to identify patients displaying the poorest disease-free-survival (**Figure R23A** and **R23B**). A more detailed analysis of the Marisa dataset demonstrated that high levels of NEMO are associated with worse prognosis in patients at stages II (n=264, p=0.0011) (**Figure R24A**), III (n=205, p=0.0078) (**Figure R24B**) and IV

(n=60, p=0.028) (**Figure R24C**). Importantly, the prognosis value of NEMO was restricted to tumors carrying high ATM expression (n=295, p=0.013), being patients with ATM high and NEMO high tumors the ones with the worst disease-free survival (**Figure R25A** and **R25B**).

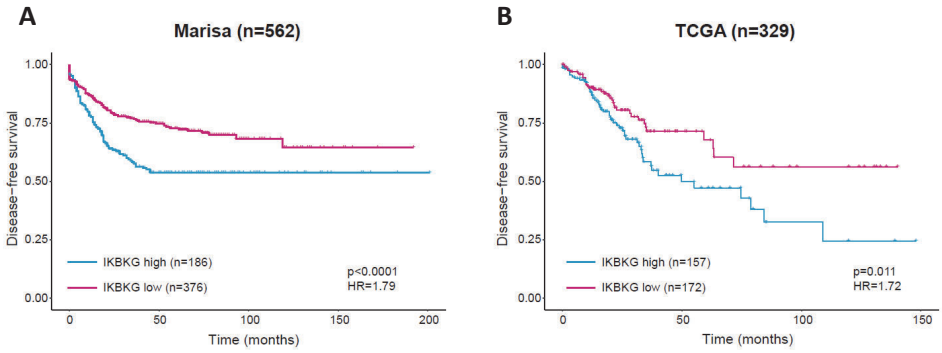

Figure R23. NEMO/IKBKG has prognostic value in CRC patients. (A and B) Kaplan-meier representation of DFS probability over time for CRC patients with high or low expression of NEMO/IKBKG in Marisa **(A)** and TCGA **(B)** datasets.

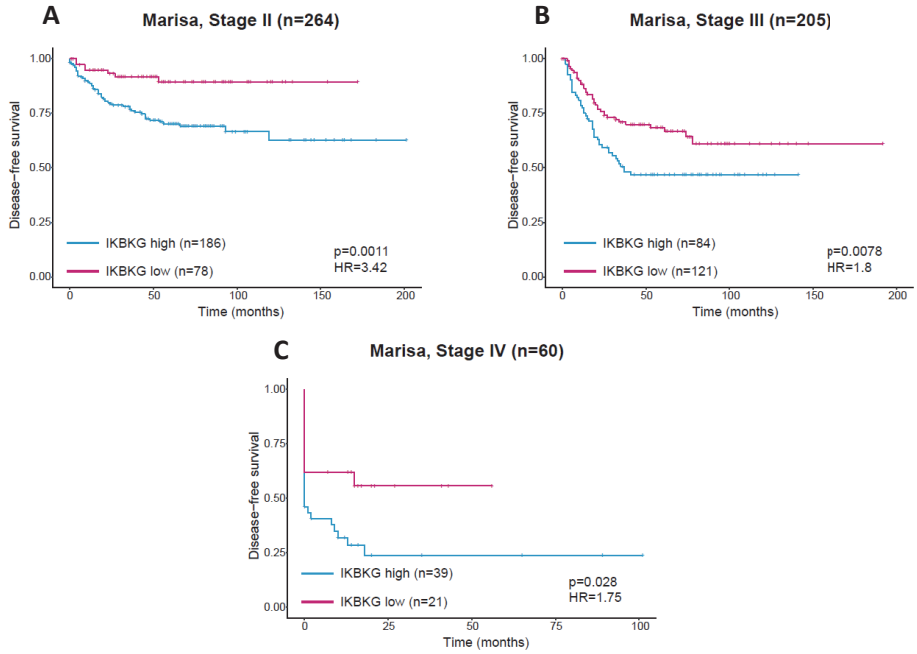

Figure R24. NEMO/IKBKG has prognostic value in stage II, stage III and stage IV patients. (A-C) Kaplan-meier representation of DFS probability over time for CRC patients classified according to NEMO/IKBKG levels of groups from stage II **(A)**, stage III **(B)** and stage IV **(C)**, from Marisa CRC dataset.

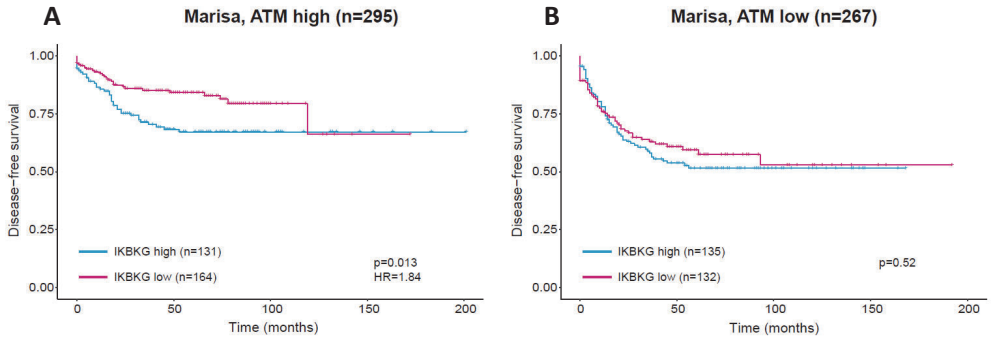

Figure R25. NEMO/IKBKG has prognostic value in CRC patients with high levels of ATM. (A and B) Kaplan-meier representation of DFS probability over time for patients with high or low expression of NEMO/IKBKG inside the group of tumors with high ATM **(A)** and low ATM **(B)** levels, from Marisa dataset.

Using the molecular classification of CRC from Guinney and collaborators[15], we found that NEMO-high tumors were categorized mostly in CMS2 (46%, n=85) and CMS4 (32%, n=59). Notably, 20% of NEMO-low tumors were categorized in CMS1 (n=76) (compared with 8% of the NEMO-high tumors (n=15) (**Figure R26A**)), which is characterized by increased microsatellite instability and high mutational load. These data are consistent with the idea that NEMO is essential for ATM function on DNA repair and genome stability maintenance.

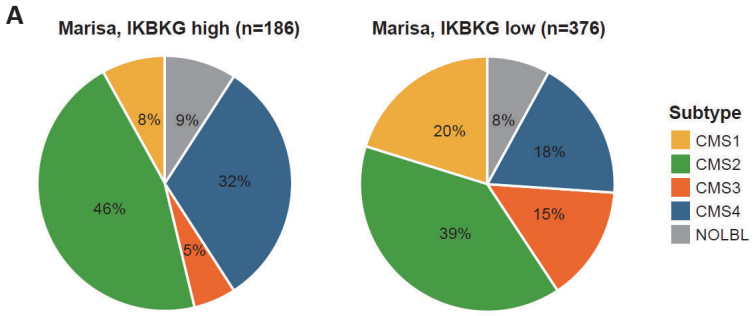

Figure R26. NEMO/IKBKG low expression is associated with higher genomic instability in CRC patients. (A) Pie charts showing the molecular subtype distribution, according to Guinney et al.[15], in patients carrying NEMO/IKBKG high and low tumors, form Marisa dataset.

RESULTS: PART II

Combination of chemotherapy with BRAF inhibitors results in effective eradication of Malignant Melanoma by preventing ATM-dependent DNA repair

Alonso-Marañón J, Villanueva A, Piulats JM, Martínez-Iniesta M, Solé L, Martín-Liberal J, Segura S, Pujol RM, Iglesias M, Bigas A, Gallardo F and Espinosa L.

Oncogene (volume 40, pages 5042–5048) (2021) DOI:10.1038/s41388-021-01879-2

Combination of chemotherapy with BRAF inhibitors results in effective eradication of Malignant Melanoma by preventing ATM-dependent DNA repair

Josune Alonso-Marañón[1,2], Alberto Villanueva[3,&], Josep Maria Piulats[4], María Martínez-Iniesta[3], Laura Solé[1,2], Juan Martín-Liberal[4], Sonia Segura[5], Ramon M. Pujol[5,2], Mar Iglesias[6], Anna Bigas[1,2,&], Fernando Gallardo[5,2,&] and Lluís Espinosa[1,2,&].

[1]Stem Cells and Cancer Research Laboratory-IMIM, Barcelona, CIBERONC, Spain.

[2]Cancer Research Program Hospital del Mar Medical Research Institute (IMIM), Barcelona, Spain.

[3]Group of Chemoresistance and Predictive Factors, Subprogram Against Cancer Therapeutic Resistance (ProCURE), ICO, Oncobell Program, IDIBELL, L'Hospitalet del Llobregat, 08908 Barcelona, Spain.

[4]Medical Oncology Department, Catalan Institute of Cancer (ICO), IDIBELL-OncoBell, Hospitalet de Llobregat, 08908 Barcelona, CIBERONC, Spain.

[5]Department of Dermatology, Institut Hospital del Mar d'Investigacions Mèdiques (IMIM) and Universitat Autònoma Barcelona.

[6]Department of Pathology, Institut Mar d'Investigacions Mèdiques, Universitat Autònoma de Barcelona, CIBERONC, Barcelona 08003, Spain.

[7]Institut Josep Carreras contra la Leucemia (IJC), Barcelona 08003, Spain

[&] Corresponding authors

Correspondence: avillanueva@iconcologia.net (A.V.), abigas@imim.es (A.B.), fgallardo@parcdesalutmar.cat (F.G.), lespinosa@imim.es (L.E.)

ABSTRACT

Invasive malignant melanoma (MM) is an aggressive tumor with no curative therapy in advanced stages. Chemotherapy has not demonstrated its efficacy in MM and current treatment for tumors carrying the most frequent BRAFV600E mutation consists of BRAF inhibitors alone or in combination with MAPK pathway inhibitors. We previously found that BRAF inhibition prevents activation of the DNA-damage repair (DDR) pathway in colorectal cancer thus potentiating the effect of chemotherapy. We now show that different chemotherapy agents inflict DNA damage in MM cells, which is efficiently repaired, associated with activation of the ATM-dependent DDR machinery. Pharmacologic inhibition of BRAF impairs ATM and DDR activation in these cells, leading to sustained DNA damage. Combination treatments involving DNA-damaging agents and BRAF inhibitors increase tumor cell death in vitro and in vivo, and impede MM regrowth after treatment cessation.

We propose to reconsider the use of chemotherapy in combination with BRAF inhibitors for MM treatment.

SIGNIFICANCE

Chemotherapy has low impact on Malignant Melanoma eradication. This lack of efficacy can be circumvented by combination treatments leading to BRAF/MEK inhibition.

INTRODUCTION

Malignant melanoma (MM) is the main cause of death by skin cancer worldwide, with about 48,000 melanoma-related deaths every year (see GLOBOCAN at http:gco.iarc.fr). MM progression primarily depends on tumor stage at diagnosis but it varies from patient to patient, likely reflecting specific characteristics of tumor cells. In advanced non-resectable MM, treatment options include MAPK and BRAF inhibitors, BRAF being the principal mutated oncogene in MM, or check-point immunotherapy. Chemotherapy (CT) or radiation therapies have shown little benefit as adjuvant or palliative strategies and alkylating agents with cytostatic activity such as temozolomide (which in the body is converted to the active metabolite MTIC that generates DNA damage through methylation of the O-6 position of guanine) are not highly active in MM. Temozolomide is able to cross the blood-brain barrier, making it useful to treat brain tumors such as glioblastoma or astrocytoma[1] and also brain metastases from different primary tumors, including MM[2]. Even though it is not an FDA approved compound, temozolomide is used for treating patients with advanced MM because of its CNS penetration and favorable toxicity profile[3]. In general, treatment choice may depend on the characteristics of the patient, the degree of dissemination of the tumor, their location in the different areas of the body and the specific weaknesses (biochemistry and genetics) of tumor cells (see https://www.mayoclinic.org/diseases-conditions/melanoma/diagnosis-treatment/drc-20374888). Despite considerable progress made in the treatment of patients with advanced MM, the majority of the patients under treatment with BRAF and MEK inhibitors experience a disease progression due to acquired resistance and new insights are needed to overcome or reverse this process. This fact highlights the importance of uncovering additional mechanisms of tumor progression and therapy resistance in MM.

As mentioned, the principal molecular pathway activated in melanocytic tumors is the MAPK, mainly associated with mutations in the serine/threonine kinase BRAF or its upstream activator NRAS. Other pathways altered in MM are CDKN2A/p16INK4A, CDK4 or p14ARF [4,5], Rac1 [6], PTEN/RAS [7] and the NF-kB kinase IKKα[8]. IKKα was found to exert multiple pro-tumorigenic functions in colorectal cancer [9–11], prostate [12], squamous cell carcinoma [13] and MM [8].

Because of the high prevalence of BRAF mutations in MM (about 50% of all MM display mutated BRAF) and its essentially contribution to tumor progression [14], several inhibitors of BRAFV600E (the principal mutated form in patients), such as Vemurafenib, Dabrafenib or Encorafenib, are currently used in the clinical practice alone or, most commonly, in combination with MEK/ERK inhibitors[15–17].

The American Food and Drug Administration (FDA) initially approved Vemurafenib (PLX4032) and Cobimetinib for advanced-stage melanoma treatment in 2011 and Dabrafenib plus Trametinib in 2013, and recently Encorafenib with Binimetinib in 2018. Paradoxically, treatment of BRAF wild type tumors with Vemurafenib results in increased MAPK signaling due to stabilization of BRAF/cRAF dimers [18,19], which can be mitigated by second-generation RAF inhibitors such as PLX7904 and PLX8394[20]. We recently demonstrated that in human colorectal cancer, BRAF not only acts through the more conventional MAPK pathway, but it is also required for IKKα activation (mainly its IKKα(p45) form) in response to damaging agents thus facilitating ATM phosphorylation and induction of ATM-dependent DNA damage repair (DDR). Consequently, BRAF or IKK inhibition in combination with CT led to irreversible DNA damage and tumor eradication both in vitro and in vivo[21].

Here, we mechanistically and functionally demonstrate the therapeutic potential of DNA damaging agents in combination with BRAF inhibitors for the eradication of MM cells. This strategy may not only prevent acquired resistance to BRAF inhibitors on those patients with BRAF-mutant MM but also offer a new therapeutic perspective for the use of BRAF inhibitors even in BRAF-WT and RAS mutated MM patients.

RESULTS AND DISCUSION

Different damaging agents activate the DDR pathway in MM cells carrying activated IKKα(p45).

We found that UV light induced DDR pathway activation in different MM cell lines as indicated by the presence of the phosphorylated forms of ATM, Chk1 and Chk2, which was associated with H2A.X phosphorylation (γH2A.X) (**Figure 1A**) in western blot (WB) assays. Different DNA damaging agents such as Temozolomide, 5-fluorouracil plus irinotecan (5-FU+iri) or ionizing radiation (IR) also imposed phosphorylation of ATM, Chk1/2 and H2A.X in SKMEL37 cells (**Figure 1B**). DDR activation by Temozolomide was time and dose dependent as shown by WB assay on SK-MEL37 cells (**Figure 1C**). In contrast with that reported in CRC cells, we detected comparable high levels of phosphorylated IKKα(p45) in untreated and treated MM cells (**Figures 1A-C**), likely as consequence of constitutive activation of the RAS/RAF pathway in these cells, which acts upstream of IKKα(p45) induction [22]. Our results indicate that MM cells are prone to activate DDR elements including ATM, Chk1/2 and H2A.X in response to different DNA damaging agents.

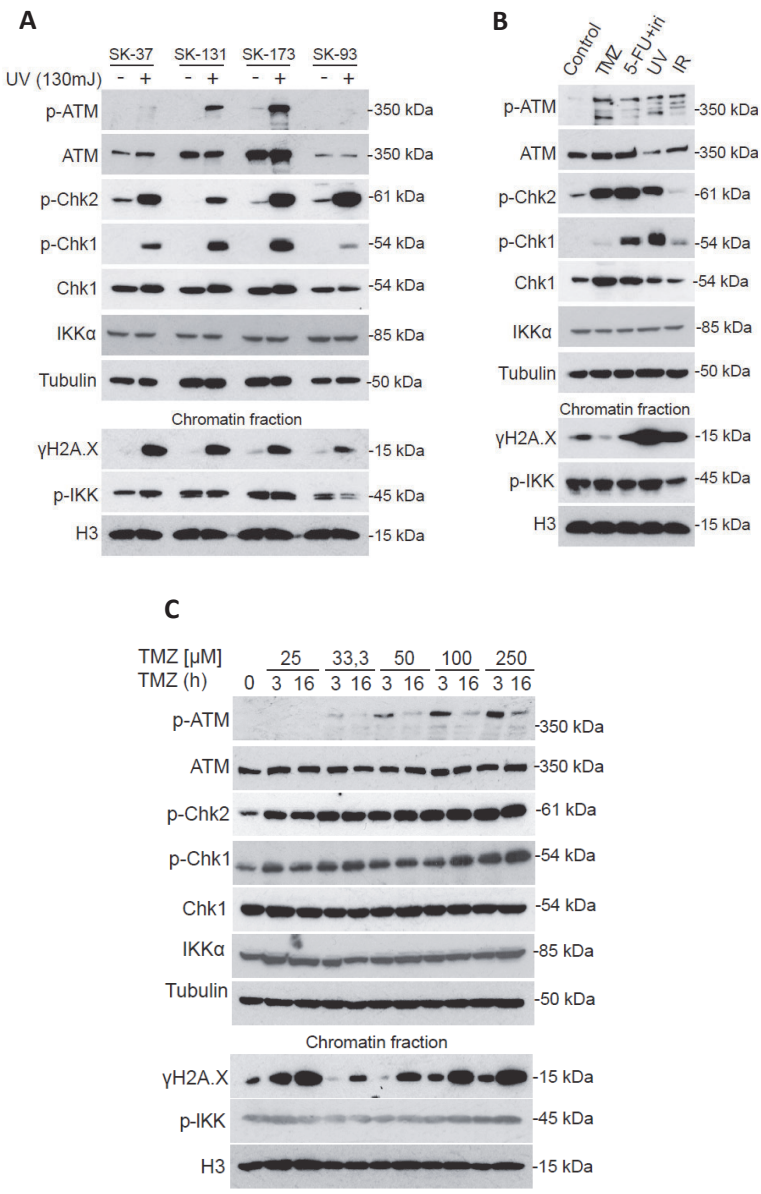

Figure 1. Different damaging agents activate the DDR pathway in MM cells carrying activated IKKα(p45). **(A)** WB analysis of four different MM cell lines (SK-MEL37, SK-MEL131, SK-MEL173 and SK-MEL93) colleted without treatment or 1h after UV exposure (130mJ). **(B)** WB analysis of SK-MEL37 treated with different DNA damaging agents: TMZ (50μM, 3h), 5-Fu+Irinotecan (50 μg/mL + 20 μg/mL, 3h), UV (130 mJ, 1h) and IR (10 Gy, 1h). **(C)** WB analysis of SK-MEL37 treated with TMZ for 3h or 16h at the indicated concentrations.

BRAF inhibition prevents ATM and DDR activation in response to DNA damage-based treatments associated with decreased IKKα induction.

We then tested whether DDR triggered by damage was dependent on BRAF and IKKα(p45) activity. Treatment of MM cells with different BRAF inhibitors imposed a variable reduction of Chk1/2 and ATM phosphorylation after Temozolomide treatment (**Figure 2A**), which parallels their specific effect on ERK1/2 and IKKα(p45) phosphorylation (**Figure 2A**) and cell growth inhibition (**Figure 2B**). In time-course assays, Vemurafenib and AZ628 similarly precluded DDR activation induced by TMZ (**Figure 2C**) and 5-FU+iri (**Figure 2D**), which was again cell line specific. In particular, whereas in the BRAF mutated cell line SK-MEL37 both inhibitors have similar effects, in the NRAS mutated cell line SK-MEL173 only the more general BRAF inhibitor AZ628 affected cell survival and DDR activation. Of note that γH2A.X levels were very variable among experiments and conditions likely reflecting that it is not only a DNA damage sensor but also a phosphorylation target of ATM.

Thus, effective inhibition of BRAF activity and IKKα(p45) phosphorylation in MM cells precludes DDR pathway function in response to DNA damaging agents.

Combination of DNA damaging agents with BRAF inhibitors imposes irreversible DNA damage and tumor cell eradication in vitro.

We speculated that limited efficacy of CT on MM might be linked, at least in part, to their DNA damage repair capacity. To test this possibility, we treated different MM cell lines with TMZ alone or in combination with the general BRAF inhibitor AZ628. Combination treatment produced a superior effect compared with single treatments in all tested MM cell lines (SK-MEL37, SK-MEL131 and SK-MEL173) after 1 week (**Figure 3A**). We observed a similar beneficial effect of drug combinations in 1-week-treatment dose response assays (**Figure 3B, left panels**). Importantly, differences between single and combination treatment were more pronounced after 72 hours of washout mainly associated with a partial reversion of single TMZ treatment effect (**Figure 3B, right panels**). These results indicate that the effects of TMZ on MM cell growth that are reversed after treatment cessation, are mainly prevented in the combination treatment with BRAF inhibitors.

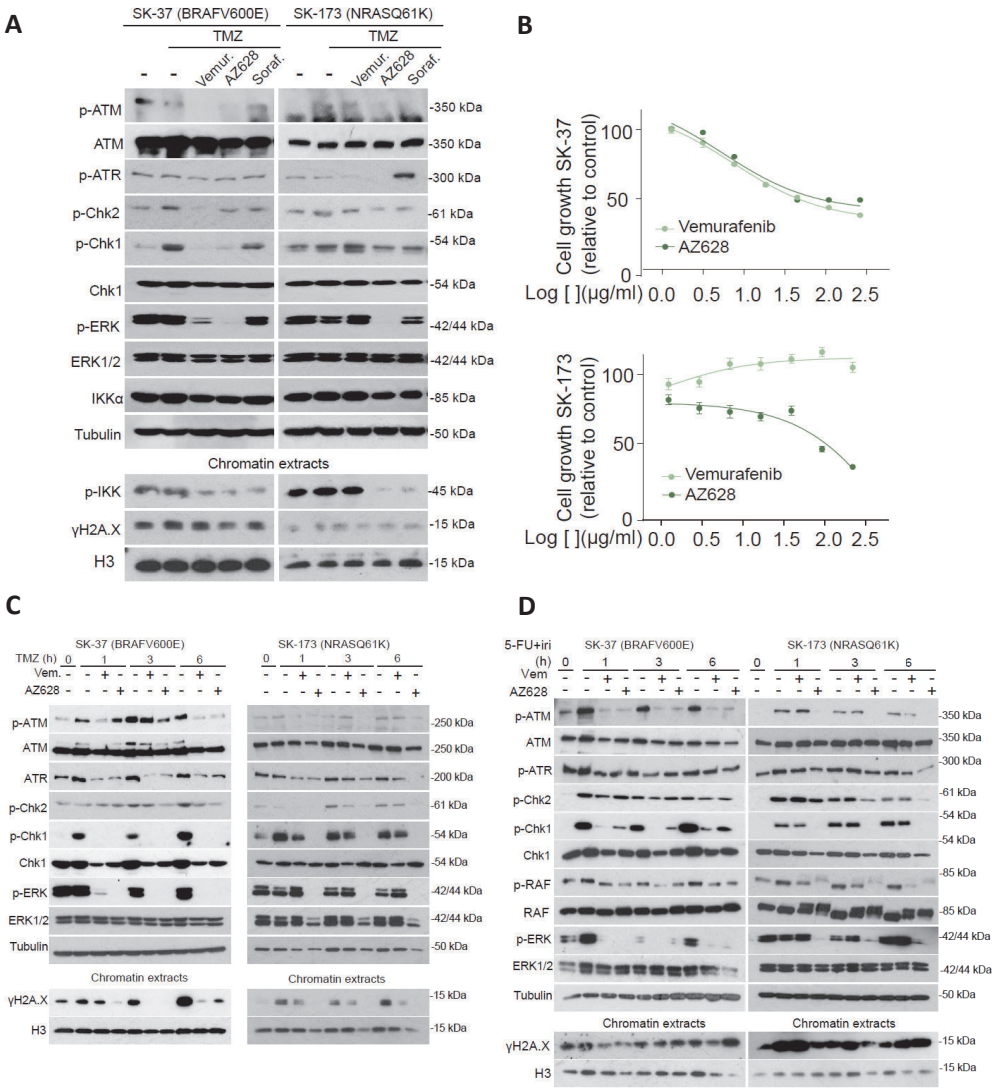

Figure 2. BRAF inhibition prevents ATM and DDR activation in response to DNA damage-based treatments. **(A**) WB analysis of SKMEL-37 and SKMEL-173 melanoma cells pre-treated with BRAF inhibitors Vemurafenib (10 µM, 16h), AZ628 (10 µM, 16h) or Sorafenib (1 µM, 16h) and then treated with Temozolomide (50 µM 3h). **(B)** Dose-response curves of two different MM cell lines (SK-MEL37 and SK-MEL173) treated for 72 hours with the BRAF inhibitors, Vemurafenib or AZ628**. (C-D)** WB analysis of SK-MEL37 and SK-MEL 173 cells treated with Temozolomide (50 µM) **(C)** or 5FU+Iri (50 µg/mL + 20 µg/mL) **(D)** for 1h, 3h and 6h alone or in combination with the BRAF inhibitors Vemurafenib or AZ628 (16h, 10 µM).

We speculated that MM cells escape from growth arrest in the single TMZ treatment as result of effective DNA repair. By Comet Assay, we determined the amount of DNA damage in SK-MEL37 cells treated under different experimental conditions. We found that TMZ treatment imposes a significant amount of DNA damage after 1 week of treatment that is completely reverted after 3 days of treatment cessation. In the combination treatment of TMZ plus AZ628 (**Figure 3C**) or Vemurafenib (**Figure 3D**), DNA damage persisted after treatment withdrawal.

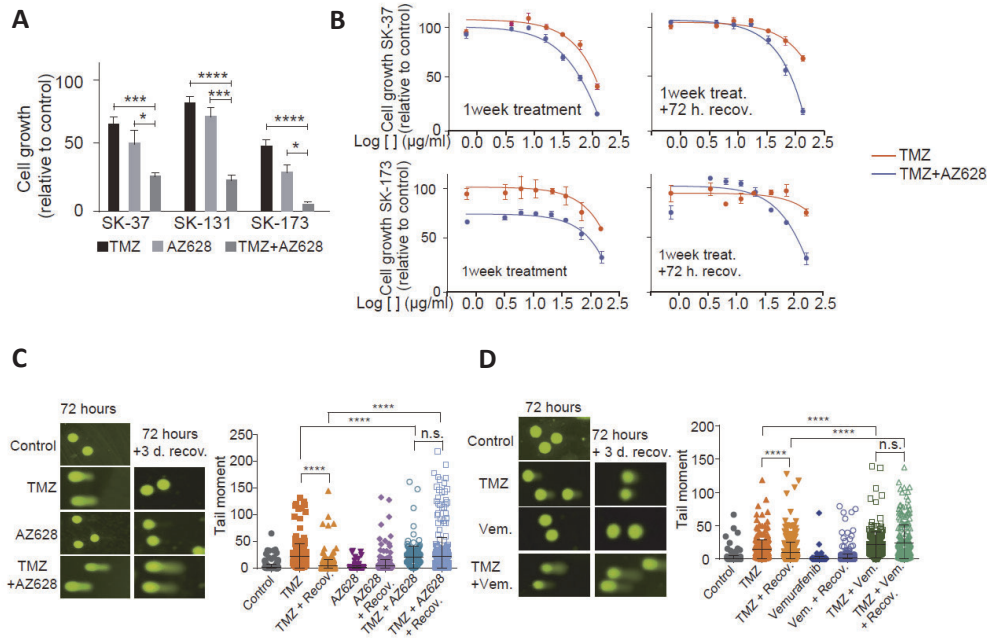

Figure 3. Combination of DNA damaging agents with BRAF inhibitors imposes irreversible DNA damage and tumor cell eradication in vitro. (A) Quantification of viability in SK-MEL37, SK-MEL131 and SK-MEL173 after treatment with Temozolomide (100 μM) and AZ628 (200 nM) for 1 week, as single treatments or in combination. **(B)** Dose-response curves of SK-MEL37 and SK-MEL173 cell lines treated as indicated with TMZ or TMZ+AZ628. Left panels show cell survival after 1 week of treatment, and right panels indicate cell survival after 1 week of treatment plus 72h of washout. **(C-D)** Comet assay of SK-MEL37 cell line treated with Temozolomide (50 μM) and AZ628 (200 nM) **(C)** or Vemurafenib (200 nM) **(D)**, alone or in combination. The tail moment was measured after 72h of treatment and 72h after treatment washout.

These results are in agreement with that obtained by Robb and collaborators in thyroid cancer cell lines carrying mutant BRAFV600E [23] and provides a mechanistic explanation for the superior effect of the combination strategy.

TMZ plus Vemurafenib treatment leads to In vivo eradication of patient-derived MM cells.

We then tested the efficacy of CT in combination with BRAF inhibitors for the eradication of patient-derived MM in vivo. We transplanted equivalent fragments of two different human MM tumors carrying the BRAFV600E mutation to nude mice. When tumors started growing, we randomly ascribed transplanted mice to the different groups of treatment: i) vehicle (n=7+5), ii) TMZ (n=6+6), iii) Vemurafenib (n=7+5) and iv) TMZ plus Vemurafenib (n=7+6). Our results demonstrated that both TMZ and Vemurafenib treatments imposed a slight delay in tumor growth when compared with vehicle treatment, which was significantly improved by the combination of TMZ plus Vemurafenib (**Figure 4A**). Analysis of tumor volume and weigh at sacrifice confirmed the higher effect of the combination treatment in comparison with TMZ and Vemurafenib alone (**Figure 4B**). More detailed analysis of tumor sections after H&E staining indicated that reduced tumor growth in the TMZ and combination treatment (TMZ plus vemurafenib) was associated to the presence of pleomorphic and anaplastic cells with enlarged nuclei, nucleoli and cytoplasms, with the combination-treated tumors displaying a significant increase in the presence of apoptotic and cariorexic cells (identified by the presence of nuclear fragment distributed throughout the cytoplasm) (**Figure 4C**). Of note that the presence of small tumors containing giant cells in the combination treated mice implies a very low tumor cellularity compared with the rest of conditions. In addition, immunohistochemistry analysis with the proliferation marker ki67 indicated a significant reduction in proliferation in the TMZ-treated tumors that was slightly higher in the TMZ+Vem treatment, which was linked to an increase in DNA damage as determine by the presence of γH2A.X positive cells (**Figure 4D**).

Together our results indicate that DNA damaging agents, which are poorly effective in the eradication of human MM, could be repurposed in therapeutic regimes with BRAF inhibitors that are currently used in the clinical practice.

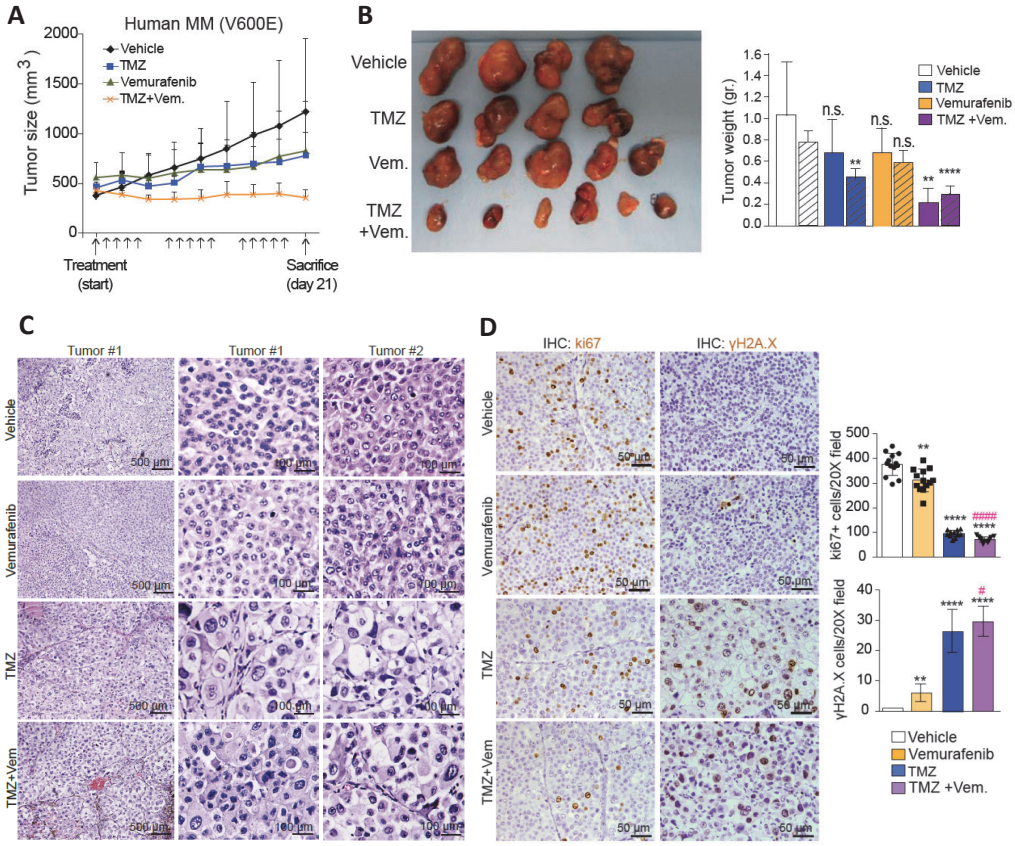

Figure 4. In vivo eradication of MM cells by combination treatment using TMZ plus Vemurafenib. (A) Growth curves of a BRAFV600E mutant patient-derived MM orthotopically implanted in nude mice and treated as indicated. Tumor volumes were determined every 2-3 days. **(B)** Photograph of tumors from each group of treatment recovered at the end of the experiment. Quantification of the weight of the tumors in the different groups of treatment (vehicle, n=7+5; TMZ, n=6+6; vemurafenib, n=7+5 and TMZ+vemurafenib, n=7+6). Dashed bars represent the analysis of a second human MM tumor analyzed. **(C)** Representative images from H&E staining of tumors in each group of treatment (low magnification images of one tumor and high magnification of two different tumors). **(D)** IHC analysis of the proliferation marker ki67 and the DNA damage marker γH2A.X and quantification of the number of ki67 and γH2A.X positive cells per 20X field from a minimum of 10 fields counted. Significance of the differences was calculated by unpaired t-test comparing the different treatments with the vehicle (*) or with single TMZ treatment (#). ****p<0.0001, **p<0.01, n.s.=non-significant.

METHODS

Cell lines

MM cell lines SK-MEL37 and SK-MEL131 (BRAF V600E) and SK-MEL173 (NRAS Q61K) were obtained from the cell line repository of Institut Mar d'Investigacions Mèdiques (IMIM). All cell lines were confirmed as mycoplasma negative by PCR, and were grown in Dulbecco's modified Eagle's medium (Invitrogen) plus 10% fetal bovine serum (Biological Industries) and were maintained in 5% CO_2 incubator at 37°C.

Cell lysis and Western Blot (WB)

Cells were lysed 20 min at 4°C in 200 µL of PBS plus 0.5% Triton X-100, 1mM EDTA, 100 mM Na-orthovanadate, 0.25 mM phenylmethylsulfonyl fluoride, and complete protease inhibitor cocktail (Roche). Lysates were analyzed by western blotting using standard SDS-polyacrylamide gel electrophoresis (SDS-PAGE) techniques. Briefly, protein samples were boiled in Laemmli buffer, run in polyacrylamide gels, and transferred onto polyvinylidene fluoride (PVDF) membranes (Millipore). The membranes were incubated overnight at 4°C with the appropriate primary antibodies. After being washed, the membranes were incubated with specific secondary horseradish peroxidase-linked antibodies from Dako and visualized using the enhanced chemiluminescence reagent from Amersham.

Cell viability assays

3000 cells were plated in 96-well plates with Dulbecco's modified Eagle's medium. After 1 day in culture, growing cells were treated with Temozolomide, AZ628 and Vemurafenib, alone or combination for 72 hours or 1 week at the indicated concentrations. Cell viability was determined using the CellTiter-Glo® 3D Cell Viability Assay (Promega) following manufacturer's instructions in an Orion II multiplate luminometer (Berthold detection systems). All the experiments were conducted in triplicate.

Comet Assay

50000 cells were plated in 12-well plates with Dulbecco's modified Eagle's medium. After 1 day in culture, melanoma cells were treated with Temozolomide alone or in combination with BRAF inhibitors AZ628 or Vemurafenib for 72 hours. Comet Assays were performed using CometAssay

Trevigen Kit (4250-050-K) following manufacturer's instructions. Pictures were taken using a Nikon Eclipse Ni-E epifluorescence microscope and tail moment was calculated using the OPENCOMET plugin for Image J.

Immunohistochemical staining (IHC)

Tissues were fixed in 4% formaldehyde overnight at room temperature and embedded in paraffin. Paraffin embedded sections of 4μm were first deparaffinized in xylene, rehydrated and endogenous peroxidase activity was blocked (20 min, 1,5%H_2O_2). IHC was performed following standard techniques with EDTA- or citrate-based antigen retrieval depending on the primary antibody used and developed with the Envision+System HRP Labelled Polymer anti-Mouse [Dako #K4001] or anti-Rabbit [Dako #K4003] and 3,3'-diaminobenzidine (DAB) from DAKO [Dako #K3468]. Images were obtained with an Olympus BX61 microscope.

Antibodies

We used antibodies against p-Chk1 (Ser345) #2348; p-Chk2 (Thr68) #2661; Chk1 #2360, p-ATR (Ser428) #2853, p-ERK (Thr202/Tyr204) #4370, ERK1/2 #9102, p-RAF #2696, BRAF #14814, p-IKK (Ser176/180) #16A6 and γH2A.X (Ser139) #2577 from Cell Signalling; p-ATM (Ser1981) 05-740 from Millipore; ATM Ab199726, IKKα Ab32041 and H3 Ab2621 from Abcam; Tubulin #T6074 from Sigma; ki67 #NCL-Ki67-MM1 from Leica Biosystems. Secondary antibodies Anti-Rabbit-HRP P0448 and Anti-Mouse-HRP P0260 were from DAKO.

Animal Studies

Fragments of human BRAF V600E mutant MM tumor obtained with the informed consent of the patient and following all recommendations of Hospital del Bellvitge Ethics Committee, the Spanish regulations, and the Helsinki declaration's Guide were transplanted and expanded in nude mice as orthoxenografts. To perform in vivo drug testing, equivalent pieces of individual tumors were implanted orthotopically as skin patches. When tumors started growing, animals were randomly ascribed to the different groups of treatment. Temozolomide (40 mg/kg) was administered intraperitoneally in 20% DMSO and Vemurafenib (75 mg/kg) was administered orally, and in the double treatment Temozolomide was given 1 hour after Vemurafenib. Animals were treated every day (expect the weekend) for 21 days and tumors measured every 2-3 days. At day 21 animals were euthanized and tumors collected, photographed and measured. In all our procedures, animals were

kept under pathogen-free conditions, and animal work was conducted according to the guidelines from the Animal Care Committee at the Generalitat de Catalunya. The Committee for Animal Experimentation at the Institute of Biomedical Research of Bellvitge (Barcelona) approved these studies.

Statistical Analysis

Statistical parameters, including number of events quantified, standard deviation and statistical significance are reported in the figures and in the figure legends. Statistical analysis has been performed using GraphPad Prism6 software (GraphPad) and $p<0.05$ is considered significant. Two-side Student's t test was used to compare differences between two groups and Two-Way ANOVA test was used to compare differences among multiple groups.

ACKNOWLEDGEMENTS

We want to thank the Bigas' and Espinosa's lab members for constructive discussions and suggestions and technical support. This work was funded by grants from Instituto de Salud Carlos III FEDER PI19/00013 to L.E., PI19/01320 to A.V. and PI19/01210 to JM.L, Generalitat de Catalunya 2017SGR135 and the "Xarxa de Bancs de tumors sponsored by Pla Director d'Oncologia de Catalunya (XBTC) and Fundacion hna to A.V. research team in the development of orthoxenografts/PDOX.

REFERENCES

1 Schreck KC, Grossman SA. Role of Temozolomide in the Treatment of Cancers Involving the Central Nervous System. Oncology (Williston Park). 2018.

2 Luke JJ, Schwartz GK. Chemotherapy in the management of advanced cutaneous malignant melanoma. *Clin Dermatol* 2013. doi:10.1016/j.clindermatol.2012.08.016.

3 Wilson MA, Schuchter LM. Chemotherapy for melanoma. In: *Cancer Treatment and Research*. 2016 doi:10.1007/978-3-319-22539-5_8.

4 Monahan KB, Rozenberg GI, Krishnamurthy J, Johnson SM, Liu W, Bradford MK *et al.* Somatic p16INK4a loss accelerates melanomagenesis. *Oncogene* 2010. doi:10.1038/onc.2010.314.

5 Buecher B, Gauthier-Villars M, Desjardins L, Lumbroso-Le Rouic L, Levy C, De Pauw A *et al.* Contribution of CDKN2A/P16 INK4A, P14 ARF, CDK4 and BRCA1/2 germline mutations in individuals with suspected genetic predisposition to uveal melanoma. *Fam Cancer* 2010. doi:10.1007/s10689-010-9379-9.

6 Krauthammer M, Kong Y, Ha BH, Evans P, Bacchiocchi A, McCusker JP *et al.* Exome sequencing identifies recurrent somatic RAC1 mutations in melanoma. *Nat Genet* 2012. doi:10.1038/ng.2359.

7 Nogueira C, Kim KH, Sung H, Paraiso KHT, Dannenberg JH, Bosenberg M *et al.* Cooperative interactions of PTEN deficiency and RAS activation in melanoma metastasis. *Oncogene* 2010. doi:10.1038/onc.2010.349.

8 Gallardo F, Padrón A, Garcia-Carbonell R, Rius C, González-Perez A, Arumí-Uria M *et al.* Cytoplasmic accumulation of NCoR in malignant melanoma: Consequences of altered gene repression and prognostic significance. *Oncotarget* 2015; **6**. doi:10.18632/oncotarget.3252.

9 Fernández-Majada V, Aguilera C, Villanueva A, Vilardell F, Robert-Moreno A, Aytés A *et al.* Nuclear IKK activity leads to dysregulated Notch-dependent gene expression in colorectal cancer. *Proc Natl Acad Sci U S A* 2007. doi:10.1073/pnas.0606476104.

10 Colomer C, Margalef P, Gonzalez J, Vert A, Bigas A, Espinosa L. IKKa is required in the intestinal epithelial cells for tumour stemness. *Br J Cancer* 2018; **118**. doi:10.1038/bjc.2017.459.

11 Margalef P, Fernández-Majada V, Villanueva A, Garcia-Carbonell R, Iglesias M, López L *et al.* A Truncated Form of IKKα Is Responsible for Specific Nuclear IKK Activity in Colorectal Cancer. *Cell Rep* 2012; **2**. doi:10.1016/j.celrep.2012.08.028.

12 Luo JL, Tan W, Ricono JM, Korchynskyi O, Zhang M, Gonias SL *et al.* Nuclear cytokine-activated IKKα controls prostate cancer metastasis by repressing Maspin. *Nature* 2007. doi:10.1038/nature05656.

13 Toll A, Margalef P, Masferrer E, Ferrándiz-Pulido C, Gimeno J, Pujol RM *et al.* Active nuclear IKK correlates with metastatic risk in cutaneous squamous cell carcinoma. *Arch Dermatol Res* 2015; **307**. doi:10.1007/s00403-015-1579-6.

14 Colombino M, Capone M, Lissia A, Cossu A, Rubino C, De Giorgi V *et al.* BRAF/NRAS mutation

frequencies among primary tumors and metastases in patients with melanoma. *J Clin Oncol* 2012. doi:10.1200/JCO.2011.41.2452.

15 Planchard D, Besse B, Groen HJM, Souquet PJ, Quoix EA, Baik CS *et al.* An open-label phase II trial of dabrafenib (D) in combination with trametinib (T) in patients (pts) with previously treated BRAF V600E–mutant advanced non-small cell lung cancer (NSCLC; BRF113928). . *J Clin Oncol* 2016. doi:10.1200/jco.2016.34.15_suppl.107.

16 Flaherty KT, Infante JR, Daud A, Gonzalez R, Kefford RF, Sosman J *et al.* Combined BRAF and MEK inhibition in melanoma with BRAF V600 mutations. *N Engl J Med* 2012. doi:10.1056/NEJMoa1210093.

17 Zaman A, Wu W, Bivona TG. Targeting oncogenic braf: Past, present, and future. Cancers (Basel). 2019. doi:10.3390/cancers11081197.

18 Poulikakos PI, Zhang C, Bollag G, Shokat KM, Rosen N. RAF inhibitors transactivate RAF dimers and ERK signalling in cells with wild-type BRAF. *Nature* 2010. doi:10.1038/nature08902.

19 Hatzivassiliou G, Song K, Yen I, Brandhuber BJ, Anderson DJ, Alvarado R *et al.* RAF inhibitors prime wild-type RAF to activate the MAPK pathway and enhance growth. *Nature* 2010. doi:10.1038/nature08833.

20 Zhang C, Spevak W, Zhang Y, Burton EA, Ma Y, Habets G *et al.* RAF inhibitors that evade paradoxical MAPK pathway activation. *Nature* 2015. doi:10.1038/nature14982.

21 Colomer C, Margalef P, Villanueva A, Vert A, Pecharroman I, Solé L *et al.* IKKα Kinase Regulates the DNA Damage Response and Drives Chemo-resistance in Cancer. *Mol Cell* 2019; **75**. doi:10.1016/j.molcel.2019.05.036.

22 Margalef P, Colomer C, Villanueva A, Montagut C, Iglesias M, Bellosillo B *et al.* BRAF-induced tumorigenesis is IKKα-dependent but NF-κB-independent. *Sci Signal* 2015; **8**. doi:10.1126/scisignal.2005886.

23 Robb R, Yang L, Shen C, Wolfe AR, Webb A, Zhang X *et al.* Inhibiting BRAF oncogene-mediated radioresistance effectively radiosensitizes BRAFV600E-mutant thyroid cancer cells by constraining DNA double-strand break repair. *Clin Cancer Res* 2019. doi:10.1158/1078-0432.CCR-18-3625.

DISCUSSION

DISCUSSION

D1. IKKα implication in DNA damage response pathway

It has been widely demonstrated that IKKα is implicated in tumor initiation and cancer progression both dependently and independently from NF-κB pathway. Specially, its nuclear-specific activities have added intricacy to its biological functions and opened the door to new mechanisms to be explored. Our group discovered a truncated form of IKKα, IKKα(p45)[209] that is localized in the nuclear compartment of cancer cells and is activated in response to damage[211]. Moreover, we demonstrated that upon damage, this active IKKα(p45) accumulates in DNA damage sites and contributes to the regulation of the DDR pathway by directly phosphorylating the DDR central element ATM[211]. In this thesis, we provided new evidence of the implication of IKKα in damage response and studied the elements involved in the regulation of this damage-induced IKKα function.

Using the novel BioID identification method, we have shown that, upon DNA damage induced by UV exposure, the interactome of IKKα changes from NF-κB-related interactors to DNA damage-related interactors, including several elements of the DDR signalling pathway, such as Chk1, Rad51, PARP1 and DNA polymerases, among others. In agreement with our results, IKKα has been previously described to be involved in p53-dependent autophagy and cell apoptosis by promoting Chk1-p53 complex formation and Chk1 activation[279,280]. Regarding DNA damage resolution, IKKα ensures NHEJ allowing 53BP1-RIF1 recruitment to DNA damage sites[211]. However, the identification of PARP1 or POLD2 in the mass spectrometry analysis suggest that it might also take part in the alternative-NHEJ repair pathway[281]. Furthermore, IKKα has also been related with HR repair pathway dysregulation through non-canonical NF-κB factor p100/p52[282,283]. These findings support the idea that the implication of IKKα in DDR signalling is beyond ATM activation.

Interestingly, we here describe the presence of a complex containing ATM and IKKα, which is stably formed in basal conditions and functions in response to damage preserving efficient DNA repair. As mentioned, previous mass spectrometry analysis of our group identified four residues of ATM (Ser1974, Ser1987, Ser2058 and Thr2059) which are direct substrates of IKKα phosphorylation upon UV exposure[211]. These four sites are distinct from ATM auto-phosphorylation sites, that includes the activation marker Ser1981[284]. However, IKKα deficiency precludes ATM phosphorylation at Ser1981 indicating that IKKα-mediated ATM phosphorylation is essential for subsequent ATM activation. We propose that phosphorylation of Ser1974, Ser1987, Ser2058 and Thr2059 by IKKα may induce a

conformational change that facilitates Ser1981 auto-phosphorylation. On the other hand, ATM has been also described to phosphorylate IKKα at Ser473 in response to cisplatin-induced damage[285]. The phosphorylation of this residue might not be related with IKKα activation, as the inhibition of ATM activity does not abrogate the phosphorylation of IKKα(p45) at Ser180[211], but it has been shown to be essential for the nuclear translocation of IKKα upon treatment[285]. This intricated relationship between IKKα and ATM and the cellular necessity to act rapidly to overcome damage enforce the idea of a IKKα-ATM complex formed previous to damage. Then, after DNA damage generation, IKKα, and subsequently ATM, will be activated downstream BRAF/TAK1/p38-MAPK and both elements will be translocated to the nucleus and accumulated in DNA damage sites, allowing the recruitment and activation of other DDR elements involved in DNA repair (**Figure D1**).

Previous publications demonstrated that the activation of IKKα(p45) is independent of NF-κB pathway since it is independent of IKKβ and NEMO presence[211]. However, at that time, we could not discard NEMO involvement in the IKKα-ATM complex regulation. As observed in the size exclusion chromatography assay, NEMO and ELKS coelute with IKKα(p45) and ATM in the same fractions in untreated and UV-exposed cells. In contrast, the coelution of IKKα-ATM and NEMO with IKKβ is reduce to one fraction upon UV treatment, supporting the concept that IKKβ is not involved in damage-dependent IKKα function. Moreover, the protein-protein interaction network from the MS data showed that NEMO is localized at the crossroad of the different condition nodes suggesting that it may play a role in the transfer from NF-κB-related interactors to DDR-related interactors.

D2. NEMO as a guide-dog for the recognition of damaged DNA by IKKα-ATM complex upon treatment.

NEMO is the regulatory element of IKK complex and is essential for canonical NF-κB activation ensuring the activity of IKKβ towards IκBα[278]. Similar to IKKα, NEMO has also been shown to shuttle between cytoplasm and the nucleus. Indeed, nuclear NEMO links the DDR pathway and NF-κB pathway via ATM[182]. Our group has already demonstrated that NEMO associates with nuclear IKKα(p45) and supports its function in the chromatin[209]. We now propose that NEMO acts also as the essential regulator of IKKα-ATM complex function (**Figure D1**).

In accordance with previous results, IKKα(p45) activation in response to damage is independent of the presence of NEMO, as well as the phosphorylation of ATM and other key DDR elements such as Chk1, Chk2 and γH2A.X. However, NEMO deficiency impairs nuclear translocation of the IKKα-ATM

complex leading to defective recruitment of activated ATM to the sites of DNA damage upon treatment. Nuclear export inhibition by CRM1 inhibitor did not result in the accumulation of nuclear ATM in NEMO KO cells, indicating that NEMO is necessary for the nuclear import of ATM. Moreover, by IF analysis, we not only observe that in the absence of NEMO there is less nuclear total ATM, but also that the remaining nuclear ATM is not able to localize the DNA damage sites in the chromatin (marked by γH2A.X dots) generated by different damaging treatments such as UV exposure and CT combination 5-Fluorouracil plus Irinotecan. This failure in the recognition of DNA damage sites might be related with a dysregulation of DNA damage sensors MRE11-RAD50-NBS1 (MRN complex) or PARP1. MRN complex is essential for detecting DBS and inducing the recruitment and activation of ATM[60]. We found that NEMO deficient cells fail to promote MRE11 and PARP1 transcription upon damage, which could contribute to the phenotype observed in the NEMO KO cells. However, further investigation of the protein levels of these sensors is required to obtain a conclusive explanation of p-ATM recruitment failure.

One question that this work opens is how ATM could be activated if it is not able to be recruited to damage sites. Classically, inactive ATM homodimers are recruited to DSBs in an MRN-dependent manner. MRN complex favours the recruitment of TIP60 that will acetylate ATM homodimers, inducing its autophosphorylation in different residues and promoting ATM monomerization[286]. However, apart from this canonical pathway, it has been described that ATM could be activated though different mechanisms. The crosstalk between different PIKK members could explain proper ATM nuclear activation, as it has been widely demonstrated that they are able to phosphorylate each other upon different stresses[287–290]. Indeed, NEMO deficient cells showed higher levels of ATR and DNA PKc that might compensate the ATM failure in damage sites and explained the comparable phosphorylation levels of H2A.X[291,292]. Furthermore, ATM could also be activated directly in the cytoplasm. For instance, it is described that in response to ROS presence cytoplasmatic ATM is activated[293].

Following this line, we propose that the lack of difference in the ATM activation in NEMO deficient cells could also be explained by cytoplasmatic activation downstream BRAF and IKKα. In response to UV exposure, IKKα(p45) is activated downstream BRAF, TAK1 and p38-MAPK in the cytoplasm and then this active IKKα(p45) is the one that translocates to the nucleus and go to damaged chromatin[211]. We have consistently shown that the interaction of ATM and IKKα is stable in basal conditions and is not dependent of NEMO. Thus, upon damage active IKKα(p45) will be able to

phosphorylate ATM. However, NEMO seems to be required for the translocation of this active IKKα-ATM complex to DNA damage sites. In fact, in the absence of NEMO, this complex maintains quite stable in the soluble cell fractions. Surprisingly, in the absence of NEMO there is an accumulation of endogenous IKKα in the chromatin extract, even though it fails to interact with γH2A.X, suggesting that effective DNA repair is linked to IKKα chromatin dissociation. Nevertheless, in order to elucidate the exact mechanism by which ATM is activated in NEMO deficient cells further investigation is required.

D3. Essential contribution of NEMO for proper DNA repair, treatment response and patient outcome.

Our observations unequivocally revealed that NEMO is required for a correct recruitment of ATM to damage sites. ATM is the master transducer of DDR signalling, since it recruits and activates numerous substrates involved in DDR and DNA repair. For that reason, it could be expected that NEMO deficient cells present defects in specific DNA repair mechanisms, such as NHEJ or HR, thus leading to increased genome instability. In this work we have not study deeply the impact of NEMO deficiency in these different DDR pathways. However, we certainly observe a reduction in the activation and recruitment of 53BP1 to DNA damage sites, suggesting that NHEJ might be affected. The impairment of DNA repair mechanisms is followed by the accumulation of total DNA damage in NEMO deficient cells, which correlates with higher sensitivity to treatment and increased cell death. Of note, even though NEMO KO cells showed more apoptotic cell population, significant differences were not observed.

In addition, we observed that NEMO deletion strongly reduced the ability of the cells to form cell colonies. IF analysis of the proliferation marker Ki67 confirmed that NEMO KO showed significantly smaller number of proliferative cells, which were found mainly in the inside of the colony, resulting in a peculiar growth expansion in culture plates. However, comparative analysis of cell cycle phase distribution did not show differences between WT and NEMO KO cells, confirming that this characteristic is independent from ATM cell cycle checkpoint function and might be related with other NEMO functions, since the cytoplasmatic ATM activity is not dependent of NEMO.

From a clinical perspective, ATM is one of the most commonly aberrant genes in sporadic cancers, however only a 10-15% of CRC tumors show mutations in ATM and they are not associated with patient prognosis[294,295]. CRC tumors are commonly characterized by chromosomal (CIN) and

microsatellite instability (MSI), associated with defective DNA repair mechanisms[6,296], which in the new molecular classification system are categorized in the CMS1 group[15]. In this study, we have provided proof-of-concept that ATM requires NEMO for its DNA repair function, being essential for maintaining genomic fidelity. In line with this findings, analysis of NEMO expression in CRC patients demonstrated that a higher percentage of patients with tumors with low expression of NEMO are categorized in this CMS1 subgroup (around 20% of patients), compared to patients with high NEMO levels (8% of patients).

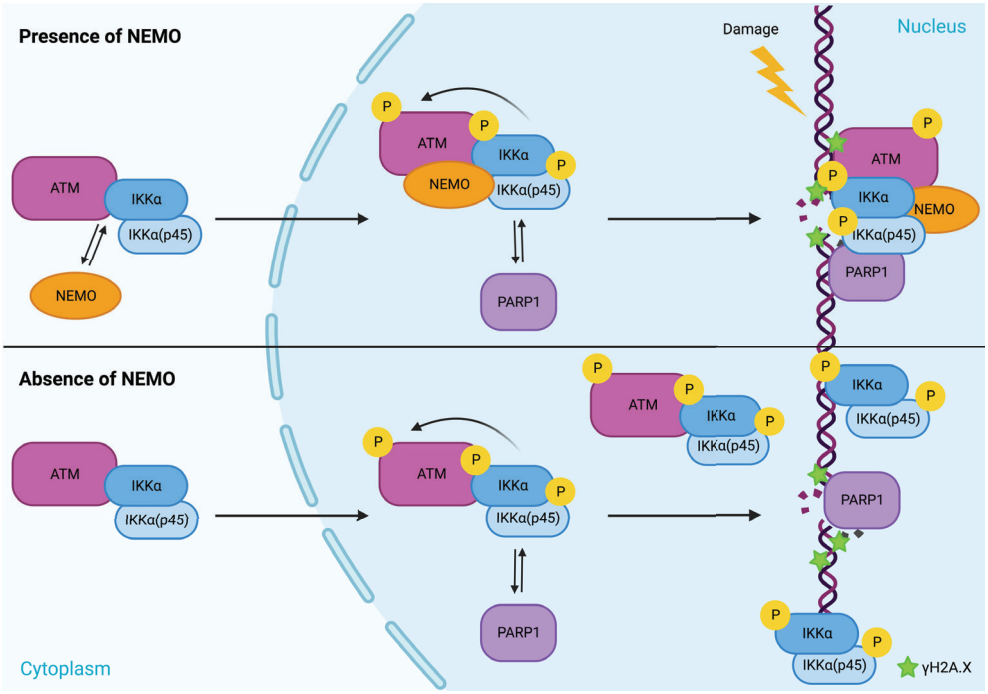

Figure D1. Schematic representation of the working model. In basal conditions, IKKα and ATM are forming a complex. Upon damage, NEMO is recruited to this complex and regulates the translocation of active ATM and IKKα to DNA damage sites. For detecting damage sites PARP1 activity is required. In the absence of NEMO, DNA is not effectively repaired, resulting in DNA damage accumulation and increased cell death. Created with BioRender.com.

Further bioinformatic analysis of different public data sets demonstrated that NEMO has prognostic value in CRC, since high levels of NEMO were associated with poorest disease-free-survival in general, but also specially in the subset of stage II patients, which is particularly relevant for the clinical context. The prognostic significance of NEMO in the outcome has already been observed in

uveal melanoma[297], but without explanation of the underlying mechanism. Importantly, and in accordance with our *in vitro* results, the prognosis value of NEMO was restricted to patients with high ATM expression tumors. Indeed, the patients with high NEMO and high ATM expression are the ones with the worst disease-free survival, which could be related with treatment resistance development due to their higher DNA repair capacity.

D4. PARP1 as the new player of IKKα-ATM-NEMO complex: therapeutic implications.

To date there is no evidence that NEMO has the ability of sensing DNA damage by itself. Therefore, the question we tried to answer was: how NEMO detects and drives the ATM- IKKα complex to the DNA damage sites? Generally, DSBs ends are recognised and bound by DNA damage sensors such as MRN complex members, Ku70-Ku80 complexes or PARP1[41]. PARP1 is also required for damage-induced NF-κB pathway activation, being its PARylation activity essential for the recruitment of elements to NEMO, including ATM[187]. The mass spectrometry analysis revealed that PARP1 is one of the damage-related IKKα new interactors, whose interaction increase response to UV exposure. However, in the absence of NEMO, the accumulation of IKKα-interacting PARP1 in the chromatin is compromised. This decrease in the levels of PARP1 in the chromatin explains the defect of the recognition of damage sites by ATM-IKKα complex in NEMO deficient cells. Indeed, depletion of PARP1, but no PARP2, totally abrogates the recruitment of active ATM to damage sites. Therefore, if in the absence of PARP1, NEMO is not able to bind to the chromatin, DNA damage will not be adequately sensed and signalled, and as a consequence, active ATM and IKKα will not be recruited thus compromising DNA repair (**Figure D1**).

The discovery of PARP1 as a second regulator of ATM-IKKα complex activity opens the door to new strategies for blocking the DDR-related IKKα function (**Figure D2**). For a long time, inhibitors of IKK members, including NEMO, have been tried to be developed to block their association with inflammation and tumorigenesis[298–300]. The majority of them are not very specific of one isoform and showed significant toxicity and side effects associated with NF-κB inhibition. Recently, several chemical compounds specific for IKKα inhibition were reported[301], however further investigation is required to be presented as new possible drugs for cancer treatment. Importantly, PARP inhibitors are already approved for cancer treatment, being especially efficient for HR-deficient cancer patient treatment by exploiting synthetic lethality[118]. We here have demonstrated that pretreatment of CRC cells with clinically approved PARP inhibitor Olaparib before CT treatments mimics NEMO

deficiency, blocking the ATM recognition of damaged sites and enhancing DNA damage up to NEMO KO cell levels treated with CT alone.

PARP inhibitors are not presently approved for CRC patient treatment, even though several studies and clinical trials have shown promising results of the viability of PARP inhibitors for improvement of response to current therapy regimens in CRC patients[302]. Specially, CRC tumor cells carrying inactivating mutations in ATM have increased sensitivity to PARP inhibition, which has also been found in gastric and lung cancers[303–305]. In line with this, it has been postulated that cells that exhibit MSI and CIN may also be susceptible to PARP inhibition[306]. For that reason, we propose that CRC patients categorized in the subgroup CMS1 could be perfect receptors of combination treatment of DNA damaging agents and PARP inhibitors, including patients with low NEMO expression levels. Oddly, PARP inhibition has not incremental effect in NEMO KO cells in the accumulation of DNA damage. Further investigation will be required, but a plausible explanation could be the gain of function of other DDR elements, such as ATR or DNA PKc, to compensate the deficiency of ATM in NEMO lacking cells. If this is the case, the combination of PARP inhibitors with DDR inhibitors (ATR inhibitors or DNA PKc inhibitors) could enhance tumor killing and overcome therapy resistance[307,308].

D5. Clinical applications of inhibition of damage-related IKKα function.

In the second part of this thesis, we study the possibility to extrapolate the previous results obtained in CRC to other solid tumors. Our group has consistently demonstrated that the nuclear truncated form of IKKα, IKKα(p45), has important alternative protumoral role in damage response and DNA repair. As mentioned above, IKKα(p45) is activated in response to damage downstream BRAF and, as we now have revealed, its function is regulated by NEMO and PARP1. Therefore, the inhibition of BRAF block the activation of IKKα(p45), abrogating the activation of key DDR elements, compromising DNA repair and potentiating the effect of CT against CRC tumor cells, both *in vitro* and *in vivo.* BRAF inhibitors are widely used in clinical practice, especially for the treatment of BRAF-mutated metastatic melanoma patients. Contrary to BRAF inhibitors, DNA damaging agents such as CT or radiotherapy have been shown very little benefit and are usually used for palliative therapy. For that reason, we aimed to investigate the potential benefits of combining BRAF inhibitors with chemotherapy treatment in Malignant melanoma (MM).

We demonstrated that DDR activation upon damage in MM cells was independent from cell BRAF status. However, the ability of BRAF inhibitors to block DDR activation it was BRAF status-dependent. For cell lines carrying BRAFV600E common mutation clinically approved inhibitor Vemurafenib was able to abrogate ATM activation and decrease cell viability. In contrast, melanoma cells with mutations in NRAS, upstream activator of BRAF, were resistant to Vemurafenib, even though comparable results were obtained when a more general BRAF inhibitor (AZ628) was used. Thus, it could not be totally discarded the potential of combination treatment in melanoma patients with NRAS mutations or non-BRAFV600E mutation through the development of more specific chemical inhibitors[309,310].

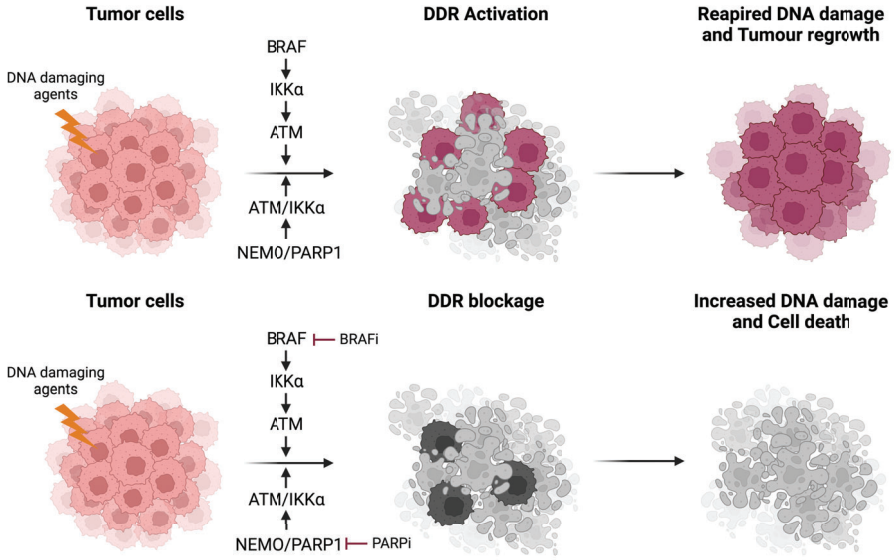

Figure D2. New therapeutic propose model. Combination DNA damaging agents in combination with chemical inhibitors of IKKα-ATM-NEMO axis, such as BRAF inhibitors or PARP inhibitors, prevents the correct function of DDR pathway, increasing the antitumoral effect of DNA damage agents for the eradication of cancer cells. Created with BioRender.com.

In addition, we have demonstrated, not only that treatment of melanoma cells with BRAF inhibitors generates more DNA damage and increase cell death upon CT treatment, but also that BRAF inhibition blocks the capacity of cells to repair damaged DNA though the abrogation of DDR activation (**Figure D2**). Consequently, cell cycle is not restored thus abolishing the possibility of

tumor cell regrowth, which is associated with tumor relapse. This superior effect of the combination therapy was confirmed *in vivo,* therefore we propose the reevaluation of chemotherapy as treatment option for advanced MM patients in therapeutic regimes with BRAF inhibitors.

Altogether, our data demonstrate that inhibition of IKKα-ATM-NEMO axis with chemical inhibitors that block the activation of DDR elements (such as BRAF inhibitors) or dysregulate the recognition of damage sites (such as PARP inhibitors) could be proposed in combination with DNA damaging agents a new therapeutic strategy for cancer patients (**Figure D2**).

CONCLUSIONS

CONCLUSIONS

PART I- The impact of NEMO in the regulation of damage-related IKKα function

1. IKKα is in a complex with ATM and NEMO under non-damaged conditions
2. The interactome of IKKα changes in response to DNA damage.
3. NEMO is not necessary for the activation of IKKα(p45), ATM and other DDR elements such as Chk1/2 upon treatment with damaging agents.
4. NEMO is essential for the translocation of the active ATM-IKKα complex to the sites of damage.
5. NEMO requires PARP1 activity for the recognition of damage sites leading to effective DNA damage resolution.
6. High levels of NEMO are predictive of poor prognosis in CRC patients.

PART II- New therapeutic strategies for Malignant melanoma (MM) patients

1. Combination of DNA damaging agents and chemical inhibitors of IKKα-ATM-NEMO axis represents a new therapeutic strategy for MM patients.
2. Activation of ATM and downstream DDR elements is reduced in MM cells upon BRAF inhibition.
3. BRAF inhibition induces accumulation of DNA damage in MM cells.
4. Combination treatment of chemotherapy and BRAF inhibitors increase MM cell death *in vitro* and *in vivo* and impede tumor regrowth.

BIBLIOGRAPHY

BIBLIOGRAPHY

1. Sung, H. *et al.* Global Cancer Statistics 2020: GLOBOCAN Estimates of Incidence and Mortality Worldwide for 36 Cancers in 185 Countries. *CA Cancer J Clin* **71**, 209–249 (2021).

2. Dekker, E., Tanis, P. J., Vleugels, J. L. A., Kasi, P. M. & Wallace, M. B. Colorectal cancer. *The Lancet* **394**, 1467–1480 (2019).

3. Dow, L. E. *et al.* Apc Restoration Promotes Cellular Differentiation and Reestablishes Crypt Homeostasis in Colorectal Cancer. *Cell* **161**, 1539–1552 (2015).

4. Keum, N. N. & Giovannucci, E. Global burden of colorectal cancer: emerging trends, risk factors and prevention strategies. *Nature Reviews Gastroenterology & Hepatology* **16**, 713–732 (2019).

5. Kuipers, E. J. *et al.* Colorectal cancer. *Nature Reviews Disease Primers* **1**, 1–25 (2015).

6. Nguyen, H. T. & Duong, H. Q. The molecular characteristics of colorectal cancer: Implications for diagnosis and therapy (review). *Oncol Lett* **16**, 9–18 (2018).

7. Fearon, E. R. Molecular genetics of colorectal cancer. *Annual Review of Pathology: Mechanisms of Disease* **6**, 479–507 (2011).

8. Li, S. K. H. & Martin, A. Mismatch Repair and Colon Cancer: Mechanisms and Therapies Explored. *Trends Mol Med* **22**, 274–289 (2016).

9. Bakhoum, S. F. & Cantley, L. C. The Multifaceted Role of Chromosomal Instability in Cancer and Its Microenvironment. *Cell* **174**, 1347–1360 (2018).

10. Shen, L. *et al.* Integrated genetic and epigenetic analysis identifies three different subclasses of colon cancer. *Proc Natl Acad Sci USA* **104**, 18654–18659 (2007).

11. Huang, Z. & Yang, M. Molecular Network of Colorectal Cancer and Current Therapeutic Options. *Front Oncol* **12**, 1360 (2022).

12. Schmitt, M. & Greten, F. R. The inflammatory pathogenesis of colorectal cancer. *Nature Reviews Immunology* **21**, 653–667 (2021).

13. O'Connell, J. B., Maggard, M. A. & Ko, C. Y. Colon Cancer Survival Rates With the New American Joint Committee on Cancer Sixth Edition Staging. *JNCI: Journal of the National Cancer Institute* **96**, 1420–1425 (2004).

14. Nagtegaal, I. D., Quirke, P. & Schmoll, H. J. Has the new TNM classification for colorectal cancer improved care? *Nature Reviews Clinical Oncology* **9**, 119–123 (2011).

15. Guinney, J. *et al.* The consensus molecular subtypes of colorectal cancer. *Nature Medicine* **21**, 1350–1356 (2015).

16. McQuade, R. M., Stojanovska, V., Bornstein, J. C. & Nurgali, K. Colorectal Cancer Chemotherapy: The Evolution of Treatment and New Approaches. *Curr Med Chem* **24**, (2017).

17. Xie, Y. H., Chen, Y. X. & Fang, J. Y. Comprehensive review of targeted therapy for colorectal cancer. *Signal Transduction and Targeted Therapy* **5**, 1–30 (2020).

18. Moiseyenko, V. M. *et al.* First-Line Cetuximab Monotherapy in KRAS/NRAS/BRAF Mutation-Negative Colorectal Cancer Patients. *Clin Drug Investig* **38**, 553–562 (2018).

19. Seeber, A., Gunsilius, E., Gastl, G. & Pircher, A. Anti-Angiogenics: Their Value in Colorectal Cancer Therapy. *Oncol Res Treat* **41**, 188–193 (2018).

20. Ganesh, K. *et al.* Immunotherapy in colorectal cancer: rationale, challenges and potential. *Nature Reviews Gastroenterology & Hepatology* **16**, 361–375 (2019).

21. Naldini, L. Gene therapy returns to centre stage. *Nature* **526**, 351–360 (2015).

22. Ciccia, A. & Elledge, S. J. The DNA Damage Response: Making It Safe to Play with Knives. *Mol Cell* **40**, 179–204 (2010).

23. Molinaro, C., Martoriati, A. & Cailliau, K. Proteins from the DNA Damage Response: Regulation, Dysfunction, and Anticancer Strategies. *Cancers* **13**, 3819 (2021).

24. Harper, J. W. & Elledge, S. J. The DNA Damage Response: Ten Years After. *Mol Cell* **28**, 739–745 (2007).

25. Lord, C. J. & Ashworth, A. The DNA damage response and cancer therapy. *Nature* **481**, 287–294 (2012).

26. Jackson, S. P. & Bartek, J. The DNA-damage response in human biology and disease. *Nature* **461**, 1071–1078 (2009).

27. Hoeijmakers, J. H. J. DNA Damage, Aging, and Cancer. *New England Journal of Medicine* **361**, 1475–1485 (2009).

28. Goetz, M. E. & Luch, A. Reactive species: A cell damaging rout assisting to chemical carcinogens. *Cancer Lett* **266**, 73–83 (2008).

29. Kunkel, T. A. DNA Replication Fidelity *. *Journal of Biological Chemistry* **279**, 16895–16898 (2004).

30. Hakem, R. DNA-damage repair; the good, the bad, and the ugly. *EMBO J* **27**, 589–605 (2008).

31. Caldecott, K. W. Single-strand break repair and genetic disease. *Nature Reviews Genetics* **9**, 619–631 (2008).

32. Chapman, J. R., Taylor, M. R. G. & Boulton, S. J. Playing the End Game: DNA Double-Strand Break Repair Pathway Choice. *Mol Cell* **47**, 497–510 (2012).

33. Kuzminov, A. Single-strand interruptions in replicating chromosomes cause double-strand breaks. *Proc Natl Acad Sci USA* **98**, 8241–8246 (2001).

34. Chatterjee, N. & Walker, G. C. Mechanisms of DNA damage, repair, and mutagenesis. *Environ Mol Mutagen* **58**, 235–263 (2017).

35. Gutierrez, R. & O'Connor, T. R. DNA direct reversal repair and alkylating agent drug resistance. *Cancer Drug Resistance* **4**, 414–423 (2021).

36. Deans, A. J. & West, S. C. DNA interstrand crosslink repair and cancer. *Nature Reviews Cancer* **11**, 467–480 (2011).

37. Li, L. Y., Guan, Y. di, Chen, X. S., Yang, J. M. & Cheng, Y. DNA Repair Pathways in Cancer Therapy and Resistance. *Front Pharmacol* **11**, 2520 (2021).

38. Dianov, G. L. & Hübscher, U. Mammalian Base Excision Repair: the Forgotten Archangel. *Nucleic Acids Res* **41**, 3483–3490 (2013).

39. Marteijn, J. A., Lans, H., Vermeulen, W. & Hoeijmakers, J. H. J. Understanding nucleotide excision repair and its roles in cancer and ageing. *Nature Reviews Molecular Cell Biology* **15**, 465–481 (2014).

40. Jiricny, J. The multifaceted mismatch-repair system. *Nature Reviews Molecular Cell Biology* **7**, 335–346 (2006).

41. Scully, R., Panday, A., Elango, R. & Willis, N. A. DNA double-strand break repair-pathway choice in somatic mammalian cells. *Nature Reviews Molecular Cell Biology* **20**, 698–714 (2019).

42. Meek, K., Dang, V. & Lees-Miller, S. P. Chapter 2 DNA-PK: The Means to Justify the Ends? *Adv Immunol* **99**, 33–58 (2008).

43. Lieber, M. R. The mechanism of double-strand DNA break repair by the nonhomologous DNA end-joining pathway. *Annu Rev Biochem* **79**, 181–211 (2010).

44. Wyatt, D. W. *et al.* Essential Roles for Polymerase θ-Mediated End Joining in the Repair of Chromosome Breaks. *Mol Cell* **63**, 662–673 (2016).

45. Mateos-Gomez, P. A. *et al.* Mammalian polymerase θ promotes alternative NHEJ and suppresses recombination. *Nature* **518**, 254–257 (2015).

46. Li, X. & Heyer, W. D. Homologous recombination in DNA repair and DNA damage tolerance. *Cell Research* **18**, 99–113 (2008).

47. Garcia, V., Phelps, S. E. L., Gray, S. & Neale, M. J. Bidirectional resection of DNA double-strand breaks by Mre11 and Exo1. *Nature* **479**, 241–244 (2011).

48. San Filippo, J., Sung, P. & Klein, H. Mechanism of Eukaryotic Homologous Recombination. *Annu Rev Biochem* **77**, 229–257 (2008).

49. Panier, S. & Boulton, S. J. Double-strand break repair: 53BP1 comes into focus. *Nature Reviews Molecular Cell Biology* **15**, 7–18 (2013).

50. Chapman, J. R., Sossick, A. J., Boulton, S. J. & Jackson, S. P. BRCA1-associated exclusion of 53BP1 from DNA: Damage sites underlies temporal control of DNA repair. *J Cell Sci* **125**, 3529–3534 (2012).

51. Symington, L. S. & Gautier, J. Double-Strand Break End Resection and Repair Pathway Choice. *Annu Rev Genet* **45**, 247–271 (2011).

52. Blackford, A. N. & Jackson, S. P. ATM, ATR, and DNA-PK: The Trinity at the Heart of the DNA Damage Response. *Mol Cell* **66**, 801–817 (2017).

53. Lempiäinen, H. & Halazonetis, T. D. Emerging common themes in regulation of PIKKs and PI3Ks. *EMBO J* **28**, 3067–3073 (2009).

54. Renwick, A. *et al.* ATM mutations that cause ataxia-telangiectasia are breast cancer susceptibility alleles. *Nature Genetics* **38**, 873–875 (2006).

55. McKinnon, P. J. ATM and ataxia telangiectasia. *EMBO Rep* **5**, 772–776 (2004).

56. O'Driscoll, M., Ruiz-Perez, V. L., Woods, C. G., Jeggo, P. A. & Goodship, J. A. A splicing mutation affecting expression of ataxia–telangiectasia and Rad3–related protein (ATR) results in Seckel syndrome. *Nature Genetics* **33**, 497–501 (2003).

57. van der Burg, M., van Dongen, J. J. M. & van Gent, D. C. DNA-PKcs deficiency in human: Long predicted, finally found. *Curr Opin Allergy Clin Immunol* **9**, 503–509 (2009).

58. Lee, J. H. & Paull, T. T. Cellular functions of the protein kinase ATM and their relevance to human disease. *Nature Reviews Molecular Cell Biology* **22**, 796–814 (2021).

59. Paull, T. T. Mechanisms of ATM Activation. *Annu Rev Biochem* **84**, 711–738 (2015).

60. Uziel, T. *et al.* Requirement of the MRN complex for ATM activation by DNA damage. *EMBO J* **22**, 5612–5621 (2003).

61. Sun, Y., Xu, Y., Roy, K. & Price, B. D. DNA Damage-Induced Acetylation of Lysine 3016 of ATM Activates ATM Kinase Activity. *Mol Cell Biol* **27**, 8502–8509 (2007).

62. Khoronenkova, S. v. & Dianov, G. L. ATM prevents DSB formation by coordinating SSB repair and cell cycle progression. *Proc Natl Acad Sci USA* **112**, 3997–4002 (2015).

63. Guo, Z., Kozlov, S., Lavin, M. F., Person, M. D. & Paull, T. T. ATM activation by oxidative stress. *Science* **330**, 517–521 (2010).

64. Sordet, O. *et al.* Ataxia telangiectasia mutated activation by transcription- and topoisomerase I-induced DNA double-strand breaks. *EMBO Rep* **10**, 887–893 (2009).

65. Tresini, M. *et al.* The core spliceosome as target and effector of non-canonical ATM signalling. *Nature* **523**, 53–58 (2015).

66. Shiloh, Y. ATM and related protein kinases: safeguarding genome integrity. *Nature Reviews Cancer* **3**, 155–168 (2003).

67. Bothmer, A. *et al.* Regulation of DNA End Joining, Resection, and Immunoglobulin Class Switch Recombination by 53BP1. *Mol Cell* **42**, 319–329 (2011).

68. Balmus, G. *et al.* ATM orchestrates the DNA-damage response to counter toxic non-homologous end-joining at broken replication forks. *Nature Communications* **10**, 1–18 (2019).

69. Chen, B. P. C. *et al.* Ataxia telangiectasia mutated (ATM) is essential for DNA-PKcs phosphorylations at the Thr-2609 cluster upon DNA double strand break. *Journal of Biological Chemistry* **282**, 6582–6587 (2007).

70. Cortez, D., Wang, Y., Qin, J. & Elledge, S. J. Requirement of ATM-dependent phosphorylation of Brca1 in the DNA damage response to double-strand breaks. *Science* **286**, 1162–1166 (1999).

71. Kijas, A. W. *et al.* ATM-dependent phosphorylation of MRE11 controls extent of resection during homology directed repair by signalling through Exonuclease 1. *Nucleic Acids Res* **43**, 8352–8367 (2015).

72. Misteli, T. & Soutoglou, E. The emerging role of nuclear architecture in DNA repair and genome maintenance. *Nature Reviews Molecular Cell Biology* **10**, 243–254 (2009).

73. Rogakou, E. P., Pilch, D. R., Orr, A. H., Ivanova, V. S. & Bonner, W. M. DNA Double-stranded Breaks Induce Histone H2AX Phosphorylation on Serine 139. *Journal of Biological Chemistry* **273**, 5858–5868 (1998).

74. Burma, S., Chen, B. P., Murphy, M., Kurimasa, A. & Chen, D. J. ATM Phosphorylates Histone H2AX in Response to DNA Double-strand Breaks . *Journal of Biological Chemistry* **276**, 42462–42467 (2001).

75. An, J. *et al.* DNA-PKcs plays a dominant role in the regulation of H2AX phosphorylation in response to DNA damage and cell cycle progression. *BMC Mol Biol* **11**, 1–13 (2010).

76. Ward, I. M. & Chen, J. Histone H2AX Is Phosphorylated in an ATR-dependent Manner in Response to Replicational Stress . *Journal of Biological Chemistry* **276**, 47759–47762 (2001).

77. Lou, Z. *et al.* MDC1 maintains genomic stability by participating in the amplification of ATM-dependent DNA damage signals. *Mol Cell* **21**, 187–200 (2006).

78. Stucki, M. *et al.* MDC1 directly binds phosphorylated histone H2AX to regulate cellular responses to DNA double-strand breaks. *Cell* **123**, 1213–1226 (2005).

79. Cimprich, K. A. & Cortez, D. ATR: an essential regulator of genome integrity. *Nature Reviews Molecular Cell Biology* **9**, 616–627 (2008).

80. Maréchal, A. & Zou, L. DNA Damage Sensing by the ATM and ATR Kinases. *Cold Spring Harb Perspect Biol* **5**, a012716 (2013).

81. Zou, L. & Elledge, S. J. Sensing DNA damage through ATRIP recognition of RPA-ssDNA complexes. *Science* **300**, 1542–1548 (2003).

82. Matsuoka, S. *et al.* ATM and ATR substrate analysis reveals extensive protein networks responsive to DNA damage. *Science* **316**, 1160–1166 (2007).

83. Stiff, T. *et al.* ATR-dependent phosphorylation and activation of ATM in response to UV treatment or replication fork stalling. *EMBO J* **25**, 5775–5782 (2006).

84. Jette, N. & Lees-Miller, S. P. The DNA-dependent protein kinase: A multifunctional protein kinase with roles in DNA double strand break repair and mitosis. *Prog Biophys Mol Biol* **117**, 194–205 (2015).

85. Graham, T. G. W., Walter, J. C. & Loparo, J. J. Two-Stage Synapsis of DNA Ends during Non-homologous End Joining. *Mol Cell* **61**, 850–858 (2016).

86. Jiang, W. *et al.* Differential phosphorylation of DNA-PKcs regulates the interplay between end-processing and end-ligation during nonhomologous end-joining. *Mol Cell* **58**, 172–185 (2015).

87. Yue, X., Bai, C., Xie, D., Ma, T. & Zhou, P. K. DNA-PKcs: A Multi-Faceted Player in DNA Damage Response. *Front Genet* **11**, 1692 (2020).

88. Zhou, Y. *et al.* Regulation of the DNA Damage Response by DNA-PKcs Inhibitory Phosphorylation of ATM. *Mol Cell* **65**, 91–104 (2017).

89. Kastan, M. B. & Bartek, J. Cell-cycle checkpoints and cancer. *Nature* **432**, 316–323 (2004).

90. Bartek, J. & Lukas, J. Chk1 and Chk2 kinases in checkpoint control and cancer. *Cancer Cell* **3**, 421–429 (2003).

91. Bartek, J. & Lukas, J. DNA damage checkpoints: from initiation to recovery or adaptation. *Curr Opin Cell Biol* **19**, 238–245 (2007).

92. Smith, J., Mun Tho, L., Xu, N. & A. Gillespie, D. The ATM–Chk2 and ATR–Chk1 Pathways in DNA Damage Signaling and Cancer. *Adv Cancer Res* **108**, 73–112 (2010).

93. Shiloh, Y. & Ziv, Y. The ATM protein kinase: regulating the cellular response to genotoxic stress, and more. *Nature Reviews Molecular Cell Biology* **14**, 197–210 (2013).

94. Shang, Z. F. *et al.* Inactivation of DNA-dependent protein kinase leads to spindle disruption and mitotic catastrophe with attenuated checkpoint protein 2 phosphorylation in response to DNA damage. *Cancer Res* **70**, 3657–3666 (2010).

95. Campisi, J. & D'Adda Di Fagagna, F. Cellular senescence: when bad things happen to good cells. *Nature Reviews Molecular Cell Biology* **8**, 729–740 (2007).

96. Gibson, B. A. & Kraus, W. L. New insights into the molecular and cellular functions of poly(ADP-ribose) and PARPs. *Nature Reviews Molecular Cell Biology* **13**, 411–424 (2012).

97. Ray Chaudhuri, A. & Nussenzweig, A. The multifaceted roles of PARP1 in DNA repair and chromatin remodelling. *Nature Reviews Molecular Cell Biology* **18**, 610–621 (2017).

98. Langelier, M. F., Planck, J. L., Roy, S. & Pascal, J. M. Structural basis for DNA damage-dependent poly(ADP-ribosyl)ation by human PARP-1. *Science* **336**, 728–732 (2012).

99. Jungmichel, S. *et al.* Proteome-wide identification of poly(ADP-Ribosyl)ation targets in different genotoxic stress responses. *Mol Cell* **52**, 272–285 (2013).

100. Hassa, P. O. & Hottiger, M. O. The diverse biological roles of mammalian PARPs, a small but powerful family of poly-ADP-ribose polymerases. *Frontiers in Bioscience* **13**, 3046–3082 (2008).

101. Krietsch, J. *et al.* Reprogramming cellular events by poly(ADP-ribose)-binding proteins. *Mol Aspects Med* **34**, 1066–1087 (2013).

102. Teloni, F. & Altmeyer, M. Readers of poly(ADP-ribose): designed to be fit for purpose. *Nucleic Acids Res* **44**, 993–1006 (2016).

103. Caldecott, K. W. DNA single-strand break repair and human genetic disease. *Trends Cell Biol* **0**, (2022).

104. Robu, M. *et al.* Role of poly(ADP-ribose) polymerase-1 in the removal of UV-induced DNA lesions by nucleotide excision repair. *Proc Natl Acad Sci USA* **110**, 1658–1663 (2013).

105. Huang, D. & Kraus, W. L. The expanding universe of PARP1-mediated molecular and therapeutic mechanisms. *Mol Cell* **82**, 2315–2334 (2022).

106. Haince, J. F. *et al.* PARP1-dependent Kinetics of Recruitment of MRE11 and NBS1 Proteins to Multiple DNA Damage Sites . *Journal of Biological Chemistry* **283**, 1197–1208 (2008).

107. Aguilar-Quesada, R. *et al.* Interaction between ATM and PARP-1 in response to DNA damage and sensitization of ATM deficient cells through PARP inhibition. *BMC Mol Biol* **8**, (2007).

108. Xie, S. *et al.* Timeless Interacts with PARP-1 to Promote Homologous Recombination Repair. *Mol Cell* **60**, 163–176 (2015).

109. Mansour, W. Y., Rhein, T. & Dahm-Daphi, J. The alternative end-joining pathway for repair of DNA double-strand breaks requires PARP1 but is not dependent upon microhomologies. *Nucleic Acids Res* **38**, 6065–6077 (2010).

110. Spagnolo, L., Barbeau, J., Curtin, N. J., Morris, E. P. & Pearl, L. H. Visualization of a DNA-PK/PARP1 complex. *Nucleic Acids Res* **40**, 4168–4177 (2012).

111. Andronikou, C. & Rottenberg, S. Studying PAR-Dependent Chromatin Remodeling to Tackle PARPi Resistance. *Trends Mol Med* **27**, 630–642 (2021).

112. Hanzlikova, H. & Caldecott, K. W. Perspectives on PARPs in S Phase. *Trends in Genetics* **35**, 412–422 (2019).

113. Kraus, W. L. & Lis, J. T. PARP Goes Transcription. *Cell* **113**, 677–683 (2003).

114. Kim, D. S. *et al.* Activation of PARP-1 by snoRNAs Controls Ribosome Biogenesis and Cell Growth via the RNA Helicase DDX21. *Mol Cell* **75**, 1270-1285.e14 (2019).

115. Kim, D. S., Challa, S., Jones, A. & Kraus, W. L. PARPs and ADP-ribosylation in RNA biology: from RNA expression and processing to protein translation and proteostasis. *Genes Dev* **34**, 302–320 (2020).

116. O'Connor, M. J. Targeting the DNA Damage Response in Cancer. *Mol Cell* **60**, 547–560 (2015).

117. O'Neil, N. J., Bailey, M. L. & Hieter, P. Synthetic lethality and cancer. *Nature Reviews Genetics* **18**, 613–623 (2017).

118. Lord, C. J. & Ashworth, A. PARP inhibitors: Synthetic lethality in the clinic. *Science* **355**, 1152–1158 (2017).

119. Feng, F. Y., de Bono, J. S., Rubin, M. A. & Knudsen, K. E. Chromatin to Clinic: The Molecular Rationale for PARP1 Inhibitor Function. *Mol Cell* **58**, 925–934 (2015).

120. Pandey, N. & Black, B. E. Rapid Detection and Signaling of DNA Damage by PARP-1. *Trends Biochem Sci* **46**, 744–757 (2021).

121. Farmer, H. *et al.* Targeting the DNA repair defect in BRCA mutant cells as a therapeutic strategy. *Nature* **434**, 917–921 (2005).

122. Li, H. *et al.* PARP inhibitor resistance: the underlying mechanisms and clinical implications. *Molecular Cancer* **19**, 1–16 (2020).

123. Fugger, K., Hewitt, G., West, S. C. & Boulton, S. J. Tackling PARP inhibitor resistance. *Trends Cancer* **7**, 1102–1118 (2021).

124. Pilié, P. G., Tang, C., Mills, G. B. & Yap, T. A. State-of-the-art strategies for targeting the DNA damage response in cancer. *Nature Reviews Clinical Oncology* **16**, 81–104 (2018).

125. Weber, A. M. & Ryan, A. J. ATM and ATR as therapeutic targets in cancer. *Pharmacol Ther* **149**, 124–138 (2015).

126. Brown, J. S., O'Carrigan, B., Jackson, S. P. & Yap, T. A. Targeting DNA repair in cancer: Beyond PARP inhibitors. *Cancer Discov* **7**, 20–37 (2017).

127. Matthews, T. P., Jones, A. M. & Collins, I. Structure-based design, discovery and development of checkpoint kinase inhibitors as potential anticancer therapies. *Expert Opin Drug Discov* **8**, 621–640 (2013).

128. Sen, R. & Baltimore, D. Inducibility of kappa immunoglobulin enhancer-binding protein Nf-kappa B by a posttranslational mechanism. *Cell* **47**, 921–928 (1986).

129. Karin, M. Nuclear factor-kappaB in cancer development and progression. *Nature* **441**, 431–436 (2006).

130. Zhang, Q., Lenardo, M. J. & Baltimore, D. 30 Years of NF-κB: A Blossoming of Relevance to Human Pathobiology. *Cell* **168**, 37–57 (2017).

131. Hayden, M. S. & Ghosh, S. Shared principles in NF-kappaB signaling. *Cell* **132**, 344–362 (2008).

132. Gilmore, T. D. & Herscovitch, M. Inhibitors of NF-kappaB signaling: 785 and counting. *Oncogene* **25**, 6887–6899 (2006).

133. Perkins, N. D. Integrating cell-signalling pathways with NF-kappaB and IKK function. *Nat Rev Mol Cell Biol* **8**, 49–62 (2007).

134. Pasparakis, M., Luedde, T. & Schmidt-Supprian, M. Dissection of the NF-kappaB signalling cascade in transgenic and knockout mice. *Cell Death Differ* **13**, 861–872 (2006).

135. Ghosh, S. & Karin, M. Missing Pieces in the NF-κB Puzzle. *Cell* **109**, S81–S96 (2002).

136. Hayden, M. S. & Ghosh, S. NF-κB, the first quarter-century: remarkable progress and outstanding questions. *Genes Dev* **26**, 203–234 (2012).

137. Smale, S. T. Dimer-specific regulatory mechanisms within the NF-κB family of transcription factors. *Immunol Rev* **246**, 193–204 (2012).

138. Yamamoto, Y. & Gaynor, R. B. IκB kinases: Key regulators of the NF-κB pathway. *Trends in Biochemical Sciences* **29,** 72–79 (2004).

139. Tam, W. F., Lee, L. H., Davis, L. & Sen, R. Cytoplasmic sequestration of rel proteins by IkappaBalpha requires CRM1-dependent nuclear export. *Mol Cell Biol* **20**, 2269–2284 (2000).

140. Karin, M. & Ben-Neriah, Y. Phosphorylation meets ubiquitination: the control of NF-[kappa]B activity. *Annu Rev Immunol* **18**, 621–663 (2000).

141. Espinosa, L. & Marruecos, L. NF-κB-Dependent and -Independent (Moonlighting) IκBα Functions in Differentiation and Cancer. *Biomedicines* **9**, (2021).

142. Mulero, M. C. *et al.* Chromatin-bound IκBα regulates a subset of polycomb target genes in differentiation and cancer. *Cancer Cell* **24**, 151–166 (2013).

143. Marruecos, L. *et al.* IκBα deficiency imposes a fetal phenotype to intestinal stem cells. *EMBO Rep* **21**, (2020).

144. Marruecos, L. *et al.* Dynamic chromatin association of IκBα is regulated by acetylation and cleavage of histone H4. *EMBO Rep* **22**, (2021).

145. Aguilera, C., Hoya-Arias, R., Haegeman, G., Espinosa, L. & Bigas, A. Recruitment of IkappaBalpha to the hes1 promoter is associated with transcriptional repression. *Proc Natl Acad Sci U S A* **101**, 16537–16542 (2004).

146. Israël, A. The IKK Complex, a Central Regulator of NF-κB Activation. *Cold Spring Harb Perspect Biol* **2**, a000158 (2010).

147. Zandi, E., Rothwarf, D. M., Delhase, M., Hayakawa, M. & Karin, M. The IkappaB kinase complex (IKK) contains two kinase subunits, IKKalpha and IKKbeta, necessary for IkappaB phosphorylation and NF-kappaB activation. *Cell* **91**, 243–252 (1997).

148. Chen, G., Cao, P. & Goeddel, D. v. TNF-induced recruitment and activation of the IKK complex require Cdc37 and Hsp90. *Mol Cell* **9**, 401–410 (2002).

149. Hinz, M. *et al.* Signal responsiveness of IkappaB kinases is determined by Cdc37-assisted transient interaction with Hsp90. *J Biol Chem* **282**, 32311–32319 (2007).

150. Sigala, J. L. D. *et al.* Activation of transcription factor NF-kappaB requires ELKS, an IkappaB kinase regulatory subunit. *Science* **304**, 1963–1967 (2004).

151. Scheidereit, C. IkappaB kinase complexes: gateways to NF-kappaB activation and transcription. *Oncogene* **25**, 6685–6705 (2006).

152. May, M. J., Marienfeld, R. B. & Ghosh, S. Characterization of the Ikappa B-kinase NEMO binding domain. *J Biol Chem* **277**, 45992–46000 (2002).

153. May, M. J., Larsen, S. E., Shim, J. H., Madge, L. A. & Ghosh, S. A novel ubiquitin-like domain in IkappaB kinase beta is required for functional activity of the kinase. *J Biol Chem* **279**, 45528–45539 (2004).

154. Liu, F., Xia, Y., Parker, A. S. & Verma, I. M. IKK biology. *Immunol Rev* **246**, 239–253 (2012).

155. Yumi, Y., Verma, U. N., Prajapati, S., Youn-Tae, K. & Gaynor, R. B. Histone H3 phosphorylation by IKK-alpha is critical for cytokine-induced gene expression. *Nature* **423**, 655–659 (2003).

156. Anest, V. *et al.* A nucleosomal function for IkappaB kinase-alpha in NF-kappaB-dependent gene expression. *Nature* **423**, 659–663 (2003).

157. Zandi, E., Chen, Y. & Karin, M. Direct phosphorylation of IkappaB by IKKalpha and IKKbeta: discrimination between free and NF-kappaB-bound substrate. *Science* **281**, 1360–1363 (1998).

158. Delhase, M., Makio, H., Chen, Y. & Karin, M. Positive and negative regulation of IkappaB kinase activity through IKKbeta subunit phosphorylation. *Science* **284**, 309–313 (1999).

159. Häcker, H. & Karin, M. Regulation and function of IKK and IKK-related kinases. *Sci STKE* **2006**, (2006).

160. Mercurio, F. *et al.* IKK-1 and IKK-2: cytokine-activated IkappaB kinases essential for NF-kappaB activation. *Science* **278**, 860–866 (1997).

161. Meylan, E. *et al.* RIP1 is an essential mediator of Toll-like receptor 3-induced NF-kappa B activation. *Nat Immunol* **5**, 503–507 (2004).

162. Yang, J. *et al.* The essential role of MEKK3 in TNF-induced NF-kappaB activation. *Nat Immunol* **2**, 620–624 (2001).

163. Ea, C. K., Deng, L., Xia, Z. P., Pineda, G. & Chen, Z. J. Activation of IKK by TNFα Requires Site-Specific Ubiquitination of RIP1 and Polyubiquitin Binding by NEMO. *Mol Cell* **22**, 245–257 (2006).

164. Clark, K., Nanda, S. & Cohen, P. Molecular control of the NEMO family of ubiquitin-binding proteins. *Nat Rev Mol Cell Biol* **14**, 673–685 (2013).

165. Lo, Y. C. *et al.* Structural basis for recognition of diubiquitins by NEMO. *Mol Cell* **33**, 602–615 (2009).

166. Sebban, H., Yamaoka, S. & Courtois, G. Posttranslational modifications of NEMO and its partners in NF-kappaB signaling. *Trends Cell Biol* **16**, 569–577 (2006).

167. Harhaj, E. W. & Dixit, V. M. Regulation of NF-κB by deubiquitinases. *Immunol Rev* **246**, 107–124 (2012).

168. Tsuchiya, Y. *et al.* Distinct B subunits of PP2A regulate the NF-κB signalling pathway through dephosphorylation of IKKβ, IκBα and RelA. *FEBS Lett* **591**, 4083 (2017).

169. Schmidt-Supprian, M. *et al.* NEMO/IKK gamma-deficient mice model incontinentia pigmenti. *Mol Cell* **5**, 981–992 (2000).

170. Maubach, G., Schmädicke, A. C. & Naumann, M. NEMO Links Nuclear Factor-κB to Human Diseases. *Trends Mol Med* **24**, 654 (2018).

171. Pobezinskaya, Y. L. *et al.* The function of TRADD in signaling through tumor necrosis factor receptor 1 and TRIF-dependent Toll-like receptors. *Nat Immunol* **9**, 1047–1054 (2008).

172. Wang, C. *et al.* TAK1 is a ubiquitin-dependent kinase of MKK and IKK. *Nature* **412**, 346–351 (2001).

173. Kanarek, N. & Ben-Neriah, Y. Regulation of NF-κB by ubiquitination and degradation of the IκBs. *Immunol Rev* **246**, 77–94 (2012).

174. Baeuerle, P. A. & Baltimore, D. I kappa B: a specific inhibitor of the NF-kappa B transcription factor. *Science* **242**, 540–546 (1988).

175. Coope, H. J. *et al.* CD40 regulates the processing of NF-kappaB2 p100 to p52. *EMBO J* **21**, 5375–5385 (2002).

176. Claudio, E., Brown, K., Park, S., Wang, H. & Siebenlist, U. BAFF-induced NEMO-independent processing of NF-kappa B2 in maturing B cells. *Nat Immunol* **3**, 958–965 (2002).

177. Dejardin, E. *et al.* The lymphotoxin-beta receptor induces different patterns of gene expression via two NF-kappaB pathways. *Immunity* **17**, 525–535 (2002).

178. Senftleben, U. *et al.* Activation by IKKalpha of a second, evolutionary conserved, NF-kappa B signaling pathway. *Science* **293**, 1495–1499 (2001).

179. He, J. Q., Saha, S. K., Kang, J. R., Zarnegar, B. & Cheng, G. Specificity of TRAF3 in its negative regulation of the noncanonical NF-kappa B pathway. *J Biol Chem* **282**, 3688–3694 (2007).

180. Sun, S. C. The non-canonical NF-κB pathway in immunity and inflammation. *Nat Rev Immunol* **17**, 545 (2017).

181. Cildir, G., Low, K. C. & Tergaonkar, V. Noncanonical NF-κB Signaling in Health and Disease. *Trends Mol Med* **22**, 414–429 (2016).

182. McCool, K. W. & Miyamoto, S. DNA damage-dependent NF-κB activation: NEMO turns nuclear signaling inside out. *Immunol Rev* **246**, 311–326 (2012).

183. Hadian, K. & Krappmann, D. Signals from the nucleus: activation of NF-kappaB by cytosolic ATM in the DNA damage response. *Sci Signal* **4**, (2011).

184. Huang, T. T., Feinberg, S. L., Suryanarayanan, S. & Miyamoto, S. The zinc finger domain of NEMO is selectively required for NF-kappa B activation by UV radiation and topoisomerase inhibitors. *Mol Cell Biol* **22**, 5813–5825 (2002).

185. Huang, T. T., Wuerzberger-Davis, S. M., Wu, Z. H. & Miyamoto, S. Sequential modification of NEMO/IKKgamma by SUMO-1 and ubiquitin mediates NF-kappaB activation by genotoxic stress. *Cell* **115**, 565–576 (2003).

186. Mabb, A. M., Wuerzberger-Davis, S. M. & Miyamoto, S. PIASy mediates NEMO sumoylation and NF-kappaB activation in response to genotoxic stress. *Nat Cell Biol* **8**, 986–993 (2006).

187. Stilmann, M. *et al.* A nuclear poly(ADP-ribose)-dependent signalosome confers DNA damage-induced IkappaB kinase activation. *Mol Cell* **36**, 365–378 (2009).

188. McCool, K. & Miyamoto, S. A PAR-SUMOnious mechanism of NEMO activation. *Mol Cell* **36**, 349–350 (2009).

189. Janssens, S., Tinel, A., Lippens, S. & Tschopp, J. PIDD mediates NF-kappaB activation in response to DNA damage. *Cell* **123**, 1079–1092 (2005).

190. Biton, S. & Ashkenazi, A. NEMO and RIP1 control cell fate in response to extensive DNA damage via TNF-α feedforward signaling. *Cell* **145**, 92–103 (2011).

191. Wu, Z. H., Shi, Y., Tibbetts, R. S. & Miyamoto, S. Molecular linkage between the kinase ATM and NF-kappaB signaling in response to genotoxic stimuli. *Science* **311**, 1141–1146 (2006).

192. Wuerzberger-Davis, S. M., Nakamura, Y., Seufzer, B. J. & Miyamoto, S. NF-kappaB activation by combinations of NEMO SUMOylation and ATM activation stresses in the absence of DNA damage. *Oncogene* **26**, 641–651 (2007).

193. Jin, H. S. *et al.* cIAP1, cIAP2, and XIAP act cooperatively via nonredundant pathways to regulate genotoxic stress-induced nuclear factor-kappaB activation. *Cancer Res* **69**, 1782–1791 (2009).

194. Miyamoto, S. Nuclear initiated NF-κB signaling: NEMO and ATM take center stage. *Cell Res* **21**, 116–130 (2011).

195. Wu, Z. H. *et al.* ATM- and NEMO-dependent ELKS ubiquitination coordinates TAK1-mediated IKK activation in response to genotoxic stress. *Mol Cell* **40**, 75–86 (2010).

196. Yang, Y. *et al.* A cytosolic ATM/NEMO/RIP1 complex recruits TAK1 to mediate the NF-kappaB and p38 mitogen-activated protein kinase (MAPK)/MAPK-activated protein 2 responses to DNA damage. *Mol Cell Biol* **31**, 2774–2786 (2011).

197. Hinz, M. *et al.* A cytoplasmic ATM-TRAF6-cIAP1 module links nuclear DNA damage signaling to ubiquitin-mediated NF-κB activation. *Mol Cell* **40**, 63–74 (2010).

198. Hinz, M. & Scheidereit, C. The IκB kinase complex in NF-κB regulation and beyond. *EMBO Rep* **15**, 46–61 (2014).

199. Park, K. J., Krishnan, V., O'Malley, B. W., Yamamoto, Y. & Gaynor, R. B. Formation of an IKKalpha-dependent transcription complex is required for estrogen receptor-mediated gene activation. *Mol Cell* **18**, 71–82 (2005).

200. Tu, Z. *et al.* IKKα Regulates Estrogen-induced Cell Cycle Progression by Modulating E2F1 Expression *. *Journal of Biological Chemistry* **281**, 6699–6706 (2006).

201. Zhang, W. *et al.* A NIK-IKKα module expands ErbB2-induced tumor-initiating cells by stimulating nuclear export of p27/Kip1. *Cancer Cell* **23**, 647–659 (2013).

202. Luo, J. L. *et al.* Nuclear cytokine-activated IKKalpha controls prostate cancer metastasis by repressing Maspin. *Nature* **446**, 690–694 (2007).

203. Huang, W. C., Ju, T. K., Hung, M. C. & Chen, C. C. Phosphorylation of CBP by IKKalpha promotes cell growth by switching the binding preference of CBP from p53 to NF-kappaB. *Mol Cell* **26**, 75–87 (2007).

204. Zhu, F. *et al.* IKKalpha shields 14-3-3sigma, a G(2)/M cell cycle checkpoint gene, from hypermethylation, preventing its silencing. *Mol Cell* **27**, 214–227 (2007).

205. Toll, A. *et al.* Active nuclear IKK correlates with metastatic risk in cutaneous squamous cell carcinoma. *Arch Dermatol Res* **307**, 721–729 (2015).

206. Fernández-Majada, V. *et al.* Aberrant cytoplasmic localization of N-CoR in colorectal tumors. *Cell Cycle* **6**, 1748–1752 (2007).

207. Fernández-Majada, V. *et al.* Nuclear IKK activity leads to dysregulated notch-dependent gene expression in colorectal cancer. *Proc Natl Acad Sci U S A* **104**, 276–281 (2007).

208. Colomer, C. *et al.* IKKα is required in the intestinal epithelial cells for tumour stemness. *Br J Cancer* **118**, 839–846 (2018).

209. Margalef, P. *et al.* A truncated form of IKKα is responsible for specific nuclear IKK activity in colorectal cancer. *Cell Rep* **2**, 840–854 (2012).

210. Margalef, P. *et al.* BRAF-induced tumorigenesis is IKKα-dependent but NF-κB-independent. *Sci Signal* **8**, (2015).

211. Colomer, C. *et al.* IKKα Kinase Regulates the DNA Damage Response and Drives Chemo-resistance in Cancer. *Mol Cell* **75**, 669-682.e5 (2019).

212. Taniguchi, K. & Karin, M. NF-κB, inflammation, immunity and cancer: coming of age. *Nat Rev Immunol* **18**, 309–324 (2018).

213. Gilmore, T. D. & Garbati, M. R. Inhibition of NF-κB signaling as a strategy in disease therapy. *Curr Top Microbiol Immunol* **349**, 245–263 (2011).

214. Vancurova, I., Uddin, M. M., Zou, Y. & Vancura, A. Combination Therapies Targeting HDAC and IKK in Solid Tumors. *Trends Pharmacol Sci* **39**, 295–306 (2018).

215. Karin, M., Yamamoto, Y. & Wang, Q. M. The IKK NF-kappa B system: a treasure trove for drug development. *Nat Rev Drug Discov* **3**, 17–26 (2004).

216. Schadendorf, D. *et al.* Melanoma. *Nature Reviews Disease Primers* **1**, 1–20 (2015).

217. Watts, C. G. *et al.* Clinical practice guidelines for identification, screening and follow-up of individuals at high risk of primary cutaneous melanoma: a systematic review. *British Journal of Dermatology* **172**, 33–47 (2015).

218. Gandini, S. *et al.* Meta-analysis of risk factors for cutaneous melanoma: II. Sun exposure. *Eur J Cancer* **41**, 45–60 (2005).

219. Chin, L. The genetics of malignant melanoma: lessons from mouse and man. *Nature Reviews Cancer* **3**, 559–570 (2003).

220. Tucker, M. A. *et al.* Clinically Recognized Dysplastic Nevi: A Central Risk Factor for Cutaneous Melanoma. *JAMA* **277**, 1439–1444 (1997).

221. Gray-Schopfer, V., Wellbrock, C. & Marais, R. Melanoma biology and new targeted therapy. *Nature* **445**, 851–857 (2007).

222. Haass, N. K., Smalley, K. S. M. & Herlyn, M. The Role of Altered Cell–Cell Communication in Melanoma Progression. *Journal of Molecular Histology* **35**, 309–318 (2004).

223. Duffy, K. & Grossman, D. The dysplastic nevus: From historical perspective to management in the modern era: Part I. Historical, histologic, and clinical aspects. *J Am Acad Dermatol* **67**, 1.e1-1.e16 (2012).

224. Shain, A. H. & Bastian, B. C. From melanocytes to melanomas. *Nature Reviews Cancer* **16**, 345–358 (2016).

225. Eddy, K., Shah, R. & Chen, S. Decoding Melanoma Development and Progression: Identification of Therapeutic Vulnerabilities. *Front Oncol* **10**, 3357 (2021).

226. Guo, W., Wang, H. & Li, C. Signal pathways of melanoma and targeted therapy. *Signal Transduction and Targeted Therapy* **6**, 1–39 (2021).

227. Wei, Z. & Liu, H. T. MAPK signal pathways in the regulation of cell proliferation in mammalian cells. *Cell Research* **12**, 9–18 (2002).

228. Arthur, J. S. C. & Ley, S. C. Mitogen-activated protein kinases in innate immunity. *Nature Reviews Immunology* **13**, 679–692 (2013).

229. Peti, W. & Page, R. Molecular basis of MAP kinase regulation. *Protein Science* **22**, 1698–1710 (2013).

230. Morrison, D. K. MAP Kinase Pathways. *Cold Spring Harb Perspect Biol* **4**, a011254 (2012).

231. Johnson, G. L. & Lapadat, R. Mitogen-activated protein kinase pathways mediated by ERK, JNK, and p38 protein kinases. *Science* **298**, 1911–1912 (2002).

232. McKay, M. M. & Morrison, D. K. Integrating signals from RTKs to ERK/MAPK. *Oncogene* **26**, 3113–3121 (2007).

233. Rincón, M. & Davis, R. J. Regulation of the immune response by stress-activated protein kinases. *Immunol Rev* **228**, 212–224 (2009).

234. Cuadrado, A. & Nebreda, A. R. Mechanisms and functions of p38 MAPK signalling. *Biochemical Journal* **429**, 403–417 (2010).

235. Stern, D. F. Keeping Tumors Out of the MAPK Fitness Zone. *Cancer Discov* **8**, 20–23 (2018).

236. Braicu, C. *et al.* A Comprehensive Review on MAPK: A Promising Therapeutic Target in Cancer. *Cancers* **11**, 1618 (2019).

237. Davies, H. *et al.* Mutations of the BRAF gene in human cancer. *Nature* **417**, 949–954 (2002).

238. Gray-Schopfer, V. C., da Rocha Dias, S. & Marais, R. The role of B-RAF in melanoma. *Cancer and Metastasis Reviews* **24**, 165–183 (2005).

239. Buchbinder, E. I. & Flaherty, K. T. Biomarkers in Melanoma: Lessons from Translational Medicine. *Trends Cancer* **2**, 305–312 (2016).

240. Monahan, K. B. *et al.* Somatic p16INK4a loss accelerates melanomagenesis. *Oncogene* **29**, 5809–5817 (2010).

241. Kong, Y. *et al.* Frequent genetic aberrations in the CDK4 pathway in acral melanoma indicate the potential for CDK4/6 inhibitors in targeted therapy. *Clinical Cancer Research* **23**, 6946–6957 (2017).

242. Buecher, B. *et al.* Contribution of CDKN2A/P16 INK4A , P14 ARF , CDK4 and BRCA1/2 germline mutations in individuals with suspected genetic predisposition to uveal melanoma. *Familial Cancer* **9**, 663–667 (2010).

243. Hodis, E. *et al.* A landscape of driver mutations in melanoma. *Cell* **150**, 251–263 (2012).

244. Nogueira, C. *et al.* Cooperative interactions of PTEN deficiency and RAS activation in melanoma metastasis. *Oncogene* **29**, 6222–6232 (2010).

245. Hemmings, B. A. & Restuccia, D. F. PI3K-PKB/Akt Pathway. *Cold Spring Harb Perspect Biol* **4**, a011189 (2012).

246. Gallardo, F. *et al.* Cytoplasmic accumulation of NCoR in malignant melanoma: consequences of altered gene repression and prognostic significance. *Oncotarget* **6**, 9284–9294 (2015).

247. Gershenwald, J. E. *et al.* Melanoma staging: Evidence-based changes in the American Joint Committee on Cancer eighth edition cancer staging manual. *CA Cancer J Clin* **67**, 472–492 (2017).

248. Schadendorf, D. *et al.* Melanoma. *The Lancet* **392**, 971–984 (2018).

249. Hayward, N. K. *et al.* Whole-genome landscapes of major melanoma subtypes. *Nature* **545**, 175–180 (2017).

250. Tremante, E. *et al.* Melanoma molecular classes and prognosis in the postgenomic era. *Lancet Oncol* **13**, e205–e211 (2012).

251. Akbani, R. *et al.* Genomic Classification of Cutaneous Melanoma. *Cell* **161**, 1681–1696 (2015).

252. Romano, E., Schwartz, G. K., Chapman, P. B., Wolchock, J. D. & Carvajal, R. D. Treatment implications of the emerging molecular classification system for melanoma. *Lancet Oncol* **12**, 913–922 (2011).

253. Mattia, G. *et al.* Cell death-based treatments of melanoma: conventional treatments and new therapeutic strategies. *Cell Death & Disease* **9**, 1–14 (2018).

254. Schreck K & Grossman S. Role of Temozolomide in the Treatment of Cancers Involving the Central Nervous System. | Semantic Scholar. *Oncology* **32**, 560–569 (2018).

255. Luke, J. J. & Schwartz, G. K. Chemotherapy in the management of advanced cutaneous malignant melanoma. *Clin Dermatol* **31**, 290–297 (2013).

256. Wilson, M. A. & Schuchter, L. M. Chemotherapy for melanoma. *Cancer Treat Res* **167**, 209–229 (2016).

257. Zaman, A., Wu, W. & Bivona, T. G. Targeting Oncogenic BRAF: Past, Present, and Future. *Cancers* **11**, 1197 (2019).

258. Flaherty, K. T. *et al.* Improved Survival with MEK Inhibition in BRAF-Mutated Melanoma. *New England Journal of Medicine* **367**, 107–114 (2012).

259. Planchard, D. *et al.* An open-label phase II trial of dabrafenib (D) in combination with trametinib (T) in patients (pts) with previously treated BRAF V600E–mutant advanced non-small cell lung cancer (NSCLC; BRF113928). *Am. J. Clin. Oncol.* **34**, 107–107 (2016).

260. Holderfield, M., Deuker, M. M., McCormick, F. & McMahon, M. Targeting RAF kinases for cancer therapy: BRAF-mutated melanoma and beyond. *Nature Reviews Cancer* **14**, 455–467 (2014).

261. Poulikakos, P. I., Zhang, C., Bollag, G., Shokat, K. M. & Rosen, N. RAF inhibitors transactivate RAF dimers and ERK signalling in cells with wild-type BRAF. *Nature* **464**, 427–430 (2010).

262. Zhang, C. *et al.* RAF inhibitors that evade paradoxical MAPK pathway activation. *Nature* **526**, 583–586 (2015).

263. Kwong, L. N. & Davies, M. A. Targeted therapy for melanoma: rational combinatorial approaches. *Oncogene* **33**, 1–9 (2013).

264. Haanen, J. B. A. G. Immunotherapy of melanoma. *European Journal of Cancer Supplements* **11**, 97–105 (2013).

265. Ribas, A. & Wolchok, J. D. Cancer immunotherapy using checkpoint blockade. *Science* **359**, 1350–1355 (2018).

266. Luke, J. J., Flaherty, K. T., Ribas, A. & Long, G. v. Targeted agents and immunotherapies: optimizing outcomes in melanoma. *Nature Reviews Clinical Oncology* **14**, 463–482 (2017).

267. Tentori, L., Lacal, P. M. & Graziani, G. Challenging resistance mechanisms to therapies for metastatic melanoma. *Trends Pharmacol Sci* **34**, 656–666 (2013).

268. Shalem, O. *et al.* Genome-scale CRISPR-Cas9 knockout screening in human cells. *Science* **343**, 84–87 (2014).

269. Roux, K. J., Kim, D. I., Burke, B. & May, D. G. BioID: A Screen for Protein-Protein Interactions. *Curr Protoc Protein Sci* **91**, 19.23.1 (2018).

270. Nahlé, S. *et al.* Defining the interactomes of proteins involved in cytoskeletal dynamics using high-throughput proximity-dependent biotinylation in cellulo. *STAR Protoc* **3**, (2022).

271. Choi, H. *et al.* SAINT: probabilistic scoring of affinity purification-mass spectrometry data. *Nat Methods* **8**, 70–73 (2011).

272. Marisa, L. *et al.* Gene expression classification of colon cancer into molecular subtypes: characterization, validation, and prognostic value. *PLoS Med* **10**, (2013).

273. Barrett, T. *et al.* NCBI GEO: archive for functional genomics data sets--update. *Nucleic Acids Res* **41**, (2013).

274. Irizarry, R. A. *et al.* Exploration, normalization, and summaries of high density oligonucleotide array probe level data. *Biostatistics* **4**, 249–264 (2003).

275. Cortazar, A. R. *et al.* CANCERTOOL: A Visualization and Representation Interface to Exploit Cancer Datasets. *Cancer Res* **78**, 6320–6328 (2018).

276. Therneau, T. M. & Grambsch, P. M. Modeling Survival Data: Extending the Cox Model. (2000).

277. Roux, K. J., Kim, D. I., Raida, M. & Burke, B. A promiscuous biotin ligase fusion protein identifies proximal and interacting proteins in mammalian cells. *J Cell Biol* **196**, 801–810 (2012).

278. Schröfelbauer, B., Polley, S., Behar, M., Ghosh, G. & Hoffmann, A. NEMO ensures signaling specificity of the pleiotropic IKKβ by directing its kinase activity toward IκBα. *Mol Cell* **47**, 111–121 (2012).

279. Tan, Q. *et al.* Selective degradation of IKKα by autophagy is essential for arsenite-induced cancer cell apoptosis. *Cell Death Dis* **11**, (2020).

280. Xu, X. *et al.* Autophagic feedback-mediated degradation of IKKα requires CHK1- and p300/CBP-dependent acetylation of p53. *J Cell Sci* **133**, (2020).

281. Layer, J. v. *et al.* Polymerase δ promotes chromosomal rearrangements and imprecise double-strand break repair. *Proc Natl Acad Sci U S A* **117**, 27566–27577 (2020).

282. Sau, A. *et al.* Persistent Activation of NF-κB in BRCA1-Deficient Mammary Progenitors Drives Aberrant Proliferation and Accumulation of DNA Damage. *Cell Stem Cell* **19**, 52–65 (2016).

283. Budke, B. *et al.* Noncanonical NF-κB factor p100/p52 regulates homologous recombination and modulates sensitivity to DNA-damaging therapy. *Nucleic Acids Res* **50**, 6251–6263 (2022).

284. Daniel, J. A. *et al.* Multiple autophosphorylation sites are dispensable for murine ATM activation in vivo. *J Cell Biol* **183**, 777–783 (2008).

285. Yoshida, K. *et al.* ATM-dependent nuclear accumulation of IKK-alpha plays an important role in the regulation of p73-mediated apoptosis in response to cisplatin. *Oncogene* **27**, 1183–1188 (2008).

286. Sabatel, H., Pirlot, C., Piette, J. & Habraken, Y. Importance of PIKKs in NF-κB activation by genotoxic stress. *Biochem Pharmacol* **82**, 1371–1383 (2011).

287. Stiff, T. *et al.* ATR-dependent phosphorylation and activation of ATM in response to UV treatment or replication fork stalling. *EMBO J* **25**, 5775–5782 (2006).

288. Shiotani, B. & Zou, L. Single-stranded DNA orchestrates an ATM-to-ATR switch at DNA breaks. *Mol Cell* **33**, 547–558 (2009).

289. Shrivastav, M. *et al.* DNA-PKcs and ATM co-regulate DNA double-strand break repair. *DNA Repair (Amst)* **8**, 920–929 (2009).

290. Yajima, H., Lee, K.-J. & Chen, B. P. C. ATR-dependent phosphorylation of DNA-dependent protein kinase catalytic subunit in response to UV-induced replication stress. *Mol Cell Biol* **26**, 7520–7528 (2006).

291. Stiff, T. *et al.* ATM and DNA-PK function redundantly to phosphorylate H2AX after exposure to ionizing radiation. *Cancer Res* **64**, 2390–2396 (2004).

292. Wang, H., Wang, M., Wang, H., Böcker, W. & Iliakis, G. Complex H2AX phosphorylation patterns by multiple kinases including ATM and DNA-PK in human cells exposed to ionizing radiation and treated with kinase inhibitors. *J Cell Physiol* **202**, 492–502 (2005).

293. Alexander, A. *et al.* ATM signals to TSC2 in the cytoplasm to regulate mTORC1 in response to ROS. *Proc Natl Acad Sci U S A* **107**, 4153–4158 (2010).

294. Randon, G. *et al.* Prognostic impact of ATM mutations in patients with metastatic colorectal cancer. *Sci Rep* **9**, (2019).

295. Choi, M., Kipps, T. & Kurzrock, R. ATM Mutations in Cancer: Therapeutic Implications. *Mol Cancer Ther* **15**, 1781–1791 (2016).

296. Li, S. K. H. & Martin, A. Mismatch Repair and Colon Cancer: Mechanisms and Therapies Explored. *Trends in Molecular Medicine* **22**, 274–289 (2016).

297. Singh, M. K. *et al.* Does NEMO/IKKγ protein have a role in determining prognostic significance in uveal melanoma? *Clin Transl Oncol* **20**, 1592–1603 (2018).

298. Yu, Z. *et al.* Characterization of a small-molecule inhibitor targeting NEMO/IKKβ to suppress colorectal cancer growth. *Signal Transduct Target Ther* **7**, (2022).

299. Carvalho, G. *et al.* Inhibition of NEMO, the regulatory subunit of the IKK complex, induces apoptosis in high-risk myelodysplastic syndrome and acute myeloid leukemia. *Oncogene* **26**, 2299–2307 (2007).

300. Zhao, J. *et al.* Development of novel NEMO-binding domain mimetics for inhibiting IKK/NF-κB activation. *PLoS Biol* **16**, (2018).

301. Anthony, N. G. *et al.* Inhibitory Kappa B Kinase α (IKKα) Inhibitors That Recapitulate Their Selectivity in Cells against Isoform-Related Biomarkers. *J Med Chem* **60**, 7043–7066 (2017).

302. Reilly, N. M., Novara, L., di Nicolantonio, F. & Bardelli, A. Exploiting DNA repair defects in colorectal cancer. *Mol Oncol* **13**, 681–700 (2019).

303. Wang, C., Jette, N., Moussienko, D., Bebb, D. G. & Lees-Miller, S. P. ATM-Deficient Colorectal Cancer Cells Are Sensitive to the PARP Inhibitor Olaparib. *Transl Oncol* **10**, 190–196 (2017).

304. Schmitt, A. *et al.* ATM Deficiency Is Associated with Sensitivity to PARP1- and ATR Inhibitors in Lung Adenocarcinoma. *Cancer Res* **77**, 3040–3056 (2017).

305. Kubota, E. *et al.* Low ATM protein expression and depletion of p53 correlates with olaparib sensitivity in gastric cancer cell lines. *Cell Cycle* **13**, 2129–2137 (2014).

306. Vilar, E. *et al.* MRE11 deficiency increases sensitivity to poly(ADP-ribose) polymerase inhibition in microsatellite unstable colorectal cancers. *Cancer Res* **71**, 2632–2642 (2011).

307. Lloyd, R. L. *et al.* Combined PARP and ATR inhibition potentiates genome instability and cell death in ATM-deficient cancer cells. *Oncogene* **39**, 4869–4883 (2020).

308. Kim, H. *et al.* Combining PARP with ATR inhibition overcomes PARP inhibitor and platinum resistance in ovarian cancer models. *Nat Commun* **11**, (2020).

309. Fedorenko, I. v., Gibney, G. T. & Smalley, K. S. M. NRAS mutant melanoma: biological behavior and future strategies for therapeutic management. *Oncogene* **32**, 3009–3018 (2013).

310. Menzer, C. & Hassel, J. C. Targeted Therapy for Melanomas Without BRAF V600 Mutations. *Curr Treat Options Oncol* **23**, 831–842 (2022).